TEL AVIV UNIVERSITY אוניברסיטת תל-אביב
Raymond and Beverly Sackler
Faculty of Exact Sciences
The Blavatnik School of Computer Science

# Minkowski Sum Construction and other Applications of Arrangements of Geodesic Arcs on the Sphere

Thesis submitted for the degree of "Doctor of Philosophy"

by

**Efraim Fogel**

This work has been carried out under the supervision of
Prof. Dan Halperin

Submitted to the Senate of Tel-Aviv University
October 2008

## Acknowledgements

This research project would not have been possible without the support of many people. I wish to express my gratitude to my advisor, Prof. Dan Halperin who was abundantly helpful and offered invaluable assistance, support, insights, and guidance. This sentense is far short of describing the magnitude of positive influence Danny had on this research and this researcher.

I would like to thank Ron Wein and Ophir Setter from Tel-Aviv University and Eric Berberich from Max-Planck-Insitut für Informatik, for ongoing and fruitful collaboration. I would also like to thank all other members of the applied computational geometry group at the computer science school in Tel-Aviv University who made the study duration festive.

I would like to thanks the members of the CGAL Editorial Board in particular and all members of the CGAL developers' community in general for sharing their wisdom through many useful advises and rich discussions.

During the years I participated in the EU-funded projects ECG (Effective Computational Geometry for Curves and Surfaces; contract No. IST-2000-26473), MOVIE (Motion Planning in Virtual Environments, contract No. IST-2001-39250) and ACS (Algorithms for Complex Shapes; contract No. IST-006413) projects. I wish to thank all the other participants in these projects, with whom I enjoyed working.

Finally, I would like to express my love and gratitude to my beloved families; for their understanding and endless love, through the duration of my studies.

# Abstract

We present two exact implementations of efficient output-sensitive algorithms that compute *Minkowski sums* of two convex polyhedra in $\mathbb{R}^3$. We do not assume general position. Namely, we handle degenerate input, and produce exact results. We provide a tight bound on the exact maximum complexity of Minkowski sums of polytopes in $\mathbb{R}^3$ in terms of the number of facets of the summand polytopes. The complexity of Minkowski sum structures is directly related to the time consumption of our Minkowski sum constructions, as they are output sensitive. We demonstrate the effectiveness of our Minkowski-sum constructions through simple applications that exploit these operations to detect collision between, and answer proximity queries about, two convex polyhedra in $\mathbb{R}^3$.

The algorithms employ variants of a data structure that represents arrangements embedded on two-dimensional parametric surfaces in $\mathbb{R}^3$, and they make use of many operations applied to arrangements in these representations. We have developed software components that support the arrangement data-structure variants and the operations applied to them. These software components are generic, as they can be instantiated with any number type. However, our algorithms require only (exact) rational arithmetic. These software components together with exact rational-arithmetic enable a robust, efficient, and elegant implementation of the Minkowski-sum constructions and the related applications. These software components are provided through a package of the Computational Geometry Algorithm Library (CGAL) [5] called `Arrangement_on_surface_2` [WFZH07a]. The code of CGAL in general, the `Arrangement_on_surface_2` package in particular, and all the rest of the code developed as part of this thesis adhere to the *Generic Programming* paradigm and follow the *Exact Geometric Computation* paradigm.

We also present exact implementations of other applications that exploit arrangements of arcs of great circles, also known as geodesic arcs, embedded on the sphere. For example, we implemented robust polyhedra central-projection and Boolean set-operations applied to point sets embedded on the sphere bounded by geodesic arcs. We use them as basic blocks in an exact implementation of an efficient algorithm that partitions an assembly of polyhedra in $\mathbb{R}^3$ with two hands using infinite translations. This application makes extensive use of Minkowski-sum constructions and other operations on arrangements of geodesic arcs embedded on the sphere. It distinctly shows the importance of exact computation, as imprecise computation might result with dismissal of valid partitioning-motions.

We have produced three movies that explain some of the concepts portrayed in this thesis [20].[1] The first movie [FFHL02] explains what Minkowski sums are and demonstrates how they are used in various applications. The second movie [FH05] demonstrates the first method we have developed to construct Minkowski-sums of convex polyhedra. The third movie [FSH08b] illustrates exact construction and maintenance of arrangements induced by geodesic arcs and applications that exploit such arrangements.

Additional information is available at the following web sites:
`http://acg.cs.tau.ac.il/projects/internal-projects/gaussian-map-cubical`

[1] Throughout the thesis a number in brackets (e.g., [20]) refers to the link list starting on page 118, and an alphanumeric string in brackets (e.g., [FFHL02]) is a standard bibliographic reference.

http://acg.cs.tau.ac.il/projects/internal-projects/arrangements-on-surfaces, http://acg.cs.tau.ac.il/projects/internal-projects/exact-complexity-of-minkowski-sums, and http://acg.cs.tau.ac.il/projects/internal-projects/arr-geodesic-sphere

Auxiliary programs, source code, data sets, and documentation can be downloaded from http://www.cs.tau.ac.il/~efif/Minkowski-sum.

# Contents

# List of Figures

# List of Tables

*The Guide is definitive. Reality is frequently inaccurate.*

Douglas Adams

# 1 Introduction

Let $P$ and $Q$ be two closed convex polyhedra in $\mathbb{R}^d$. The Minkowski sum of $P$ and $Q$ is the convex polyhedron $M = P \oplus Q = \{p + q \,|\, p \in P, q \in Q\}$. A polyhedron $P$ translated by a vector $t$ is denoted by $P^t$. *Collision Detection* is a procedure that determines whether $P$ and $Q$ overlap. The *Separation Distance* $\pi(P, Q)$ and *the Penetration Depth* $\delta(P, Q)$ defined as

$$\pi(P, Q) = \min\{\|t\| \,|\, P^t \cap Q \neq \emptyset, t \in \mathbb{R}^d\} \ ,$$
$$\delta(P, Q) = \inf\{\|t\| \,|\, P^t \cap Q = \emptyset, t \in \mathbb{R}^d\}$$

are the minimum distances by which $P$ has to be translated so that $P$ and $Q$ intersect or become interior disjoint, respectively. The problems of finding the distances above can also be posed given a normalized vector $r$ that represents a direction, in which case the minimum distance sought is in direction $r$. The *Directional Penetration-Depth*, for example, is defined as

$$\delta_r(P, Q) = \inf\{\alpha \,|\, P^{\alpha\vec{r}} \cap Q = \emptyset, \alpha \in \mathbb{R}\} \ .$$

## 1.1 Main Contribution

We present two exact and robust implementations of efficient output-sensitive algorithms to compute the Minkowski sum [FFHL02] of two convex polyhedra, polytopes for short, in $\mathbb{R}^3$ [FH05, FH07, FSH08a, BFH+09a]. The implementations are exact and robust, as they handle all degenerate cases, and guarantee exact results. We demonstrate the effectiveness of our Minkowski-sum computations through simple applications that exploit these operations to detect collision, and compute the Euclidean separation-distance between, and the directional penetration depth of, two polytopes in $\mathbb{R}^3$.

We compare our Minkowski-sum constructions with three other methods that produce exact results we are aware of. One is a simple method that computes the convex hull of the pairwise sums of vertices of two polytopes. The second is based on Nef polyhedra embedded on the sphere, and the third is based on linear programming. We conducted experiments with a broad family of polytopes and compared the performance of our methods with the performance of the other. The results reported in Table 3.5 clearly shows that both our methods are significantly faster.

Each method we have developed uses a different variant of Gaussian maps, also known as normal diagrams or slope diagrams, to maintain dual representations of polytopes. Each method employs a different variant of a generic data-structure that represents *arrangement* embedded on two-dimensional parametric surfaces in $\mathbb{R}^3$ to maintain the dual representations. (Arrangements embedded on two-dimensional parametric surfaces are subdivisions of the surface, as induced by curves embedded on the surface. They play a central role in this thesis; see Chapter 2 for a formal definition and Figure 2.1 for an illustration.) Each method makes use of many operations applied to arrangements in the corresponding representations.

We present a tight bound on the exact maximum complexity of Minkowski sums of polytopes in $\mathbb{R}^3$ [FHW07]. In particular, we prove that the maximum number of facets of the Minkowski sum of $k$ polytopes with $m_1, m_2, \ldots, m_k$ facets respectively is bounded from above by $\sum_{1\leq i<j\leq k}(2m_i-5)(2m_j-5)+\sum_{1\leq i\leq k} m_i+\binom{k}{2}$. Given $k$ positive integers $m_1, m_2, \ldots, m_k$, we describe how to construct $k$ polytopes with corresponding number of facets, such that the number of facets of their Minkowski sum is exactly $\sum_{1\leq i<j\leq k}(2m_i-5)(2m_j-5)+\sum_{1\leq i\leq k} m_i+\binom{k}{2}$. When $k=2$, for example, the expression above reduces to $4m_1m_2-9m_1-9m_2+26$.

We also present an exact implementation of an efficient algorithm that partitions an assembly of polyhedra in $\mathbb{R}^3$ with two hands using infinite translations [FH08]. This application makes extensive use of Minkowski-sum constructions and other operations on arrangements of arcs of great circles, also known as geodesic arcs, embedded on the sphere, such as polyhedra central-projection and Boolean set-operations of point sets embedded on the sphere bounded by geodesic arcs. The assembly partitioning demonstrates the importance of exact computation, as imprecise computation might result with dismissal of valid partitioning-motions.

Both methods that construct Minkowski sums and the related applications are implemented on top of the Computational Geometry Algorithms Library (CGAL) [FT07], and are mainly based on the arrangement package of the library [FWH04, WFZH07b, FHK+07, BFH+07, BFH+09b], which supports arrangements embedded on two-dimensional parametric surfaces and operations on them. We have redesigned, re-implemented, and significantly extended the package exploiting advanced programming techniques to yield a package that is easy to use, to extend, and to adapt to a variety of applications.

The package contains a general framework for computing the zone of a single curve embedded on a two-dimensional parametric surface and a general framework for sweeping a set of such curves. The former framework is used, for example, to insert curves one at a time into the arrangement. The latter framework is used, for example, to compute the arrangement induced by a collection of curves, and to compute the overlay of two arrangements. Other

operations, such as point location and vertical ray shooting, are supported as well.

The design dictates the separation between the topological and geometric aspects of the two-dimensional subdivision. This separation is advantageous, as it allows users to employ the package with their own representation of any special family of curves. They must however supply a relevant component called *geometry traits* class that handles the specific family of curves they are interested in, which mainly involves algebraic computation. The separation is enabled by a modular design and conveniently implemented within the *generic-programming* paradigm. The separation is a key aspect of the package, as well as of other central CGAL components, such as the various triangulation packages [BDTY00] and convex-hull algorithms (see [cga07] for more details), has been forced since its early stages, and heightened by our new design.

The package comes with many geometric traits classes that handle all kinds of curves organized in a structured hierarchy. In particular, we mention the geometric traits class that handles continuous piecewise linear curves, referred to as polylines and the geometric traits class that handles geodesic arcs embedded on the sphere [FSH08b, FSH08a, BFH$^+$09a]. The former are of particular interest, as they can be used to approximate more complex curves in the plane. At the same time they are easier to deal with in comparison to higher-degree algebraic curves, as rational arithmetic is sufficient to carry out exact computations on polylines. The latter is broadly used by the assembly-partitioning application and by the second method that constructs Minkowski sums.

The implementation of the package as well as the implementation our Minkowski-sum constructions, collision detection, and assembly partitioning applications handle degenerate input and produce exact results, as long as the underlying number type supports the arithmetic operations $+$, $-$, $*$, and / in unlimited precision over the rationals,[1] such as the rational number type `CGAL::Gmpq` based on GMP — Gnu's Multi Precision library [12].

## 1.2 Background: Minkowski Sums

Minkowski sums are closely related to proximity queries [LM04]. For example, the minimum separation distance between two polytopes $P$ and $Q$ is equal to the minimum distance between the origin and the boundary of the Minkowski sum of $P$ and the reflection of $Q$ through the origin [CC86]. Computing Minkowski sums, collision detection and proximity calculation constitute fundamental tasks in computational geometry [HKL04, LM04, Sha04]. These operations are ubiquitous in robotics, solid modeling, design automation, manufacturing, assembly planning, virtual prototyping, and many more domains; see, e.g., [BdLT97, EOR92, KR91, Lat91, VKSM05].

The wide spectrum of ideas expressed in the massive amount of literature published about the subject during the last three decades has inspired the development of quite a few useful solutions. For an extensive overview about the subject and a comprehensive list of packages see [LM04]. However, only recent advances in the implementation of computational-geometry algorithms and data structures made our exact, robust, and efficient implementation possi-

[1] Commonly referred to as a *field* number type.

ble. The exact geometric-computation paradigm [Yap04] designed for implementing computational geometry algorithms particularly prevails in CGAL. While in general the underlying arithmetic is highly time consuming compared to machine floating-point arithmetic, major efficiency is gained by computing predicates only to sufficient precision to evaluate them correctly; see Section 1.3.2 and e.g., [PF06].

Various methods to compute the Minkowski sum of two polyhedra in $\mathbb{R}^3$ have been proposed. The goal is typically to compute the boundary of the sum provided in some representation. The combinatorial complexity of the Minkowski sum of two polyhedra of $m$ and $n$ features respectively can be as high as $\Theta(m^3n^3)$. One common approach to compute it is to decompose each polyhedron into convex pieces, compute pairwise Minkowski sums of pieces of the two, and finally the union of the pairwise sums. Computing the exact Minkowski sum of non-convex polyhedra is naturally expensive. Therefore, researchers have focused on computing an approximation that satisfies some criteria, such as the algorithm presented by Varadhan and Manocha [VM06]. They guarantee a two-sides Hausdorff distance bound on the approximation, and ensure that it has the same number of connected components as the exact Minkowski sum. Computing the Minkowski sum of two convex polyhedra remains a key operation, and this is what we focus on. The combinatorial complexity of the sum can be as high as $\Theta(mn)$ when both polyhedra are convex. For the complexity of the intermediate case, where only one polyhedron is convex, cf. [AS97, Sha04].

Convex decomposition is not always possible, as in the presence of non-convex curved objects. In these cases other techniques must be applied, such as approximations using polynomial/rational curves in 2D [kLsKE98]. Seong at al. [SKS02] proposed an algorithm to compute Minkowski sums of a subclass of objects; that is, surfaces generated by slope-monotone closed curves. Flato and Halperin [AFH02] presented algorithms based on CGAL for robust construction of planar Minkowski sums. While the citations in this paragraph refer to computations of Minkowski sums of non-convex polyhedra, and we concentrate on the convex cases, the latter is of particular interest, as our method makes heavy use of the same software components, in particular the CGAL arrangement package, which went through a few phases of improvements [FWH04, WFZH07b, BFH+07, BFH+09b] since its usage in [AFH02]; see Section 1.3.3 for more details.

A particular accomplishment of the *kinetic framework* in two dimensions introduced by Guibas *et al.* [GRS83] was the definition of the *convolution* operation in two dimensions, a superset of the Minkowski sum operation, and its exploitation in a variety of algorithmic problems. Basch *et al.* extended its predecessor concepts and presented an algorithm to compute the convolution in three dimensions [BGRR96]. An output-sensitive algorithm for computing Minkowski sums of polytopes was introduced in [GS87]. Gritzmann and Sturmfels [GS93] obtained a polynomial time algorithm in the input and output sizes for computing Minkowski sums of $k$ polytopes in $\mathbb{R}^d$ for a fixed dimension $d$, and Fukuda [Fuk04] provided an output-sensitive polynomial algorithm for variable $d$ and $k$. Ghosh [Gho93] presented a unified algorithm for computing 2D and 3D Minkowski sums of both convex and non-convex polyhedra based on a *slope diagram* representation. Computing the Minkowski sum amounts to computing the slope diagrams of the two objects, *merging them* (see details in Section 3.2.2,) and extracting the boundary of the Minkowski sum from the merged diagram. Wu *et al.* [WSD03] introduced an improved version of Ghosh' algorithm for convex

polyhedra using vector operations. Bekker and Roerdink [BR01] provided a variation on the same idea. The slope diagram of a 3D convex polyhedron can be represented as a 2D object, essentially reducing the problem to a lower dimension. We follow the same approach, but use exact computation.

We postpone a formal definition of arrangements to the next chapter. In fact, we temporary put Minkowski sums and arrangements aside to provide relevant programming background material.

## 1.3 Background: Programming

### 1.3.1 Generic Programming

Several definitions of the term *generic programming* have been proposed since it was first coined around the early sixties, along with the introduction of the Lisp programming language. Here we confine ourself to the classic notion first described by Musser *et al.* [MS88], who considered generic programming as a discipline that consists of the gradual lifting of concrete algorithms abstracting over details, while retaining the algorithm semantics and efficiency. Within this context, several approaches have been put into trial through the introduction of new features in existing computer languages, or even new computer languages all together. The software described in this thesis is written in C++, a programming language that is well equipped for writing software according to the generic-programming paradigm through the extensive use of class templates and function templates.

#### Concepts and Models

One crucial abstraction supported by all contemporary computer languages is the subroutine (also known as procedure or function, depending on the programming language). Another abstraction supported by C++ is that of abstract data typing, where a new data type is defined together with its basic operations. C++ also supports object-oriented programming, which emphasizes packaging data and functionality together into units within a running program, and is manifested in hierarchies of polymorphic data-types related by inheritance. It allows referring to a value and manipulating it without needing to specify its exact type. As a consequence, one can write a single function that operates on a number of types within an inheritance hierarchy. Generic programming identifies a more powerful abstraction (perhaps less tangible than other abstractions). It is a formal hierarchy of polymorphic abstract requirements on data types referred to as *concepts*, and a set of classes that conform precisely to the specified requirements, referred to as *models*. Models that describe behaviors are referred to as *traits* classes [Mye98]. Traits classes typically add a level of indirection in template instantiation to avoid accreting parameters to templates.

A generic algorithm has two parts: The actual instructions that describe the steps of the algorithm, and a set of requirements that specify which properties its argument types must satisfy. The following `swap()` function is an example of the first part of a generic algorithm.

```
template <typename T> void swap(T & a, T & b) {
  T tmp = a; a = b; b = tmp;
}
```

When the function call is compiled, it is instantiated with a data type that must have an assignment operator. A data type that fulfils this requirement is a model of a concept commonly called *Assignable* [Aus99]. The `int` data type, for example, is a model of this concept, so it can be used to instantiate the function template [Aus99] [25].

A concept is a set of requirements divided into four categories, namely, associated types, valid expressions, invariants, and complexity guarantees. When a type meets all requirements of a concept, the type is considered a *model* of the concept. When a concept extends the requirements of another concept, the former is said to be a *refinement* of the latter.

**Associated Types** are auxiliary types. For example, a type that represents a two-dimensional point, namely `Point_2`, is required by the arrangement geometry traits concept; see Section 2.5.

**Valid Expressions** are C++ expressions that must compile successfully. For example, `p = q`, where `p` and `q` are both objects of type `Point_2`. Valid expressions identify the set of operations a model of the concept must be able to perform.

**Invariants** are run-time characteristics such as time and space complexity bounds. In our context invariants typically take the form of preconditions and postconditions, which must always be satisfied. For example, a condition that requires that an input point $p$ lies on an input curve $c$ on invocation to a predicate that accepts both $p$ and $c$ as parameters. Having preconditions typically minimizes the concept, as the operations provided by a model must operate only on restricted arguments. Formally, removing preconditions from, and introducing postconditions to, a requirement set results with a refined concept.

**Complexity Guarantees** are maximum limits on the computing resources consumed by the various expressions.

### Traits Classes

The name "traits class" comes from a standard C++ design pattern [Mye98], which provides a way of associating information with a compile-time entity (typically a type). For example, the standard class-template `std::iterator_traits<T>` looks roughly like this:

```
template <typename Iterator> struct iterator_traits {
  typedef ... iterator_category;
  typedef ... value_type;
  typedef ... difference_type;
  typedef ... pointer;
  typedef ... reference;
};
```

Iterators play an important role in generic programming: A function that operates on a range of objects usually accepts two iterators that specify this range. The traits' `value_type`

specifies the type of object the iterators are pointing at, while the `iterator_category` can be used to select more efficient algorithms depending on the iterator's capabilities.

A key property of trait classes is that they are non-intrusive. Namely, they allow us to associate information with arbitrary types, without interfering with the internal representation of those types. Thus, it is possible to define a traits class also for built-in types and types defined in third-party libraries.

Within the context of CGAL, for example, a typical traits class is required to define nested types of geometric objects and support predicates involving objects of these types. Some algorithms also require the provision of constructions by the traits class.

Let us continue with an easy geometric example. Consider a function that accepts a set of points, given by the range `[pts_begin, pts_end)`,[2] and computes the minimal axis-parallel rectangle that contains all points in the range. It does so by locating the points with extremal $x$ and $y$-coordinates, and then constructs the bounding iso-rectangle accordingly:

```
template <typename InputIterator, typename Traits>
typename Traits::Iso_rectangle_2
bounding_rectangle(InputIterator pts_begin, InputIterator pts_end) {
  Traits traits;
  InputIterator curr = pts_begin;
  InputIterator left, right, top, bottom;
  left = right = top = bottom = curr++;
  while (curr++ != pts_end) {
      if (traits.compare_x(*curr, *left) == SMALLER) left = curr;
      else if (traits.compare_x(*curr, *right) == LARGER) right = curr;
      if (traits.compare_y(*curr, *bottom) == SMALLER) bottom = curr;
      else if (traits.compare_y(*curr, *top) == LARGER) top = curr;
  }
  return traits.construct_iso_rectangle(*left, *right, *bottom, *top);
}
```

The requirements that an instantiated traits class must satisfy in this case are as follows: It has to defined the nested type `Iso_rectangle_2` (and implicitly also a point type say `Point_2`). Moreover, it should supply two three-valued predicates[3] that compare two points by their $x$-coordinates and by their $y$-coordinates, respectively. It should also support the construction of an axis-parallel iso-rectangle from four points that specify its extremal $x$ and $y$-coordinates. Note, however, that the actual representation of points and rectangles (the coordinate system, the number-type used to represent the coordinates, etc.) and the implementation of the traits-class operations is entirely decoupled from the function `bounding_rectangle()` we have introduced.

Consider an imaginary generic implementation of a data structure that handles geometric arrangements embedded on two-dimensional parametric surfaces in space called `Arrangement_on_surface_2`. Its prototype is listed below. This template class must be

[2] This notation means that `pts_begin` points to the first point in the range, while `pts_end` points after the range ends (it is therefore called a *past-the-end iterator*, and need not point to any valid point object).

[3] The predicate return value is `SMALLER`, `EQUAL`, or `LARGER`.

instantiated with a traits class that in turn defines a type that represents a certain family of curves, and some functions (or function objects; see [10] for an exact definition) that operate on curves of this family.

```
template <typename Traits> class Arrangement_on_surface_2 { ... };
```

Traits classes that handle families of curves embedded on parametric surfaces are intricate, as they model involved concepts. The precise definitions of these concepts and their refinement hierarchy are described in Section 2.5.

One important objective is to minimize the set of requirements the traits concept imposes. A tight traits concept may save tremendously in analysis and programming of classes that model the concept. Another important reason for striving for the minimal set of requirements is to avoid computing the same algebraic entity in different ways. The importance of this is amplified in the context of computational geometry, as a non tight model that consists of duplicate, but slightly different, implementations of the same algebraic entity, can lead to artificial degenerate conditions, which in turn can drastically impair the performance.

Most traits classes in CGAL are parameterized by a model of the *Kernel* concept. The choice of a particular model determines, among the other, the type of arithmetic used, as explained in the following sections. One can easily switch between different models of the *Kernel* concept, but here lies a trap, as Section 1.3.2 reveals. A kernel model that supports exact arithmetic must be used to ensure robustness, although inexact arithmetic could be used at a certain risk.

### Libraries

Alexander Stepanov began exploring the potential of compile-time polymorphism for revolutionizing software development in 1979. With the help of several other researchers his work evolved into a prime generic-programming library — the Standard Template Library (STL). This library had became part of the C++ standard library in 1994, approximately one year before early development of CGAL started; see Section 1.3.3 for details about the evolution of CGAL.

Through the years a few other generic-programming libraries emerged. One notable library in the context of computational geometry is LEDA (Library of Efficient Data Types and Algorithms), a library of combinatorial and geometric data types and algorithms [MN00] [17]. Early development of LEDA started in 1988, ten years before the first public release of CGAL became available. In some sense LEDA is a predecessor of CGAL, although the two libraries are headed in different directions. While LEDA is mostly a large collection of fundamental graph related and general purpose data-structures and algorithms, CGAL is a collection of large and complex data-structures and algorithms focusing on geometry.

A noticeable influence on generic programming is conducted by the BOOST online community, which encourages the development of free C++ software gathered in the BOOST library collection [3]. It is a large set of portable and high quality C++ libraries that work well with, and are in the same spirit as, the C++ Standard Template Library. The BOOST Graph Library (BGL) [SLL02], which consists of generic graph-algorithms, serves a particularly important role in our context. An arrangement instance, for example, can be adapted as a

BGL graph, and passed as input to generic algorithms already implemented in the BGL, such as the Dijkstra shortest path algorithm. We use the BGL to compute the strongly connected components of a directed graph — a phase in the assembly partitioning operation; see Section 5.3.8 for more details about the application of this operation.

### 1.3.2 Geometric Programming

Implementing geometric algorithms and data structures is notoriously difficult, much harder than may seem when just considering the algorithm as described in a paper or a book. In the traditional computational-geometry literature two assumptions are usually made to simplify the design and analysis of geometric algorithms. First, inputs are in "general position". That is, degenerate input (e.g., three curves intersecting at a common point) is precluded. Secondly, operations on real numbers yield accurate results (the "real RAM" model [PS85], which also assumes that each basic operation takes constant time). Unfortunately, these assumptions do not hold in practice, as degenerate input is commonplace in practical applications and numerical errors are inevitable. Thus, an algorithm implemented without keeping this in mind may yield incorrect results, get into an infinite loop, or just crash, while running on a degenerate, or nearly degenerate, input (see [KMP+08, Sch00] for examples). These pitfalls have become well known, and have been the subject of intensive research [Sch00, Yap04].

Indeed, the last decade has seen significant progress in the development of software for computational geometry. The mission of such a task, which Kettner and Näher [KN04] call *geometric programming*, is to develop software that is correct, efficient, flexible (namely adaptable and extensible[4]), and easy to use.

#### Separation of Topology and Geometry

The use of the generic-programming paradigm enables a convenient separation between the topology and the geometry of data structures.[5] This is a key aspect in the design of geometric software, and is put into practice, for example, in the design of CGAL polyhedra, CGAL triangulations, and our CGAL arrangements. This separation allows the convenient abstraction of algorithms and data structures in combinatorial and topological terms, regardless of the specific geometry of the objects at hand and the algebra used to represent them. This abstraction is realized through class and function templates that represent specific data-structures and algorithmic frameworks, respectively. Consider again our imaginary `Arrangement_on_surface_2` class template from the previous section; its improved prototype is listed below. It is instantiated with two classes. The first, referred to as a *geometric traits* class, defines the set of geometric-object types and the operations on objects of these types. The second, defines the topological-object types and the operations required to maintain the

[4] *Adaptability* refers to the ability to incorporate existing user code, and *extendibility* refers to the ability to enhance the software with more code in the same style.

[5] In this context, we sometimes say *combinatorics* instead of topology, and say *algebra* or *numerics* instead of geometry. We always mean the same thing: The separation between the abstract, graph-like structure (the topology) from the actual embedding on the surface (the geometry).

incident relations among objects of these types.

```
template <typename Geometry_traits, typename Topology_traits>
class Arrangement_on_surface_2 { ... };
```

An immediate advantage of the separation between the topology and the geometry of data structures is that users with limited expertise in computational geometry can employ the data structure with their own special type of objects. They must however supply the relevant traits class, which mainly involve algebraic computations. A traits class also encapsulates the number types used to represent coordinates of geometric objects and to carry out algebraic operations on them. It encapsulates the type of coordinate system used (e.g., Cartesian, Homogeneous), and the geometric or algebraic computation methods themselves. Naturally, a prospective user of the package that develops a traits class would like to face as few requirements as possible in terms of traits development.

Another advantage gained by the use of generic programming is the convenient handling of numerical issues to expedite exact geometric computation. We arrive at this conclusion at the end of the next section. In a geometric algorithm each computational step is either a construction step or a conditional step based on the result of a predicate. The former produces a new geometric object such as the intersection point of two segments. The latter typically computes the sign of an expression used by the program control. Different computational paths lead to results with different combinatorial characteristics. Although numerical errors can sometimes be tolerated and interpreted as small perturbations in the input, they may lead to invalid combinatorial structures or inconsistent state during a program execution. Thus, it suffices to ensure that all predicates are evaluated correctly to eliminate inconsistencies and guarantee combinatorially correct results. This is easier said than done, but nowadays possible, as the next section exposes.

### Exact Geometric Computation

The need for robust software implementations of computational-geometry algorithms has driven many researchers over the last decade to develop variants of the classic algorithms that are less susceptible to degenerate inputs. The approaches taken to overcome the difficulties in robustly implementing geometric algorithms can be roughly divided into two categories: (i) Exact computing, and (ii) fixed-precision approximation. In the latter approach the algorithms are modified so that they can consistently cope with the limited precision of computer arithmetic. In the former, which is the approach taken by CGAL in general and the arrangement package in particular, ideal computer arithmetic is emulated for the specific type of objects being manipulated, and the code is prepared for successfully handling degenerate input.

Advances in computer algebra enabled the development of efficient software libraries that offer exact arithmetic manipulations on unbounded integers, rational numbers (GMP — Gnu's multi-precision library [12]), and algebraic numbers (the CORE library [KLPY99] [6] and the numerical facilities of LEDA [MN00, Chapter 4] [17]). These exact-number types serve as fundamental building-blocks in the robust implementation of many geometric applications in general (see [Yap04] for a review) and of those that employ arrangements in particular.

Exact Geometric Computation (EGC), as summarized by Yap [Yap04], simply amounts to ensuring that we never err in predicate evaluations. EGC represents a significant relaxation from the naive concept of numerical exactness. We only need to compute to sufficient precision to make the correct predicate evaluation. This has led to the development of several techniques such as precision-driven computation, lazy evaluation, adaptive computation, and floating-point filters, some of which are implemented in CGAL, such as numerical filtering. Here, computation is carried out using a number type that supports only inexact arithmetic (e.g., double-precision floating-point arithmetic), while applying a filter that checks whether the computation has reached a stage of uncertainty, an event referred to as a *filter failure* in the hacker's jargon. When a filter failure occurs, the computation is re-done using exact arithmetic.

Switching between number types and exact computation techniques, and choosing the appropriate components that best suit the application needs, is conveniently enabled through the generic-programming paradigm, as it typically requires only a minor code change reflected in the instantiating of just a few data types.

### 1.3.3 Computational Geometry Algorithms Library

#### CGAL Chronicles

Several research groups in Europe started to develop small geometry libraries on their own in the early 1990s. A consortium of several sites in Europe and Israel was founded in 1995 to cultivate the labor of these groups and gather their produce in a common library called CGAL — the Computational Geometry Algorithms Library. The goal was to promote the research in computational geometry and translate the results into useful, reliable, and efficient programs for industrial and academic applications [Ove96, cga07, KN04, FGK+00], the very same goal that governs CGAL development efforts to date.

An INRIA startup, GEOMETRY FACTORY [11] was founded in January 2003. The company sells CGAL commercial licenses, support for CGAL, and customized developments based on CGAL.

In November 2003, when Version 3.0 was released, CGAL became an Open Source Project [5], allowing new contributions from various resources. Most parts of CGAL are now distributed under the GNU Lesser General Public License (GNU LGPL).

CGAL has evolved through the years and is now representing the state-of-art in implementing computational geometry software in many areas. The implementations of the CGAL software modules described in this thesis are complete and robust, as they handle all degenerate cases. They rigorously adhere to the generic-programming paradigm to overcome problems encountered when effective computational geometry software is implemented. A glimpse at the structure of CGAL is given in the following subsection.

#### CGAL Content

CGAL is written in C++ according to the generic-programming paradigm described above. It has a common programming style, which is very similar to that of the STL. Its ap-

plication programming-interface (API) is homogeneous, and allows for a convenient and consistent interfacing with other software packages and applications. The library consists of about 900,000 lines of code divided among approximately 4,000 files. CGAL also comes with numerous examples and demos. The manual comprises about 3,500 pages. There are approximately 65 chapters arranged in 14 parts. The `Arrangement_on_surface_2` package, for example, consists of about 140,000 lines of code divided among approximately 300 files, described in about 300 pages of a didactic manual.

One distinguished piece consists of the geometric kernels [FGK+00]. A geometric kernel consist of types of constant size non-modifiable geometric primitive objects (e.g., points, lines, triangles, circles, etc.) and operations on objects of these types.

Another distinguished piece, referred to as the "Support Library" consists of non-geometric facilities, such as circulators, random generators, and I/O support for interfacing CGAL with various visualization tools (i.e., input and output streams). An important contribution of this piece is the number-type support. This piece also contains extensive debugging utilities that handle warnings and errors that may result from unfulfilled conditions.

The rest of the library offers a collection of geometric data structures and algorithms such as convex hull, polygons and polyhedra and operations on them (Boolean operations, polygon offsetting), 2D and 3D triangulations, Voronoi diagrams, surface meshing and surface subdivision, search structures, geometric optimization, interpolation, and kinetic data-structures. The 2D arrangements and its related data-structures naturally fit in. These data structures and algorithms are parameterized by traits classes that define the interface between them and the primitives they use. In many cases, a kernel can be used as a traits class, or at least the subtypes of a kernel can be used as components of traits classes for these data structures and algorithms.

### CGAL Arrangement Package History

CGAL contains an elaborate and efficient implementation of a generic data-structure that represents an arrangement induced by general types of curves embedded on a two-dimensional parametric surface in $\mathbb{R}^3$, but it has not been like this from the beginning. The first version of the CGAL arrangement package supported only line segments, circular arcs, and restricted types of parabolas embedded in the plane.

While the first version supported only limited types of curves, it was originally designed with the vision of supporting general curves [FHH+00, Han00, HH00]. This vision was reflected, among the other, through the separation between the topological and the geometric aspects enabled by the generic-programming paradigm (see Section 1.3.2). Most of the principles related to the topology, e.g., the use of a *doubly-connected edge list* (DCEL) to maintain the incident relations between the arrangement cells (i.e., vertices, halfedges, and faces) were conceived from the start. However, the types of curves that induce arrangements (see Section 2.5) gradually expanded. A couple of years after the introduction of CGAL arrangement Wein extended its implementation to support arcs of conics [Wei02]. The arsenal of geometric traits continues to grow to date.

Following the requirements that emerged from the ECG project[6], together with Wein we improved and refined the software design of the CGAL arrangement package [FWH04]. This new design formed a common platform for a preliminary comparison between different approaches to handle arcs of conics [FHW+04]. Two years later in a joint effort with Wein and Zukerman the whole package was revamped [WFZH05] leading to more compact, easier-to-use, and efficient code.

CGAL Version 3.2 released in 2006 included an arrangement package that supported only bounded curves in the plane. This forced users to clip unbounded curves before inserting them into the arrangement; it was the user responsibility to clip without loss of information. However, this solution is generally inconvenient and outright insufficient for some applications. For example, representing the minimization diagram defined by the lower envelope of unbounded surfaces in $\mathbb{R}^3$ [Mey06] generally requires more than one unbounded face, whereas an arrangement of bounded clipped curves contains a single unbounded face.

CGAL Version 3.3 released a year later in 2007 already included an arrangement package that handled unbounded planer curves. As a matter of fact it included much more. Together with Berberich, Melhorn, and Wein we observed the possibility to maximize code reuse by generalizing the various algorithms applied to arrangements and their implementations so that they could be employed on a large class of surfaces and curves embedded on them [BFH+07, BFH+09b]. Indeed, the algorithms and their implementations were designed with the vision of supporting general curves embedded on parametric surfaces. However, only a few geometric traits-classes that supported unbounded curves in the plane were included in Version 3.3.

A future version of CGAL, expected to be released in 2010, is planned to include an arrangement package that constructs, maintains, and operates on arrangements embedded on certain two-dimensional orientable parametric surfaces. The package already exists as a prototypical CGAL package under the new name `Arrangement_on_surface_2` to better reflect its capabilities. For example, it includes (i) a geometric traits that handles geodesic arcs embedded on the sphere [FSH08b, BFH+09a], (ii) a geometric traits that handles intersections between quadric surfaces embedded on a quadric [BFH+07, BFH+09a], and (iii) a geometric traits that handles intersections between arbitrary algebraic surfaces and a parameterized Dupin cyclide embedded on the Dupin cyclide [BK08, BFH+09a]. The references to the arrangement software in this thesis in general and in Chapter 2 in particular pertain to this latest version.

The leap in arrangement technology expressed by the ability to construct and maintain arrangements embedded on two-dimensional parametric surfaces immediately affects other components in CGAL, such as the `Boolean_set_operations_2` package. Only little effort is now required to support Boolean set-operations on point sets bounded by general curves embedded on two-dimensional parametric surfaces.

[6]ECG is a Shared-Cost RTD (FET Open) Project of the European Union devoted to Effective Computational Geometry for curves and surfaces [7].

## 1.4 Thesis Outline and Related Publications

The rest of this thesis is organized as follows. In Chapter 2 we give an overview of the CGAL arrangement package, which provides the common infrastructure for all software solutions described in this thesis. This chapter contains selected sections from several papers and from a book chapter we have co-authored, and it provides new material that has not been published yet. In particular, the chapter contains a description of the architecture of the arrangement generic data-structure, part of which also appeared in the chapter *Arrangement* of the book *Effective Computational Geometry for Curves and Surfaces* [FHK+07]. The chapter contains a description of advanced programming techniques applied in the context of arrangement, parts of which appeared in a joint work with R. Wein and B. Zukerman, and published in the journal *Computational Geometry — Theory and Application* (special issue on CGAL) [WFZH07b]. Preliminary results were first introduced in (i) the proceedings of the $12^{th}$ *Annual European Symposium on Algorithms (ESA)* [FWH04] and (ii) the $1^{st}$ *Workshop of Library-Centric Software Design* [WFZH05]. The chapter also presents arrangements induced by general curves and embedded on parametric surfaces, and it offers a detailed description of a particular type of arrangement, namely arrangements of geodesic arcs on the sphere. The presentation of general arrangements embedded on parametric surfaces is based on a joint work with E. Berberich, K. Melhorn, and R. Wein. Preliminary results of this work were first published at the $23^{rd}$ *European Workshop on Computational Geometry (EWCG)* [BFHW07]. Improved results appeared in the proceeding of the $15^{th}$ *Annual European Symposium on Algorithms (ESA)* [BFH+07], and mature results were presented in a manuscript [BFH+09b]. The discussion about particular arrangements embedded on spheres is based on joint work with O. Setter. Preliminary results of this work were first published at the $24^{th}$ *European Workshop on Computational Geometry (EWCG)* [FSH08a]. A movie rendering the results of this work was presented at the $24^{th}$ *Annual Symposium on Computational Geometry (SoCG)*. The proceeding of this symposium contains the related extended abstract [FSH08b]. Mature results were presented in a manuscript [BFH+09a].

In Chapter 3 we present two different complete, yet efficient, implementations of output-sensitive algorithms to compute the Minkowski sum of two polytopes in $\mathbb{R}^3$. We describe how the input polytopes in polyhedral-mesh representation both methods accept are converted into the corresponding internal representations unique to each method. We provide the theoretical concepts both methods rely on, and detailed descriptions specific to each method. The first method was also published in the journal *Computer Aided Design* [FH07]. A preliminary version of this paper appeared in the proceedings of the $8^{th}$ *Workshop on Algorithm Engineering and Experimentation (Alenex'06)* [FH06]. The second method appeared in the publications [FSH08a, FSH08b, BFH+09a] mentioned above. We compare our Minkowski-sum constructions with other methods that produce exact results, and provide a summary of a performance analysis of our methods.

Chapter 4 provides a tight bound on the exact maximum complexity of Minkowski sums of $k$ polytopes in $\mathbb{R}^3$ in terms of the number of facets of the polytope summands. It is based on collaborative work with C. Weibel. The results of this work were introduced in the proceedings of the $23^{rd}$ *annual Symposium on Computational Geometry (SoCG)* [FHW07], and were accepted for publication in the journal *Discrete and Computational Geometry* [FHW].

We use this opportunity to thank Shakhar Smorodinsky for fruitful discussions conducted while we were investigating the bound above. The chapter provides a proof of the upper bound, and establishes the lower bound through a construction procedure.

Chapter 5 introduces an exact implementation of an efficient algorithm to obtain a partitioning motion given an assembly of polyhedra in $\mathbb{R}^3$ — a solution to a problem in the domain of assembly planning. This application uses several types of operations on arrangements of geodesic arcs embedded on the sphere as basic blocks. In this context the chapter introduces exact implementations of additional applications that exploit geodesic arcs embedded on the sphere, such as polyhedra central-projection and Boolean set-operations applied to point sets embedded on the sphere bounded by geodesic arcs. Great parts of this chapter are extracts from a paper recently published in the $8^{th}$ *International Workshop on Algorithmic Foundations of Robotics (WAFR)* [FH08]. Specific background of assembly planning is provided at the beginning of the chapter.

We refer the reader to some ongoing research and future prospects and conclude in Chapter 6.

The software access-information along with some further design details are provided in the Appendix.

*A common mistake that people make when trying to design something completely foolproof is to underestimate the ingenuity of complete fools.*

Douglas Adams

# 2 Arrangements on Surfaces

Given a finite collection $\mathcal{C}$ of geometric objects (such as lines, planes, or spheres) the *arrangement* $\mathcal{A}(\mathcal{C})$ is the subdivision of the space where these objects reside into cells as induced by the objects in $\mathcal{C}$. In this thesis we deal only with arrangements embedded on certain two-dimensional orientable parametric surfaces in $\mathbb{R}^3$, i.e., planes, cylinders, spheres, tori, and surfaces homeomorphic to them. In this case the objects in $\mathcal{C}$ embedded on the surface $S$ are curves that divide $S$ into a finite number of cells of dimension 0 (*vertices*), 1 (*edges*) and 2 (*faces*). Figure 2.1 shows various types of arrangements embedded on two-dimensional parametric surfaces.

The `Arrangement_on_surface_2`[1] package of CGAL [WFZH07a] is a generic implemen-

[1] As a convention, CGAL prescribes the suffix _2 for all data structures of planar objects and the suffix _3 for all data structures of 3D objects. In the case of arrangements on surfaces the suffix _2 indicates the dimension of the parameter space of the embedding surface.

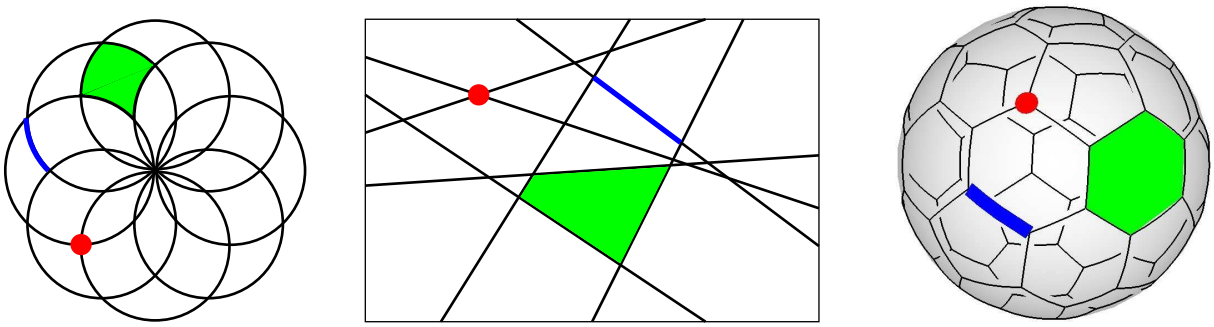

(a) (b) (c)

Figure 2.1: (a) An arrangement of circles in the plane, (b) an arrangement of lines in the plane, and (c) an arrangement of geodesic arcs on the sphere.

tation of a complete software package that constructs and maintains arrangements embedded on two-dimensional parametric surfaces [FHK+07, FWH04, WFZH07b, BFH+07, BFH+09b] (see Section 1.3.3 for the history of the package). As arrangements are ubiquitous in computational geometry and have many theoretical and practical applications( see, e.g., [dBvKOS00, AS00, Hal04]), many potential users in academia and in industry can benefit from the `Arrangement_on_surface_2` package.

As mentioned in Section 1.3.2 CGAL in general and the `Arrangement_on_surface_2` package of CGAL in particular follow the Exact Geometric Computation paradigm. The developed code covers all cases to successfully handle degenerate input, while ideal computer arithmetic is emulated. While the CGAL package supports arrangements induced by general algebraic curves of arbitrary degree, the constructions and uses of arrangements described in this thesis require only rational arithmetic. This is a key property that enables efficient implementations of all the algorithms presented in the thesis.

CGAL arrangements and their related components are the results of ongoing collaborative research we were, and still are, deeply involved with; see Section 1.3.3 for the evolution of the arrangement package. We, in particular, had a significant impact on specific topics within this research area as follows: We came up with great parts of the geometry-traits concept hierarchy, and the corresponding sets of minimal requirements (see Section 2.5); we contributed the geometry-traits module for polylines (see Section 2.5.4) and the geometry and topology traits modules for geodesic arcs embedded on the sphere (see Section 2.6); we led the design of the Boolean set-operation architecture (See Section 2.7.1), and we provided solutions to numerous issues encountered during the development of all these components. This chapter provides a comprehensive overview of these components, with a slight emphasis on asspects related to our work. It explains how arrangements induced by any type of curves can be constructed, maintained, and used by other applications.

## 2.1 Related Work

Both closely related MAPC [KCMK00] [19] and ESOLID [CKF+04] [8] libraries consist of an arrangement-construction module for algebraic curves. However, these implementations make some general-position assumptions on the input curves. The LEDA library [MN00] includes geometric facilities that allow the robust construction and maintenance of planar maps of line segments that may contain degeneracies. However, the resulting planar maps are represented as simple graphs that cannot fully describe the topological structure of the arrangement. For example, it is impossible to encode the containment relation between disconnected components of the graph (i.e., to keep track of the holes contained in a face; see Section 2.3.2). LEDA-based implementation of arrangements of conic curves and of cubic curves were developed under the EXACUS project [BEH+05] [9].

CGAL's arrangement package was the first complete software implementation, designed for constructing arrangements of arbitrary planar curves and supporting operations and queries on such arrangements. The package was employed by many users to develop a variety of applications in various domains. For example, it was used to solve geometric optimization problems [Rog03, COLYKT03], to construct Minkowski sums efficiently [AFH02,

FH07, FSH08b], to design snap-sounding algorithms [HP02], to construct envelopes of surfaces [Mey06]. It was used in motion planning [HH03, WvH07], assembly partitioning [FH08], cartography [DHH01], and several other applications [1, 16]. The package was also used to compute arrangements of quadrics [BHK+05] by considering the planar arrangements of their projected intersection curves. A better approach to compute such arrangements [BFH+07, BFH+09a] was introduced once the package started to support arrangement on parametric surfaces, which also enables the computation of arrangements embedded on Dupin cyclides [BK08]. The torus, for example, is a Dupin cyclide.

Sweeping the plane with a line is one of the most fundamental algorithmic mechanisms in computational geometry. The `Arrangement_on_surface_2` package includes a generic implementation of an elaborate version of this mechanism exploited by several higher-level operations supported by the package.

The famous sweep-line algorithm of Bentley and Ottmann [BO79] was originally formulated for sets of non-vertical line segments, with the "general position" assumption that no three segments intersect at a common point and no two segments overlap. Many generalizations have been introduced ever since, such as the ability to handle more general curves [SH89] and to deal with degeneracies(see [dBvKOS00, Section 2.1] and [MN00, Section 10.7] for a discussion about degeneracies induced by line segments).

Effective algorithms for manipulating arrangements of curves have been a topic of considerable interest in recent years with an emphasis on exactness and efficiency of implementation [FHK+07]. Mehlhorn and Seel [MS03] propose a general framework for extending the sweep-line algorithm to handle unbounded curves; however, their implementation can only handle lines in the plane. Arrangements on spheres are covered by Andrade and Stolfi [AS01], Halperin and Shelton [HS98], and recently Cazals and Loriot [CL06]. Cazals and Loriot have developed a software package that can sweep over a sphere and compute exact arrangements of circles on it.

The LEDA external package (LEP) `SphereGeometry` [18] handles geodesic arcs on the sphere using an implicit representation, which enables the use of exact rational arithmetic to handle objects of this type. The package contains implementations of basic algorithms related to geodesic arcs on a sphere, such as computing the spherical convex hull, the union of two spherical polygons, and the width of a three-dimensional set of points. It does not, however, support arrangements.

## 2.2 Parametric Surfaces

A parametric surface $S$ is defined by a continuous function $f_S : \mathbb{P} \to \mathbb{R}^3$, where the domain $\mathbb{P} = U \times V$ is a rectangular two-dimensional parameter space with bottom, top, left, and right boundaries, and the range $S = f_S(\mathbb{P})$. $U$ and $V$ are open, half-open, or closed intervals with endpoints in $\mathbb{R} \cup \{-\infty, +\infty\}$.We use $u_{\min}$, $u_{\max}$, $v_{\min}$, and $v_{\max}$ to denote the endpoints of $U$ and $V$, respectively. For example, the standard parameterization of the plane is $f_S(u, v) = (u, v, 0)$, where $U = V = (-\infty, +\infty)$, and the unit sphere is commonly parameterized as $f_S(u, v) = (\cos u \cos v, \sin u \cos v, \sin v)$, where $\mathbb{P} = [-\pi, \pi] \times [-\frac{\pi}{2}, \frac{\pi}{2}]$.

A *contraction point* $p \in S$ is a singular point, which is the mapping of a whole boundary of

the domain $\mathbb{P}$. For example, if the top boundary is contracted, we have $\forall u \in U, f_S(u, v_{\max}) = p'$ for some fixed point $p' \in \mathbb{R}^3$. An *identification curve* $C \subset S$ is a continuous curve, which is the mapping of opposite closed boundaries of the domain $\mathbb{P}$. If the left and right boundaries are identified, we have $\forall v \in V, f_S(u_{\min}, v) = f_S(u_{\max}, v)$, (and similarly for the bottom and top boundaries). For example, consider the sphere as parameterized above. Its contraction points are $(0, 0, \pm 1)$, as $f_S(u, -\frac{\pi}{2}) = (0, 0, -1)$ and $f_S(u, \frac{\pi}{2}) = (0, 0, 1)$ for all $u$. Its identification curve is $\{f_S(\pi, v) \mid -\frac{\pi}{2} \leq v \leq \frac{\pi}{2}\}$, as $f_S(-\pi, v) = f_S(+\pi, v)$ for all $v$.

A *parameterizable curve* $\gamma$ is a continuous function $\gamma : I \to \mathbb{P}$ where $I$ is an open, half-open, or closed interval with endpoints 0 and 1, and $\gamma$ is injective, except for at a finite number of points. If $0 \notin I$, $\lim_{t \to 0+} \gamma(t)$ exists (in the closure of $\mathbb{P}$) and lies in an open side of the boundary. Similarly, if $1 \notin I$, $\lim_{t \to 1-} \gamma(t)$ exists and lies in an open side of the boundary. A curve $C$ in $S$ is the image of a curve $\gamma$ in the domain.

A curve is *closed in the domain* if $\gamma(0) = \gamma(1)$; in particular, $0 \in I$ and $1 \in I$. A curve is *closed in the surface S (or simply closed)* if $f_S(\gamma(0)) = f_S(\gamma(1))$. A curve $\gamma$ has two *ends*, the 0-end $\langle \gamma, 0 \rangle$ and the 1-end $\langle \gamma, 1 \rangle$. If $d \in I$, the $d$-end has a geometric interpretation. It is a point in $\mathbb{P}$. If $d \notin I$, the $d$-end has no geometric interpretation. You may think of it as a point on an open side of the domain or an initial or terminal segment of $\gamma$. If $d \notin I$, we say that the $d$-end of the curve is open. Consider for example the equator curve on the sphere as parameterized above. This curve is given by $\gamma(t) = (\pi(2t-1), 0)$, for $t \in [0, 1]$. The 0-end of $\gamma$ is the point $(-\pi, 0)$ in $\mathbb{P}$ and a point on the equator of the sphere. It is closed on the sphere, but non-closed in $\mathbb{P}$.

A *u-monotone curve* is the image of a curve $\gamma$, such that if $t_1 < t_2$, then $u(\gamma(t_1)) < u(\gamma(t_2))$ for $t_1 < t_2$. A *vertical curve* is the image of a curve $\gamma$, such that $u(\gamma(t)) = c$ for all $t \in I$ and some $c \in U$ and $v(\gamma(t_1)) < v(\gamma(t_2))$ for $t_1 < t_2$. For instance, every Meridian curve of a sphere parameterized as above is vertical. A *weakly u-monotone curve* is either vertical or $u$-monotone.[2]

The `Arrangement_on_surface_2` package handles inducing curves that are decomposable into parameterizable weakly $u$-monotone curves as defined above. Any two weakly $u$-monotone curves must intersect only a finite number of times or overlap only in a finite number of sections, if at all. The curves must be embedded on parameterizable surfaces as defined above. A curve can be unbounded or reach the boundaries of the embedding surface. A boundary may define a contraction point or an identification curve.[3] We allow non-injectivity on the boundary, denoted $\partial\mathbb{P}$, and require bijectivity only in $\mathbb{P} \setminus \partial\mathbb{P}$ (the interior of $\mathbb{P}$). More precisely, we require that $f_S(u_1, v_1) = f_S(u_2, v_2)$ and $(u_1, v_1) \neq (u_2, v_2)$ imply $(u_1, v_1) \in \partial\mathbb{P}$ and $(u_2, v_2) \in \partial\mathbb{P}$. Informally, we require that all geometric operations defined in Section 2.5 be applicable on our curves.

Code reuse is maximized by generalizing the prevalent algorithms and their implementations originally designed to operate on arrangements embedded in the plane. The generalized code handles features embedded in the modified surface $\widetilde{S} : f_{\widetilde{S}} = f_S(u, v) \mid (u, v) \in \mathbb{P} \setminus \partial\mathbb{P}$ defined over the interior of the parameter space, where identification curves, contraction points, and points at infinity are removed. Specific code that handles unbounded features

[2] $u$-monotone curves refer to weakly $u$-monotone curves hereafter.

[3] We do not support surfaces that contain a contracted identification curve.

or features that reach the boundaries is added to yield a complete implementation.

## 2.3 The Arrangement Package Architecture

The main class of the package, namely `Arrangement_on_surface_2`, constructs and maintains the embedding of a set of continuous weakly $u$-monotone curves that are pairwise disjoint in their interiors on a two-dimensional parametric surface in $\mathbb{R}^3$. It provides the necessary capabilities for maintaining the embedded graph, while associating geometric data with the vertices, edges, and faces of the graph. The embedded graph is represented using a *doubly-connected edge list* (DCEL) [dBvKOS00, Section 2.2], which maintains the incidence relations on its features [WFZH07b]. Each edge of the subdivision is represented by two halfedges with opposite orientation, and each halfedge is associated with the face to its left. It is based on an implementation of a halfedge data-structure (HDS) [Ket07b] also used by the polyhedral-surfaces package [Ket99, Ket07a].

An important guideline in the design is to decouple the arrangement representation from the various algorithms that operate on it. Thus, the `Arrangement_on_surface_2` class provides only a restricted set of methods for locally modifying the arrangement; see Section 2.3.2. Non-trivial algorithms that involve geometric operations are implemented as free (global) functions that use the interface of the arrangement class; see Section 2.4. For example, the package offers free functions for *incremental* or *aggregated* insertion of curves that may not necessarily be $u$-monotone, and the insertion location of which are unknown *a priori*. Each input curve is subdivides into several $u$-monotone subcurves before inserted using one of the member methods listed in Section 2.3.2.

### 2.3.1 The Data Structure

The `Arrangement_on_surface_2<GeometryTraits,TopologyTraits>` class-template must be instantiated with two types as follows:

- A geometry-traits class, which defines the abstract interface between the arrangement data-structure and the geometric primitives it uses. It is tailored to handle a specific family of curves, and it encapsulates implementation details, such as the number type used, the coordinate representation (i.e., Cartesian or homogeneous), the algebraic computation methods, and auxiliary data stored with the geometric objects, if present; see Section 2.5 for more details.

- A topology-traits class, which adapts the underlying DCEL to the embedding modified surface $\widetilde{S}$. It determines whether the embedded surface is bounded, or otherwise whether a boundary defines a contraction point or an identification curve. If the inducing curves are confined to the modified parameter space, the tasks of the topology-traits class are minimal. However, in other cases it maintains the features that escape the modified parameter space $\widetilde{\mathbb{P}}$.

The underlying DCEL in turn associates a point with each vertex and a $u$-monotone curve with each halfedge pair, where the geometric types of the point and the $u$-monotone curve

are defined by the geometry-traits class. Users may extend the default DCEL data-structure, in order to attach additional data to the DCEL records, as explained in Section 2.3.3.

The `Arrangement_on_surface_with_history_2` class-template represents an arrangement of general curves embedded on a two-dimensional parametric surface, and maintains the construction history of the arrangement. Input curves that induce the arrangement are split into $u$-monotone subcurves that are pairwise disjoint in their interior, and these subcurves are the embeddings of the arrangement halfedges. While using the `Arrangement_on_surface_2` class we lose track of the connection between input curves and their final embeddings, in the `Arrangement_on_surface_with_history_2` data-structure each embedded $u$-monotone curve is extended to store a pointer to the input curve associated with it, or a container of curve pointers in case the embedded $u$-monotone curve is an overlapping section of several input curves.

The `Arrangement_on_surface_with_history_2` class is a simple *decorator*[4] for `Arrangement_on_surface_2`. It inherits from an `Arrangement_on_surface_2` class-template instantiated with a geometry-traits class that extends the $u$-monotone curve type. It also stores the set of input curves, and maintains a data structure that enables efficient traversal of all halfedges induced by given input curves. The cross-pointers between input curves and arrangement halfedges are maintained using an *observer* (see Section 2.4.4) that keeps track of each change that involves an arrangement halfedge and updates its underlying curve accordingly.

Users can traverse the original curves of each arrangement halfedge, or iterate over all halfedges induced by a given input curve. Tracing back the curve (or curves) that induced an arrangement edge is essential in a variety of applications that use arrangements, such as robot motion planning; see, e.g., [HH03]. It is possible, for example, to efficiently remove a curve from the arrangement by deleting all edges it induces.

Arrangements embedded in the plane are very common and, at least as far as the arrangement package of CGAL is concerned, have a longer history than their generalization for two-dimensional surfaces in $\mathbb{R}^3$. The `Arrangement_2` class-template represents a planar subdivision. It maintains the embedding of continuous weakly $u$-monotone curves in the $xy$ plane, parameterized the natural way. That is, the two parameters $u$ and $v$ are directly mapped to $x$ and $y$, respectively. Thus, $u$-monotonicity implies $x$-monotonicity and vice versa. The `Arrangement_2` class-template is parameterized with a geometry-traits class and with a DCEL data-structure. It inherits from an `Arrangement_on_surface_2` class-template instantiated with the geometry traits template parameter and with a specific topology-traits class suitable for the plane. The dedicated topology traits is instantiated with the DCEL template parameter. Similarly the `Arrangement_with_history_2` class-template represents a planar subdivision, and maintains the construction history of the arrangement.

The package offers various operations on arrangements stored in these representations, such as point location, insertion of curves, removal of curves, and overlay computation.

[4] A decorator attaches additional responsibilities to an object dynamically [GHJV95].

### 2.3.2 Member Operations

The interface of `Arrangement_on_surface_2` consists of various methods that enable the traversal of arrangement features. The class supplies iterators over its vertices, halfedges, or faces. The classes `Vertex`, `Halfedge`, and `Face`, nested in the `Arrangement_on_surface_2` class, supply in turn methods for local traversals. For example, it is possible to visit all halfedges incident to a specific vertex. Halfedges stored in doubly-connected lists form chains. The chains define the inner and outer connected components of the boundary (CCB) of each face. A bounded face in the `Arrangement_2` data structure has a single outer CCB representing the outer boundary of the face, and may have several inner CCBs representing its holes. However, a face in the general `Arrangement_on_surface_2` data structure may have several inner and outer CCBs; see Section 2.6. Naturally, it is possible to traverse all the halfedges along the inner and outer boundaries of a given face.

Alongside with the traversal methods, the arrangement class also supports several methods that modify the arrangement. The functions `insert_in_face_interior(C,f)` (Figure 2.2 (a)), `insert_from_left_vertex(C,v)` (Figure 2.2 (b)), `insert_from_right_vertex(C,v)`) (Figure 2.2 (c)), and `insert_at_vertices(C,v1,v2)` (Figure 2.2 (d)) create an edge that corresponds to a $u$-monotone curve $C$, whose interior is disjoint from existing edges and vertices. The choice of which one to use depends on whether the curve endpoints are associated with existing non-isolated arrangement vertices: (i) If both curve endpoints do not correspond to any existing vertex, `insert_in_face_interior()` is used to generate a new hole inside an existing face. (ii) If exactly one endpoint corresponds to an existing Dcel vertex, one of the functions `insert_from_left_vertex()` or `insert_from_right_vertex()` is called, depending on which endpoint is associated with an existing vertex. It forms an "antenna" emanating from an existing connected component. (iii) Otherwise, both endpoints correspond to existing vertices, and `insert_at_vertices()` is called to connect these vertices using a pair of twin halfedges. These functions hardly involve any geometric operations, if at all.[5] They accept topologically related parameters, and use them to operate directly on the Dcel records, thus saving algebraic operations, which are especially expensive when high-degree curves are involved.

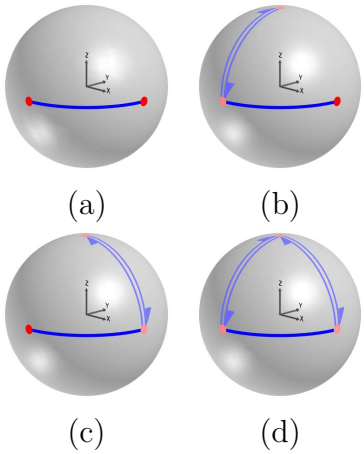


Figure 2.2: The arrangement immediate insertion methods. The newly inserted curve is drawn in bright blue. Vertices created as a result of the insertion are drawn in bright red.

Other modification methods included in the arrangement class enable users to split an edge into two, to merge two edges incident to a common vertex, and to remove an edge from the arrangement. It is also possible to insert a point in the interior of a given face, creating an isolated vertex that corresponds to this point, or to remove an isolated vertex from the arrangement.

[5] Unless we force checking preconditions. In this case the precondition evaluation involves geometric computation.

### 2.3.3 Cell Extension

As mentioned above the `Arrangement_on_surface_2` is parameterized by a topological traits, which in turn is parameterized by a DCEL class. Users may extend the default DCEL data-structure, in order to attach additional data to the DCEL records. The default DCEL model simply associates a point with each DCEL vertex and a $u$-monotone curve with each halfedge pair. Although it is possible to store auxiliary data with the curves or points by extending their respective types (see Section 2.5.3), it is sometimes necessary to extend the vertex, halfedge, or face topological features of the DCEL. Many times it is desired to associate extra data with the arrangement faces only. For example, when an arrangement represents the subdivision of a country into regions associated with their population density. In this case there is no alternative other than to extend the DCEL face, as there is no geometry-traits class entity that corresponds to an arrangement face. A similar mechanism for extending topological features with auxiliary attributes can be found in other components of CGAL, such as the triangulation packages [PY07] and the polyhedral-surfaces package [Ket07a].

## 2.4 The Arrangement Facilities

### 2.4.1 Sweep Line

The `Arrangement_on_surface_2` package offers a generic implementation of the sweep-line algorithm [dBvKOS00, Section 2.1] in form of a class template called `Sweep_line_2`. It handles any set of arbitrary $u$-monotone curves, and serves as the foundation of a family of concrete operations, such as computing all intersection points induced by a set of curves, constructing an arrangement of curves, aggregately inserting a set of curves into an existing arrangement, and computing the overlay of two arrangements. A concrete algorithm is realized through a sweep-line visitor, a template parameter of `Sweep_line_2`, which follows the *visitor* design-pattern [GHJV95], and models the concept *SweepLineVisitor_2*. In this case, a visitor defines an operation based on the sweep-line algorithm to be performed on an arrangement without the need to change the arrangement structure. Users may introduce their own sweep based algorithms by implementing an appropriate visitor class.[6]

Another parameter of the `Sweep_line_2` class-template is the geometry-traits class, which must be instantiated with a model of the *ArrangementXMonotoneTraits_2* concept; see Section 2.5 for the precise definition of this concept. It defines the minimal set of geometric primitives, among the other, required to perform the sweep-line algorithm briefly described next.

An imaginary vertical curve is swept over the surface from left to right, transforming the static two-dimensional problem into a dynamic one-dimensional one. At each time during the sweep a subset of the input $u$-monotone curves intersect this vertical line in a certain order. The subset of curves and their order along the sweep line may change as the line moves along the $u$-axis, implying a change in the topology of the arrangement, only at a

[6]The BOOST Graph Library, for example, uses visitors [SLL02, Section 12.3] to support user-defined extensions to its fundamental graph algorithms.

finite number of *event points*, namely intersection points of two curves and left endpoints or right endpoints of arcs of curves. The event points, namely endpoints and all the intersection points that have already been discovered, are stored in a $uv$-lexicographic order in a dynamic event queue, named the *$U$-structure*. The ordered sequence of segments intersecting the imaginary vertical line is stored in a dynamic structure called the *$V$-structure*. Both structures are maintained as balanced binary trees that enable their efficient maintenance using an advanced implementation of red-black trees [Wei05].

During the sweep-line process the event objects in the $U$-structure are sorted lexicographically, and the subcurve objects are stored in the $V$-structure in the same order as the lexicographic order of their intersection with the imaginary sweep-line. The `Sweep_line_2` class performs only the operations required to maintain the $U$-structure and the $V$-structure, while the visitor class is responsible for producing the actual output of the algorithm. Whenever the sweep-line class handles an event point $p$, it sends a notification to its visitor. Using this information, the visitor can access the subcurves incident to $p$ and the neighboring subcurves from above and below.

### 2.4.2 Map Overlay

The map overlay of two planar subdivisions $\mathcal{S}_1$ and $\mathcal{S}_2$ is a planar subdivision $\mathcal{S}$, such that there is a face $f$ in $\mathcal{S}$ if and only if there are faces $f_1$ and $f_2$ in $\mathcal{S}_1$ and $\mathcal{S}_2$ respectively, such that $f$ is a maximal connected subset of $f_1 \cap f_2$ [dBvKOS00, Section 2.3]. The overlay of two two-dimensional subdivisions embedded on a surface is defined similarly.

The overlay of two given arrangements, conveniently referred to as the "blue" and the "red" arrangements, is straightforwardly implemented using a sweep-line visitor. A consolidated set of the "blue" and "red" curves is processed, while the imaginary vertical line is swept over the surface. The $u$-monotone curve type is extended with a color attribute (whose value is either `BLUE` or `RED`); see Section 2.5.3. Using the extended type we filter out unnecessary computations. For example, we ignore monochromatic intersections, and compute only red–blue intersection points (or overlaps). This way the arrangement of a consolidated set of "blue" and "red" curves is computed efficiently.

The overlay visitor needs to construct a Dcel that properly represents the overlay of two input arrangements, the Dcel's of which are potentially independently extended (see Section 2.3.3). A face in the overlay arrangement corresponds to overlapping regions of the blue and red faces. An edge in the overlay arrangement is due to a blue edge, a red edge, or an overlap of two differently colored edges. An overlay vertex is due to a blue vertex, a red vertex, a coincidence of two differently colored vertices, or an intersection of a blue and a red curve. In each case, the data associated with the overlay Dcel feature should be computed from the red and blue Dcel features that induce it. To this end, the overlay visitor is parameterized by an overlay-traits module, which defines the merging operations between various Dcel features, achieving maximum genericity and flexibility for the users. The instantiated overlay traits models the *OverlayTraits* concept. The concept requires the provision of ten functions that handle all possible cases as follows:

1. A new vertex $v$ is induced by coinciding vertices $v_r$ and $v_b$.

2. A new vertex $v$ is induced by a vertex $v_r$ that lies on an edge $e_b$.
3. An analogous case of a vertex $v_b$ that lies on an edge $e_r$.
4. A new vertex $v$ is induced by a vertex $v_r$ that is contained in a face $f_b$.
5. An analogous case of a vertex $v_b$ contained in a face $f_r$.
6. A new vertex $v$ is induced by the intersection of two edges $e_r$ and $e_b$.
7. A new edge $e$ is induced by the overlap of two edges $e_r$ and $e_b$.
8. A new edge $e$ is induced by the an edge $e_r$ that is contained in a face $f_b$.
9. An analogous case of an edge $e_b$ contained in a face $f_r$.
10. A new face $f$ is induced by the overlap of two faces $f_r$ and $f_b$.

We apply the overlay operations in four different ways in this thesis; see Sections 3.2.2, 3.3.2, 5.3.6, and 5.3.7 for the different applications. Each application requires the provision of a different set of the ten functions above.

### 2.4.3 Zone Construction

The zone [Hal04] of a $u$-monotone curve $C$ in an arrangement $\mathcal{A}$ is the set of cells of $\mathcal{A}(\mathcal{C})$ intersected by the curve $C$.

The `Arrangement_on_surface_2` package includes the `Arrangement_zone_2` class-template, which computes the zone of an arrangement. Similar to the `Sweep_line_2` template, the `Arrangement_zone_2` template is parameterized with a zone visitor, a model of the concept *ZoneVisitor_2*, and it serves as the foundation of a family of concrete operations, such as inserting a single curve into an arrangement and determining whether a query curve intersects with the curves of an arrangement.

The zone of a curve $C$ is computed by locating the left endpoint of $C$ in the arrangement, and then "walking" along the curve towards the right endpoint, keeping track of the vertices, edges, and faces crossed on the way (see, for example, [dBvKOS00, Section 8.3] for the computation of the zone of a line in an arrangement of lines).

It is sometimes necessary to compute the zone of a curve in an arrangement without actually inserting the curve. In other situations, the entire zone is not required, as in the case of a process that only checks whether a query curve passes through an existing arrangement vertex; if the answer is positive, the process can terminate as soon as the vertex is located. While the sweep-line algorithm operates on a set of input $u$-monotone curves and its visitors can just use the notifications they receive to construct their output structures, the zone-computation algorithm operates on an arrangement object and its visitors may modify the same arrangement object as the computation progresses. This makes the interaction of the main class with its visitors slightly more intricate.

### 2.4.4 Observers

Some arrangement-based algorithms and applications should be bound to a specific arrangement instance and receive notifications on various topological changes this arrangement undergoes. This is not just a convenience, but crucial to the usability of the package, as it might be the only way for providing an algorithm with a certain input, such as data that

should be bound to the topological features of the arrangement, and is available only during construction; see Section 2.3.3 for an example.

The `Arrangement_on_surface_2` package supports a notification mechanism, which follows the *observer* design-pattern [GHJV95]. In this case of one-to-many dependency a set of observes depend on a single arrangement, so that when the arrangement changes state, all its dependents are notified and updated automatically. Using this mechanism it is possible to attach any number of observer instances to a specific arrangement, such that all attached observers get notified on local and global changes the arrangement undergoes.

The `Arr_observer<Arrangement>` class-template, parameterized by an arrangement type, stores a pointer to an arrangement object, and is capable of receiving notifications just before a structural change occurs in the arrangement and immediately after such a change takes place. Hence, each notification comprises of a pair of "before" and "after" functions (e.g., `before_split_face()` and `after_split_face()`). The `Arr_observer` class-template serves as a base class for other observer classes and defines a set of virtual notification functions, giving them all a default empty implementation. The interface of the base class is designed to capture all possible changes that arrangements can undergo, with a minimal set of topological events.

The set of functions can be subdivided into three categories as follows:

1. Notifiers of changes that affect the entire topological structure. Such changes occur when the arrangement is cleared or when it is assigned with the contents of another arrangement.

2. Notifiers of a *local* change to the topological structure, such as the creation of a new vertex or an edge, the splitting of an edge or a face, the formation of a new hole inside a face, the removal of an edge, etc.

3. Notifiers of a *global* change initiated by a free (global) function, and called by the free function (e.g., incremental or aggregate insert; see Section 2.3). This category consists of a single pair of notifiers, neither of them is called by methods of the `Arrangement_on_surface_2` class-template itself. Issuing point-location queries (or any other queries for that matter) between the calls to the "before" and "after" functions of this pair is forbidden.[7]

See [WF05] for a detailed specification of the arrangement observer class sketched above.

Each arrangement object stores a list of pointers to `Arr_observer` objects, and whenever one of the structural changes listed in the first two categories above is about to take place, the arrangement object invokes the appropriate function of each of its observers. It also does so immediately after the change has taken place. In addition, a free function may choose to trigger a similar notification, which falls under the third category above.

[7]This constraint improves the efficiency of the maintenance of auxiliary data structures for the relevant point-location strategies, which have to update their data structures according to the changes the arrangement undergoes (see Section 2.4.5 for more details). Since no point-location queries are issued between the invocation of `before_global_change()` and `after_global_change()`, it is not necessary to perform an update each time a local topological change occurs, and it is possible to postpone the updates until after the global operation is completed.

In case the new observer is attached to a non-empty arrangement, its constructor may extract the relevant data from the non-empty arrangement using various traversal methods offered by the public interface of the `Arrangement_on_surface_2` class, and update any internal data stored in the observer. This is necessary, for example, in case of the non-stateless point-location strategies, as shown in the next section.

### 2.4.5 Point Location

Point location is defined as follows: Given a point, find the arrangement cell that contains it. The `Arrangement_on_surface_2` package provides the means to answer this query. Typically, the result of the point-location query is one of the arrangement faces, but in degenerate situations the query point can lie on an edge, or it may coincide with a vertex. Since the arrangement representation is decoupled from the algorithms that operate on it, the `Arrangement_on_surface_2` class does not support point-location queries directly. Instead, the package provides a set of classes that are capable of answering such queries, all are models of the concept *ArrangementPointLocation_2*. Each model employs a different algorithm or *strategy* for answering queries. A model of this concept must define the `locate()` function, which accepts an input query point and returns an object representing the arrangement cell that contains this point (a polymorphic `CGAL::Object` instance that can either be a `Face_handle`, a `Halfedge_handle`, or a `Vertex_handle`).

The following models of the concept *ArrangementPointLocation_2* are included in the `Arrangement_on_surface_2` package.

- `Arr_naive_point_location` locates the query point naively, by exhaustively scanning all arrangement cells. It is the only strategy with unlimited support; see Section 2.6.

- `Arr_walk_along_a_line_point_location` simulates a reverse traversal along an imaginary vertical ray emanating from the query point toward infinity. It starts from the unbounded face of the arrangement and moves downward toward the query point until it locates the arrangement cell containing it.

- `Arr_landmarks_point_location<Generator>` uses an auxiliary generator class to create a set of "landmark" points, whose location in the arrangement is known. Given a query point, it uses a nearest-neighbor search structure (e.g., Kd-tree) to find the nearest landmark, and then traverses the straight-line segment connecting this landmark to the query point.[8] See [HH08] for more details.

- `Arr_trapezoidal_ric_point_location` implements Mulmuley's point-location algorithm [Mul90], which is based on the vertical decomposition of the arrangement into

[8]The "landmarks" strategy, requires that the arrangement is instantiated with a geometry-traits class that models the *ArrangementLandmarksTraits_2* concept, which adds two requirements to the basic *ArrangementBasicTraits_2* concept: (i) Approximating the coordinates of a given point $p$ using the double-precision arithmetic, and (ii) constructing a $u$-monotone curve that connects two given points $p$ and $q$, where $p$ represents a landmark point and $q$ is the query point. Most traits classes included in the arrangement package are models of this refined concept.

pseudo-trapezoids, and maintains a history directed acyclic graph (DAG) on top of the decomposition.

The last two strategies have query times that are shorter than the query times of the first two. However, they require preprocessing and consume more space, as they maintain auxiliary data structures. The first two strategies do not require any extra data and operate directly on the Dcel that represents the arrangement. For a complete survey see [HH08].

Each of the "landmarks" point-location class and the trapezoidal point-location class uses an observer to receive notifications whenever the arrangement is modified. For example, the default generator employed by the "landmarks" strategy uses the arrangement vertices as landmarks, so whenever a new vertex is created (by the insertion of a new edge, by the splitting of an existing edge, or by the insertion of an isolated point), it should be inserted into the nearest-neighbor search structure maintained by the respective landmark class. The usage of the notification mechanism makes it possible to associate several point-location objects with the same arrangement simultaneously.

The "landmarks" and the trapezoidal point-location strategies are both characterized by very efficient query time at the cost of time-consuming preprocessing. Naturally, these strategies exhibit better overall performance when the number of arrangement updates is relatively small compared to the number of issued queries. For a report on extensive experiments with the various point-location strategies see [HH08].

## 2.5 Geometry-Traits Concepts

The implementations of the various algorithms that construct and manipulate arrangements are generic, as they are independent of the type of curves they handle. All steps of the algorithms are enabled by the minimal set of geometric primitives gathered in the geometry-traits class, a model of a geometry-traits concept. The geometry-traits concept is factored into a hierarchy of refined concepts. The refinement hierarchy is defined according to the identified minimal requirements imposed by different algorithms that operate on arrangements, thus alleviating the production of traits classes that handle complicated curves, and increasing the usability of the algorithms. The requirements listed by the geometry-traits concepts include only the utterly essential types and operations, and fully specify all the preconditions that the input must satisfy, as these may simplify the implementation of models of this concept even further.

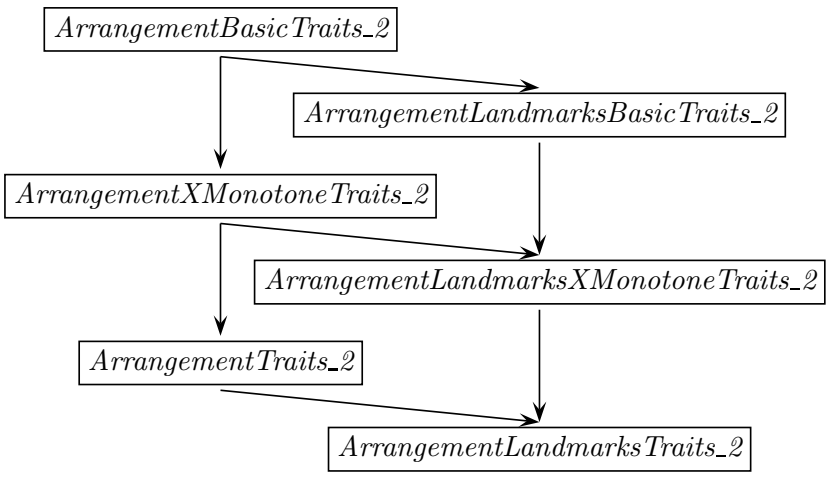


Figure 2.3: Refinement hierarchy of geometry-traits concepts.

The following sections are dedicated to a detailed description of the hierarchy. We list the minimal requirements of each layer in the hierarchy, and provide formal definitions for the required operations. The letters $x$ and $y$ are used in the code to refer to the two surface parameters, as arrangements embedded in the $xy$-plane are more common and familiar. The names of required nested types (e.g., `X_monotone_curve_2`) and valid expressions (e.g., `compare_x`) are faithful to the original source code. However, we use the letters $u$ and $v$ in the formal definitions below to refer to the two surface parameters, as these definitions apply to the general case of arrangements embedded on surfaces. Let $\mathrm{cmp}_u()$ and $\mathrm{cmp}_v()$ denote two predicates that accept two points and compare them by their $u$-coordinates and by their $v$-coordinates respectively. We use the following notation. For a point $p$, $(u_p, v_p)$, denotes a pre-image, and for a curve $C$, $\gamma$ denotes a pre-image, that is, $p = f_S(u_p, v_p)$ and $C(t) = f_S(\gamma(t))$ for all $t \in I$.

The basic concept *ArrangementBasicTraits_2* requires the definition of the types `Point_2` and `X_monotone_curve_2`. The latter represents a $u$-monotone curve, and the former is the type of the endpoints of the curves, representing a point on the surface. This concept lists the minimal set of predicates on objects of these two types sufficient to enable the operations provided by the `Arrangement_on_surface_2` class-template itself, namely the insertion of bounded $u$-monotone curves that are interior disjoint from any vertex and edge in the arrangement. All points and curves in the set below are required to have an inverse pre-image in $\mathbb{P} \setminus \partial\mathbb{P}$. In particular all curves are $u$-monotone.

---

`Compare_x_2`: Compare two points by their $u$-coordinates.

`Compare_xy_2`: Compare two points lexicographically by their $u$ and then by their $v$-coordinates.

`Construct_min_2`: Return the lexicographically smaller (left) endpoint of a given curve.

`Construct_max_2`: Return the lexicographically larger (right) endpoint of a given curve.

`Is_vertical_2`: Determine whether a weakly $u$-monotone curve is vertical.

`Compare_y_at_x`: Given a point $p$ and a curve $C$, such that the $u_p$ lies in the $u$-range of $C$, determine whether $p$ is above, below, or lies on $C$. More precisely, if $C$ is vertical, determine whether $p$ lies on $C$, or above or below $C$. Otherwise, since $u(\gamma(0)) \leq u_p \leq u(\gamma(1))$ must hold and $C$ is $u$-monotone, there must be a unique $0 \leq t' \leq 1$, that satisfies $u(\gamma(t')) = u_p$. Return $\mathrm{cmp}_v(p, \gamma(t'))$.

`Compare_y_at_x_right`: Given two curves $C_1$ and $C_2$ that share a common left endpoint $p$, determine the relative position of the two curves immediately to the right of $p$. More precisely, return $\mathrm{cmp}_v(\gamma_1(\epsilon_1), \gamma_2(\epsilon_2))$, where $\epsilon_1, \epsilon_2 > 0$ are infinitesimally small.

`Compare_y_at_x_left`: Given two curves $C_1$ and $C_2$ that share a common right endpoint $p$, determine the relative position of the two curves immediately to the left of $p$. More precisely, return $\mathrm{cmp}_v(\gamma_1(1-\epsilon_1), \gamma_2(1-\epsilon_2))$, where $\epsilon_1, \epsilon_2 > 0$ are infinitesimally small. This is an *optional* requirement with ramifications in case it is not fulfilled; see Section 2.5.1.

---

The set of predicates listed above is also sufficient for answering point-location queries by the various point-location strategies, with a small exception of the "landmarks" strategy, which requires a traits class that models the refined concept *ArrangementLandmarksTraits_2*. This

is described in Section 2.4.5.

Constructing arrangements induced by $u$-monotone curves that may intersect in their interior, requires an arrangement instantiated with a traits class that models the concept *ArrangementXMonotoneTraits_2*. This concept refines the basic arrangement-traits concept described above, as it requires an additional method for computing intersections between $u$-monotone curves, among the other. An intersection point between two curves is also represented by the `Point_2` type. The refined traits concept also requires methods for splitting curves at these intersection points to obtain pairs of interior disjoint subcurves and merging pairs of subcurves. In summary, a model of the refined concept must provide the additional operations bellow. All points and curves in the set below are required to have an inverse pre-image in $\mathbb{P} \setminus \partial\mathbb{P}$. In particular all curves are $u$-monotone.

---

`Intersection_2`**:** Compute the intersections between two given curves $C_1$ and $C_2$.
`Split_2`**:** Split a given curve $C$ at a given point $p$, which lies in the interior of $C$, into two interior disjoint subcurves.
`Merge_2`**:** Merge two mergeable curves $C_1$ and $C_2$ into a single curve $C$.
`Is_mergeable_2`**:** Determine whether two curves $C_1$ and $C_2$ that share a common endpoint can be merged into a single continuous curve representable by the traits class.

---

The further refined concept *ArrangementTraits_2* enables the construction of arrangements induced by *general* curves. A model of the refined concept must define a third type that represents a general (not necessarily $u$-monotone) curve, named `Curve_2`. It also has to supply a method that subdivides a given curve into simple $u$-monotone subcurves, and possibly isolated points.[9] We refer to the entire hierarchy of refinements defined above as a single "abstract" concept called *NoBoundaryTraits*, as it represents concepts the models of which handle curves that must have inverse pre-images in $\mathbb{P} \setminus \partial\mathbb{P}$. We use this abstract concept to simplify the description of the hierarchy defined below.

The package introduces additional concepts, models of which are able to handle unbounded curves or curves that reach the boundaries, the endpoints of which coincide with contraction points or lie on identification curves; see Figure 2.4. The "abstract" *HasBoundaryTraits* sub-hierarchy lists additional predicates required to handle both curves that reach or approach the boundaries of the parameter space. It has no models. The refined *BoundedBoundaryTraits* and *UnboundedBoundaryTraits* sub-hierarchies list additional predicates required to handle bounded and unbounded curves, respectively. The

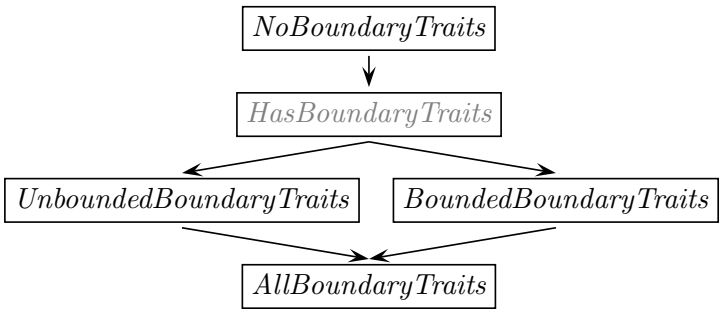


Figure 2.4: Abstract refinement hierarchy of geometry-traits concepts for arrangement on surfaces.

[9] For example, the curve $(x^2 + y^2)(x^2 + y^2 - 1) = 0$ is comprised of two $u$-monotone circular arcs, which together form the unit circle, and a singular isolated point at the origin.

geometry-traits class that handles arcs of great circles models the *BoundedBoundaryTraits* concept, as the parameter space is bounded in all four directions. Finally, the *AllBoundaryTraits* sub-hierarchy refines all the above. A model of this concept can handle unbounded curves in some directions and bounded curves in others.

In the rest of this section all curves are required to be $u$-monotone. The *HasBoundaryTraits* concept requires the following additional operations:

---

`Parameter_space_in_x_2`: Given a curve $C$ and an index $d \in \{0, 1\}$ that identifies one of its ends, determine the location of its pre-image in the domain $\mathbb{P}$ along the $u$ dimension. More precisely, determine whether $u(\gamma(d))$ is equal to $u_{\min}$, $u_{\max}$, or falls in between. In case of an unbounded curve, determine whether $\lim_{t \to d} u(\gamma(t))$ is equal to $-\infty$ or $+\infty$.

`Parameter_space_in_y_2`: Given a curve $C$ and an index $d \in \{0, 1\}$ that identifies one of its ends, determine the location of its pre-image in the domain $\mathbb{P}$ along the $v$ dimension. More precisely, determine whether $v(\gamma(d))$ is equal to $v_{\min}$, $v_{\max}$, or falls in between. In case of an unbounded curve, determine whether $\lim_{t \to d} v(\gamma(t))$ is equal to $-\infty$ or $+\infty$.

`Compare_x_near_boundary_2`: There are two predicates:

1. Given a point $p$, the inverse of which is in $\mathbb{P} \setminus \partial\mathbb{P}$, a curve $C$, and an index $d \in \{0, 1\}$ that identifies an end of $C$, compare the $u$ coordinates of $p$ and a point along $C$ near its given end. More precisely, return $\mathrm{cmp}_u(p, \gamma(|d - \epsilon|))$, where $\epsilon > 0$ is infinitesimally small.
2. Given two curves $C_1$ and $C_2$ and two corresponding indices $d_1, d_2 \in \{0, 1\}$ that identify two ends of $C_1$ and $C_2$ respectively, compare the $u$ coordinates of two points along $C_1$ and $C_2$ respectively near their given ends. More precisely, return $\mathrm{cmp}_u(\gamma_1(|d_1 - \epsilon_1|), \gamma_2(|d_2 - \epsilon_2|))$, where $\epsilon_1, \epsilon_2 > 0$ are infinitesimally small.

See Section 2.6.1 for an example.

`Compare_y_near_boundary_2`: Given two curves $C_1$ and $C_2$, and a single index $d \in \{0, 1\}$ that identifies two ends of $C_1$ and $C_2$, compare the $v$ coordinates of two points along $C_1$ and $C_2$ respectively near the given ends. More precisely, return $\mathrm{cmp}_v(\gamma_1(|d - \epsilon_1|), \gamma_2(|d - \epsilon_2|))$, where $\epsilon_1, \epsilon_2 > 0$ are infinitesimally small. See Section 2.6.1 for an example.

---

The *UnboundedBoundaryTraits* concept requires the following additional operations:

---

`Is_bounded_2`: Given a curve $C$ and an index $d \in \{0, 1\}$ that identifies an end of $C$, determine whether the curve end is bounded.

---

The *BoundedBoundaryTraits* concept requires the following additional operations:

---

`Is_on_x_identification_2`: This predicate applies only to a parameterization that has a vertical identification curve. Given a point $p$ (respectively a curve $C$), determine whether $p$ (respectively $C$) lies on the vertical and identified sides of the boundary. More precisely, determine whether $u_p \in \{u_{\min}, u_{\max}\}$. (Respectively, determine whether

$u(\gamma(t)) \in \{u_{\min}, u_{\max}\}, \forall t \in [0,1]$.

`Is_on_y_identification_2`: This predicate applies only to a parameterization that has a horizontal identification curve. Given a point $p$ (respectively a curve $C$), determine whether $p$ (respectively $C$) lies on the horizontal and identified sides of the boundary. More precisely, determine whether $v_p \in \{v_{\min}, v_{\max}\}$ for all pre-images of $p$. (Respectively, determine whether $v(\gamma(t)) \in \{v_{\min}, v_{\max}\}, \forall t \in [0,1]$.)

`Is_on_x_contraction_2`: This predicate applies only to a parameterization that has a contracted vertical boundary. determine whether $p$ coincides with a contraction point. More precisely, determine whether $u_p$ is equal to $u_{\min}$ or $u_{\max}$.

`Is_on_y_contraction_2`: This predicate applies only to a parameterization that has a contracted horizontal boundary. determine whether $p$ coincides with a contraction point. More precisely, determine whether $v_p$ is equal to $v_{\min}$ or $v_{\max}$.

`Compare_x_on_identification_2`: This predicate applies only to a parameterization that has a horizontal identified sides of the boundary. Given two points $p_1$ and $p_2$ that lie on the horizontal identification arc, compare their $u$-coordinates.

`Compare_y_on_identification_2`: This predicate applies only to a parameterization that has a vertical identified sides of the boundary.. Given two points $p_1$ and $p_2$ that lie on the vertical identification arc, compare their $v$-coordinates.

---

All traits-class operations are implemented as function objects (*functors*) according to CGAL's guidelines. This allows extending the geometric types above, without the need to redefine the methods that operate on them; see [HHK+07] for details on the extensible kernel. For a detailed specification of the various concept requirements see [WF05].

### 2.5.1 The Geometry-Traits Adaptor

The geometry-traits adaptor class-template implements geometric operations that are not provided by a model of the geometry-traits concept itself, using the operations supplied by a model of the geometry-traits concept as basic blocks. It decreases the effort required to develop geometry-traits models, and at the same time increases the usability of the geometry-traits models, adapting them for extended uses. A geometry-traits type is injected as a template parameter into the adaptor class, which inherits from it, centralizing all geometric operations. In cases where the efficiency of methods is crucial, a developer has a way to override these methods with optimized ones.

For example, in order to determine whether a point $p$ is in the $u$-range of a $u$-monotone curve $C$, the adaptor simply compares $p$ to the endpoints of $C$. It checks whether $p$ lies to the right of the left endpoint and to the left of the right endpoint.

In some cases, the geometry-traits adaptor class uses a *tag-dispatching* mechanism to select the appropriate implementation of a geometry-traits class operation. Tag dispatching is a technique that uses function overloading to dispatch a function *at compile time*, based on properties of the types of the arguments the function accepts [4]. This mechanism enables users to implement their traits class with a reduced or alternative set of operations. The adaptor respects the tags listed below every geometry-traits class must define.

`Has_left_category`: A Boolean tag that indicates whether the traits class provides the predicate `compare_y_at_x_left`, which compares two $u$-monotone curves to the *left* of a common right endpoint. This predicate is required only by some point-location strategies and by the zone-computation algorithm. While in some cases it is fairly easy for the traits-class implementer to provide it, in other cases it can be rather difficult, or even quite impossible. When this tag is false, the traits-class adaptor resorts to a somewhat less efficient algorithm that uses (other) existing traits-class predicates.

`Has_merge_category` A Boolean tag that indicates whether a model of the *ArrangementX-MonotoneTraits_2* supports the merge of $u$-monotone curves. If the tag is true, the traits class must provide the two operations `merge_2` and `is_mergeable_2`. The merger operation is used to eliminate redundant features in the arrangement. For example, if we have a T-shaped structure formed by two line segments, and the vertical segment forming the "leg" is removed, then it is possible to merge the two horizontal sub-segments. When the *has-merge* tag is false, the adaptor simply declares any pair of curves as non-mergeable. The only effect on the arrangement is that we cannot remove redundant vertices (of degree two) following the deletion of edges.

`Boundary_category`: A quadruple tag that categorizes the traits class according to the hierarchy described in Figure 2.4. The adaptor provides empty implementations of the operations that are never invoked, yet required for smooth compilation.

### 2.5.2 Geometry-Traits Models

Table 2.1: Geometry-traits models

| Curve Family | Degree | Surface | Boundness | Arithmetic |
|---|---|---|---|---|
| linear segment | 1 | plane | bounded | rational |
| linear segments, rays, lines | 1 | plane | unbounded | rational |
| piecewise linear curves | $\infty$ | plane | bounded | rational |
| circular arcs, linear segments | $\leq 2$ | plane | bounded | rational |
| algebraic curves | $\leq 2$ | plane | unbounded | algebraic |
| quadric projections | $\leq 4$ | plane | unbounded | algebraic |
| algebraic curves | $\leq 3$ | plane | unbounded | algebraic |
| algebraic curves | $\leq n$ | plane | unbounded | algebraic |
| planar Bézier curves | $\leq n$ | plane | unbounded | algebraic |
| univariate polynomials | $\leq n$ | plane | unbounded | algebraic |
| geodesic arcs on sphere | $\leq 2$ | sphere | bounded | rational |
| quadric intersection arcs | $\leq 4$ | quadric | unbounded | algebraic |
| Dupin cyclide intersection arcs | $\leq n$ | Dupin cyclides | bounded | algebraic |

The large number of geometry-traits models already implemented enables the construction and maintenance of arrangements induced by many different types of curves. The package itself contains several models of the geometry-traits concept. A few other models have been developed by other groups of researchers. Models are distinguished not only by the different families of curve they handle, but also by their suitability for constructing and

maintaining arrangements with different characteristics. For example, there are two distinct models that handle line segments [WFZH07b]. One caches information in the curve records, while the other retains the minimal amount of data. While operations on arrangements instantiated with the former model consume more space, they are more efficient for dense arrangements (namely, arrangements induced by curves with a large number of intersections). Another model handles not only (bounded) line-segments, but also rays and lines [BFH+07, BFH+09b]. There are traits models for non-linear curves, such as circular arcs [dCPT07], conic curves [Wei02, BEH+02, EKP+04], cubic curves [EKSW04], and quartic curves that are the projection of the intersection of two quadric surfaces [BHK+05], and there are traits classes for arcs of graphs of rational univariate polynomial functions [LPT08, WFZH07b]. There is even a traits class that handles algebraic curves of arbitrary degrees [EK08]. There is also a traits class that handles Bézier curves [HW07]. There is a traits class for geodesic arcs embedded on the sphere [FSH08b, BFH+09a], (see Section 2.6), another one for intersections of quadrics embedded on a quadric [BFH+07, BFH+09a], and another one for intersections of arbitrary algebraic surfaces with a Dupin cyclide embedded on the Dupin cyclide [BK08, BFH+09a]. Finally, there is a model that handles continuous piecewise linear curves, referred to as polylines, (see Section 2.5.4).

### 2.5.3 Geometry-Traits Extension

Traits-class decorators are used to extend the geometric entities defined by the traits class with additional, possibly non-geometric, data. An alternative way to achieve this is to extend the geometric types of the kernel, as the kernel is fully adaptable and extensible [HHK+07]. However, this indiscriminating extension may lead to an undue space-consumption, as every geometric object is extended, regardless of its use. It also requires nontrivial knowledge about the kernel structure and the techniques to extend it.

There is a decorator that enables the extension of the (general) curve and the $u$-monotone curve types with distinct types of data, and there is a convenient one, where the data attached to the $u$-monotone curve type is a set of objects, the type of which is attached to the (general) curve type. This set usually contains a single data object, unless the $u$-monotone curve corresponds to an overlapping section of two curves or more. When a curve with a data field $d$ is split into $u$-monotone subcurves, each subcurve is associated with a singleton set $\{d\}$. When two $u$-monotone curves overlap, the decorator takes the union of their data sets, and associates it with the resulting overlapping subcurve.

### 2.5.4 A Geometry-Traits Model that Handles Polylines

Polylines are of particular interest, as they can be used to approximate more complex curves. At the same time handling them is easier than handling higher-degree algebraic curves, as rational arithmetic is sufficient to carry out exact computations on polylines.

The geometry-traits model that handles polylines is a class-template called `Arr_polyline_traits_2`. It must be instantiated with a geometry-traits class that models the concept *ArrangementLinearTraits*. This concept refines the *ArrangementTraits* concept, as it adds a variant — it must handle line segments. This variant cannot be enforced by the

compiler, but rather be verified at run time. A polyline curve is represented as a vector of `SegmentTraits::X_monotone_curve_2` objects (namely segments). The polyline-traits class does not perform any geometric operations directly. Instead, it solely relies on the functionality of the instantiated segment-traits class. For example, when we need to determine the position of a point with respect to a $u$-monotone polyline, we use binary search to locate the relevant segment that contains the point in its $u$-range, then we compute the position of the point with respect to this segment. Thus, operations on $u$-monotone polylines of size $m$ typically take $O(\log m)$ time.

Users are free to choose the underlying segment-traits class based on the number of expected intersection points (see discussion above in Section 2.5.2). Moreover, it is possible to instantiate the polyline-traits class-template with a traits class that handles segments with some additional data attached to them (see Section 2.5.3). This makes it possible to associate different data objects with the different segments that compose a polyline.

## 2.6 Arrangements of Geodesic Arcs on the Sphere

In this section we concentrate on the particular category of arrangements embedded on surfaces, where the embedding space is the sphere, and the inducing objects are geodesic arcs. There is an analogy between this class of arrangements and the class of planar arrangements induced by linear curves (i.e., segments, rays, and lines), as properties of linear curves in the plane can be often, but not always, adapted to geodesic arcs on the sphere.

An arrangement of geodesic arcs embedded on the sphere is defined as an instance of the `Arrangement_on_surface_2` class-template instantiated with appropriate geometry- and topology-traits classes, namely `Arr_geodesic_arc_on_sphere_traits_2` and `Arr_spherical_topology_traits_2`, respectively. The geometry-traits class is tailored to handle geodesic arcs as efficiently as possible, and defines the parameterization used: $\mathbb{P} = [-\pi + \alpha, \pi + \alpha] \times [-\frac{\pi}{2}, \frac{\pi}{2}]$, $f_S(u, v) = (\cos u \cos v, \sin u \cos v, \sin v)$, where $\alpha$ is a variable that must be set at compile time, and is by default 0. This parameterization induces two contraction points $p_s = (0, 0, -1)$ and $p_n = (0, 0, 1)$, referred to as the south and north pole respectively, and an identification curve that coincides with the opposite Prime (Greenwich) Meridian. We developed the topology-traits class to support not only arrangements of geodesic arcs, but any type of curves embedded on the sphere parameterized as above, without compromising the performance of the operations gathered in the traits class. We hope that this topology-traits class will come in handy in the future for constructing and maintaining arrangements induced by types other than geodesic arcs, such as general circular arcs, which appear in arrangements induced by intersections of spheres embedded on the sphere [CL06]. The topology-traits class initializes the DCEL to have a single face, the embedding of which, is the entire sphere. It is designed to retain the variant that this face always contains the north pole during modifications the arrangement may undergo. The topology-traits class is required, for example, to inform its users that the top and bottom boundaries of the parameter space are contracted and the left and right boundaries are identified. It maintains a search structure of vertices that coincide with the contraction points or lie on the identification arc.

The figure to the right is a snapshot of a movie [FSH08b] that demonstrates, among the other, the sweep-line procedure carried out on the sphere. The red vertical arc that connects the poles is the imaginary sweep-line. The yellow vertex have been processed already. The dark blue arcs are curves that have been processed already and inserted into the arrangement. The light blue arcs are curves that are to be processed as the sweep line advances.

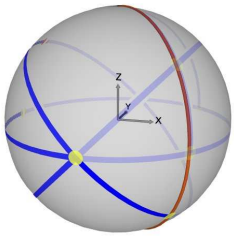


### 2.6.1 The Geometry-Traits Model

The geometry-traits class for geodesic arcs on the sphere is parameterized with a geometric kernel [HHK+07] that encapsulates the number type used to represent coordinates of geometric objects and to carry out algebraic operations on those objects. The implementation handles all degeneracies, and is exact, as long as the underlying number type is rational, even though the embedding surface is a sphere. We are able to use high-performance kernel models instantiated with exact rational number-types for the implementation of this geometry-traits class, as exact rational arithmetic suffices to carry out all necessary algebraic operations. The ability to robustly construct arrangements of geodesic arcs on the sphere, and robustly apply operations on them using only (exact) rational arithmetic is a key property that enables an efficient implementation.

A point in our arrangement is defined to be an unnormalized vector in $\mathbb{R}^3$, representing the place where the ray emanating from the origin in the relevant direction pierces the sphere. An arc of a great circle is represented by its two endpoints, and by the plane that contains the endpoint vectord and goes through the origin. The orientation of the plane and the source and target points determine which one of the two great arcs is considered.

The point type is extended with an enumeration that indicates whether the vector (i) pierces the south pole, (ii) pierces the north pole, (iii) intersects the identification arc, or (iv) is in any other direction. An arc of a great circle is extended with three Boolean flags that indicate whether any one of the $x, y, z$ coordinates of the normal of the plane that defines the arc vanishes. These flags are used to minimize the number of invocations of the geometry-traits operations, which has a drastic effect on the performance of arrangement operations at the account of a slight increase in space consumption. This representation enables an exact yet efficient implementation of all geometric operations required by the geometry-traits concept using exact rational arithmetic, as normalizing vectors (that represent directions and plane normals) is completely avoided.

We describe in details four predicates, namely `Compare_x_2`, `Compare_xy_2`, `Compare_x_near_boundary_2`, and `Compare_y_near_boundary_2`; see Section 2.5 for the complete set of the concept requirements. The former compares two points $p_1$ and $p_2$ by their $u$-coordinates. The concept admits the assumption that the input points do not coincide with the contraction points and do not lie on the identification arc. Recall that points are in fact unnormalized vectors that represent directions in $\mathbb{R}^3$. We project $p_1$ and $p_2$ onto the $xy$-plane to obtain two-dimensional unnormalized vectors $\hat{p_1}$ and $\hat{p_2}$, respectively. We compute the intersection between the identification arc and the $xy$-plane to obtain a third two-dimensional unnormalized vector $\hat{d}$. Finally, we test whether $\hat{d}$ is reached strictly before

$\hat{p_2}$ is reached, while rotating counterclockwise starting at $\hat{p_1}$. This geometric operation is supported by every geometric kernel of CGAL. In the figure on the right $\hat{d}$ is reached strictly before $\hat{p_2}$ is reached. Therefore, the $u$-coordinate of $p_1$ is larger than the $u$-coordinate of $p_2$.

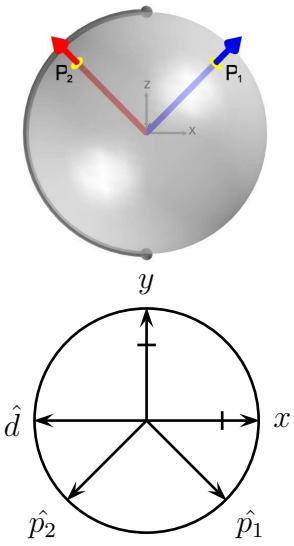


The predicate `Compare_xy_2` compares two points $p_1$ and $p_2$ lexicographically. It first applies `Compare_x_2` to compare the $u$-coordinates of the two points. If the $u$-coordinates are equal, it applies a predicate that compares the $v$-coordinates of two points with identical $u$-coordinates, referred to as `Compare_y_2`. This predicate first compares the signs of the $z$-coordinates of the two unnormalized input vectors. If they differ, it concludes that the point with the positive $z$-coordinate has a $v$-coordinate that is larger than the $v$-coordinate of the point with the negative $z$-coordinate. If the signs are identical, it compares the squares of their normalized $z$-coordinates, essentially avoiding the square-root operation. If the sign of the (unnormalized) $z$-coordinates of both points is positive (resp. negative), the point with the larger (resp. smaller) square of normalized $z$-coordinate has a larger $v$-coordinate.

The predicates above accept points, the pre-images of which, lie in the interior of the parameter space. However, there is also a need to lexicographically compare the ends of arcs, the pre-images of which reach the boundary of the parameter space. The predicate `Compare_x_near_boundary_2` accepts either (i) a point, the pre-image of which lies in the interior of the parameter space, and an arc end, or (ii) two arc ends. Such an arc end is provided by a vertical arc and an index that identifies one of the two ends of the arc, and must coincide with one of the contraction points. The first variant compares the $u$-coordinates of the input point and a point along the input arc near its given end, whereas the second variant compares the $u$-coordinates of two points along the input arcs near their respective given ends. Recall, that the $u$-coordinates of all points along a vertical arc are the same ($C_4$ and $C_5$ in the figure above). Thus, we can compare the $u$-coordinate of an arbitrary point on a vertical arc that lie inside the parameter space. For example, for the second case, we compare the two vectors perpendicular to the normals to the planes that define the vertical arcs, respectively, e.g., the $u$-coordinate of a point on the arc $C_4$ near its top end is smaller than the $u$-coordinate of a point on the arc $C_5$ near its top end, and in particular it is smaller than the $u$-coordinate of the bottom end of $C_5$. The `Compare_y_near_boundary_2` predicate compares the $v$-coordinate of two arcs ends, the pre-images of which lie on the same (left or right) identified side of the boundary of the parameter space. We use the aforementioned `Compare_y_2` predicate to compare the end points. If the points are equal, we compare the normals to the plane that define the arcs. In our example, the left end of $C_1$ is smaller than the left end of $C_2$, which is smaller than the left end of $C_3$.

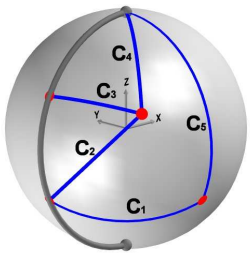


All the required geometric types listed in the traits concept are maintained using only rational numbers. All required geometric operations are implemented using only rational

arithmetic.[10] Degeneracies, such as overlapping arcs that occur during intersection computation, are properly handled. The end result is a robust yet efficient implementation.

## 2.7 Applications

Arrangement on surfaces have many applications this thesis falls short to list. However, we do list a few samples we were involved (or remotely involved) with the implementation of which, i.e., Regularized Boolean Set-Operations, Envelopes of Surfaces, and Voronoi diagrams. Minkowski sum construction is covered in details in the following chapter. The Boolean set-operation results, minimization diagrams, maximization diagrams and Voronoi diagrams, (see Section 2.7.2 for definitions), and Minkowski-sums are all represented as arrangements, and as such can be passed as input to consecutive operations on arrangements supported by the `Arrangement_on_surface_2` package and its derivatives.

### 2.7.1 Regularized Boolean Set-Operations

Together with R. Wein and B. Zuckerman we have developed a package that supports Boolean set-operations on point sets bounded by $u$-monotone curves embedded on two-dimensional parametric surfaces in $\mathbb{R}^3$ [FWZH07]. In particular, it contains the implementation of *regularized* Boolean set-operations, intersection predicates, and point containment predicates. A regularized Boolean set-operation op$^*$ can be obtained by first taking the interior of the resulting point-set of an *ordinary* Boolean set-operation ($P$ op $Q$) and then by taking the closure [Hof04]. That is, $P$ op$^*$ $Q$ = closure(interior($P$ op $Q$)). Regularized Boolean set-operations appear in constructive solid geometry (CSG), because regular sets are closed under regularized Boolean set-operations, and because regularization eliminates lower dimensional features, namely isolated vertices and "antennas" (namely, dangling edges), thus simplifying and restricting the representation to physically meaningful solids. Ordinary Boolean set-operations, which distinguish between the interior and the boundary of a polygon, are not implemented within this package. However, we implemented a specialized ordinary union operation as part of an assembly partitioning application; see Chapter 5.

The operands and results of the regularized operations are general polygons that may have holes. The boundaries of a general polygon and of holes, if present, are general $u$-monotone curves. The `Arrangement_on_surface_2` class is employed to represent a point set embedded on a two-dimensional parametric surface as an arrangement. A point set is typically constructed from a single general polygon or a collection of interior disjoint general polygons. The underlying arrangement must be instantiated with a geometry traits that models the concept *Gener-*

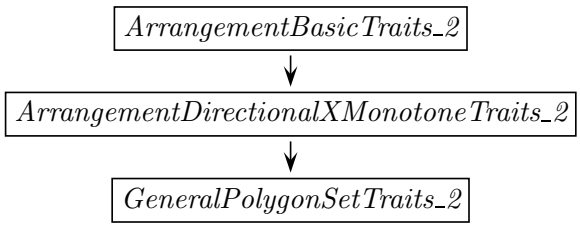


Figure 2.5: Refinement hierarchy of geometry traits concepts for Boolean set-operations.

[10] Points are represented as unnormalized vectors; The coordinates of such points are converted into machine floating-point only for rendering purposes.

*alPolygonSetTraits_2*. This concept refines the concept *ArrangementDirectionalXMonotoneTraits_2*, which in turns refines the concept *ArrangementBasicTraits_2* (see Section 2.5).

The *ArrangementDirectionalXMonotoneTraits_2* concept treats its $u$-monotone curves as objects directed from one endpoint appointed to be the source to the other endpoint appointed to be the target. Thus, it requires few additional operations on $u$-monotone curves:

---

`Compare_endpoints_xy_2`: Given a $u$-monotone curve $C$, compare the source and target points of $C$ lexicographically.

`Construct_opposite_2`: Given a $u$-monotone curve $C$, construct the opposite curve of $C$ (namely, swap the source and target endpoints of $C$).

`Intersection_2`: Compute the intersections between two given curves $C_1$ and $C_2$.

`Merge_2`: Merge two mergeable curves $C_1$ and $C_2$ into a single curve $C$.

`Is_mergeable_2`: Determine whether two curves $C_1$ and $C_2$ that share a common endpoint can be merged into a single continuous curve representable by the traits class.

---

Most traits classes bundled in the `Arrangement_on_surface_2` package and distributed with CGAL, are models of the concept *ArrangementDirectionalXMonotoneTraits_2*.[11]

The *GeneralPolygonSetTraits_2* concept requires its models to define a type that represents a general polygon and another one that represents general polygon with holes in addition to the `Point_2` and `X_monotone_curve_2` types that must be defined by all models of the generalized concept. It also requires the provision of several operations that operate on these two types listed below.

---

`Construct_polygon_2`: Given a sequence $\mathcal{C}$ of $u$-monotone curves, construct a general polygon that has $\mathcal{C}$ as its outer boundary.

`Construct_curves_2`: Given a general polygon $P$, obtain the sequence of $u$-monotone curves that comprise the boundary of $P$.

`Construct_general_polygon_with_holes_2`: Given a general polygon $P$ and a (possibly empty) set of holes $\mathcal{H}$, construct a general polygon with holes that has $P$ as its outer boundary and $\mathcal{H}$ as its holes.

`Construct_outer_boundary`: Given a general polygon-with-holes $P$, obtain the general polygon that is its outer boundary.

`Construct_holes`: Given a general polygon-with-holes $P$, obtain the holes of $P$ if any.

`Is_unbounded`: Given a general polygon-with-holes $P$, determine whether it has an outer boundary.

---

[11] The `Arr_polyline_traits_2` traits class is not a model of the *ArrangementDirectionalXMonotoneTraits_2* concept, as the $u$-monotone curve it defines is always directed from left to right. Thus, an opposite curve cannot be constructed.

### 2.7.2 Envelopes

Lower envelopes of functions on parametric surfaces are defined in a way similar to the standard definition of lower envelopes of bivariate functions in space [Hal04]. Let $S$ be a two-dimensional parametric surface is $\mathbb{R}^3$. Given a set of bivariate functions $F = \{f_1, \ldots, f_n\}$, where $f_i : S \to \mathbb{R}$, their *lower envelope* $\Psi(u, v)$ is defined to be their point-wise minimum $\Psi(u, v) = \min_{1 \le i \le n} f_i(u, v)$. The *minimization diagram* $\mathcal{M}(F)$ of the set $F$ is the two-dimensional map obtained by the projection of the lower envelope onto $S$. Upper envelopes and maximization diagrams are defined analogously for the point-wise maximum of the functions.

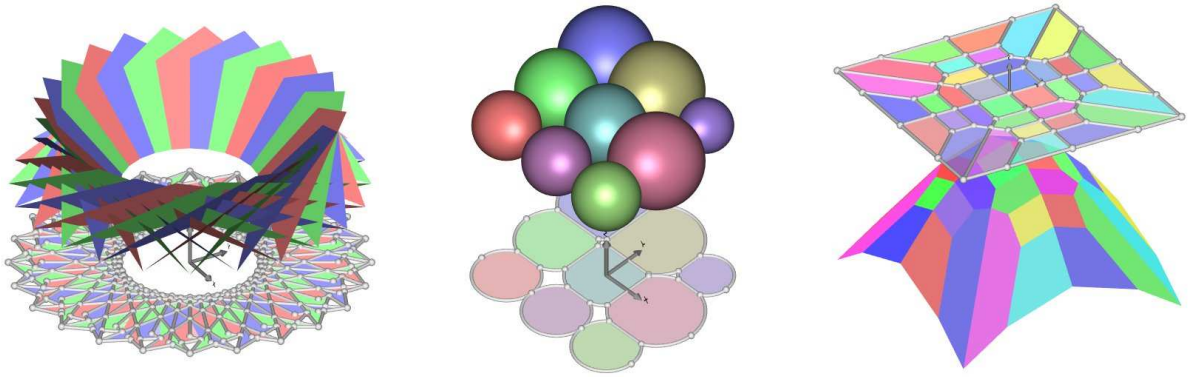

(a) (b) (c)

Figure 2.6: Lower envelopes of various types of surfaces (a) The lower envelope of triangles. (b) The lower envelope of spheres. (c) The lower envelope of planes. (The minimization diagrams is drawn above the planes for clarity.)

The `Envelope_3` package of CGAL [Mey06, MWZ07] computes the lower (or the upper) envelope of a set of surfaces in $\mathbb{R}^3$. It is based on the `Arrangement_on_surface_2` package, and like the base package, it handles degenerate input, and produces exact results. An arrangement data-structure is used to represent the resulting minimization diagram [Hal04]. The envelope computation is enabled by a traits class — a model of the concept *EnvelopeTraits_3*, which refines the *ArrangementTraits_2* concept. The `Envelope_3` package currently contains three models of the *EnvelopeTraits_3* concept that can be used to compute the envelope of triangles, spheres, and planes, respectively; see Figure 2.6 for an illustration. Other models of the *EnvelopeTraits_3* concept have been developed, for example, a traits class that enables the computation of the envelope of a set of quadric surfaces [BM07].

### 2.7.3 Voronoi Diagrams

Voronoi diagrams were thoroughly investigated, and were used to solve many geometric problems, since introduced by Shamos and Hoey to the field of computer science [SH75] (although their origin dates back centuries ago; see [OBSC00]). The concept of computing cells of points that are closer to a certain object than to any other object, among a finite number of objects, was extended to various kinds of geometric sites, ambient spaces, and distance functions, e.g., power diagrams of circles in the plane, multiplicatively weighted

Voronoi diagrams, additively weighted Voronoi diagrams [AK00]. This space decomposition is strongly connected to arrangements [ES86], a property that yields a very general approach for computing Voronoi diagrams.

Given a set of $n$ points $P = \{p_1, \ldots, p_n\}$, $p_i \in S$, we define $R(P, p_i) = \{x \in S \mid \rho(x, p_i) < \rho(x, p_j), j \neq i\}$, where $\rho(p_i, p_j)$ is some given distance function.[12] $R(P, p_i)$ is the region of all points that are closer to $p_i$ then to any other point in $P$. The Voronoi diagram of $P$ over $S$ is defined to be the regions $R(P, p_1), R(P, p_2), \ldots, R(P, p_n)$ and their boundaries. Edelsbrunner and Seidel [ES86] observed the connection between Voronoi diagrams in $\mathbb{R}^d$ and lower envelopes in $\mathbb{R}^{d+1}$ of the corresponding distance functions to the sites. From the above definitions it is clear that if $f_i : S \to \mathbb{R}$ is set to be $f_i(x) = \rho(x, p_i)$, for $i = 1, \ldots, n$, then the minimization diagram of $\{f_1, \ldots, f_n\}$ over $S$ is exactly the Voronoi diagram of $P$ over $S$.

K. E. Hoff *et al.* developed a technique for computing generalized 2D and 3D Voronoi diagrams using interpolation-based polygon rasterization hardware [HKL+99]. The hardware is used to draw the discrete and approximate lower envelope of the site-distance functions. Following similar principles, O. Setter *et al.* developed a new framework to compute different types of Voronoi diagrams embedded on certain parametric surfaces in an exact manner [SSH08]. The framework is based on the exact computation of the lower envelope of the site-distance functions over the surface [Mey06]. It provides a reduced and convenient interface between the construction of the diagrams and the construction of envelopes, which in turn are computed using the `Envelope_3` package [MWZ07]. Obtaining a new type of Voronoi diagrams only amounts to the provision of a geometry-traits class that handles the type of bisector curves of the new diagram type. Essentially, every type of Voronoi diagram, the bisectors of which can be handled by a geometry traits class, can be implemented using this framework. In particular the geometry-traits class for geodesic arcs embedded on the sphere enables Voronoi diagrams of points on the sphere and their generalization, power diagrams, also known as Laguerre Voronoi diagrams, on the sphere, as the bisector curves between point sites on the sphere are great circles [NLC02, OBSC00], and so are the bisectors between circle sites on the sphere under the Laguerre distance [Sug02]; see Figure 2.7. Power diagrams on the sphere have several applications similar to the applications of power diagrams in the plane. For example, determining whether a point is included in the union of circles on the sphere, and finding the boundary of the union of circles on the sphere [IIM85, Sug02].

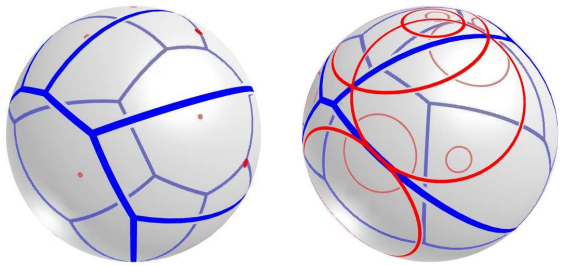

(a) (b)

Figure 2.7: Voronoi diagrams on the sphere. (a) The Voronoi diagram of 14 random points. (b) The power diagram of 10 random circles.

[12] In certain cases, the distance to a site may depend on various parameters associated with the site, e.g., in the cases of Möbius diagrams or anisotropic diagrams.

We implicitly construct envelopes of distance functions defined over the sphere to compute Voronoi diagrams. The image to the right illustrates the distance function from $(0,0) \in [-\pi,\pi]\times[-\frac{\pi}{2},\frac{\pi}{2}]$ on the sphere in the parameter space. The great circle bisector of two point sites on the sphere is the intersection of the sphere and the bisector plane of the points in $\mathbb{R}^3$ (imposed by the Euclidean metric).

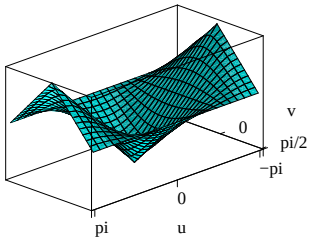


If a point on the sphere is given as a general vector in $\mathbb{R}^3$, it must be normalized. If the normalization results with a point with irrational coordinates, then it must be approximated to a point that lies exactly on the sphere [CDR92]. Once approximated, all further computations are carried out using exact rational arithmetic.

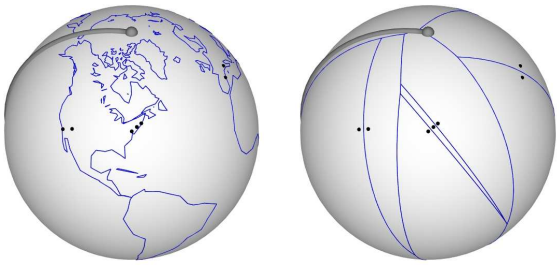

(a) (b)

Figure 2.8: Arrangements on the sphere.

Figure 2.8 (a) on the left shows an arrangement on the sphere induced by (i) the continents and some of the islands on earth, and (ii) the institutions that hosted SoCG during this millennium, which appear as isolated vertices. The sphere is oriented such that College Park, MD, USA is at the center. The arrangement consists of 1054 vertices, 1081 edges, and 117 faces. The data was taken from gnuplot [13] and google maps [14]. Figure 2.8 (b) shows an arrangement that represents the Voronoi diagram of the nine cities, the institutions above are located at, namely College Park, Gyeongju, Sedona, Pisa, New York, San Diego, Barcelona, Medford, and Hong Kong.

As mention above Voronoi diagrams, among the other, are represented as arrangements and can be passed as input to consecutive operations on arrangements supported by the `Arrangement_on_surface_2` package and its derivatives. The figure on the right shows the overlay of the two arrangements shown in Figure 2.8.

*Efficiency is just intelligent laziness.*

Anonymous

# 3

# Minkowski Sum Construction

We present two exact and robust implementations of efficient output-sensitive algorithms to compute the Minkowski sum of two polytopes in $\mathbb{R}^3$. We demonstrate the effectiveness of our Minkowski-sum computations through simple applications that exploit these operations to detect collision, and compute the Euclidean separation distance between, and the directional penetration depth of, two polytopes in $\mathbb{R}^3$. In Chapter 5 we show a more involved application of these operations.

Each method we have developed uses a different variant of Gaussian maps to maintain dual representations of polytopes. Each method employs a different variant of two-dimensional arrangements to maintain the dual representations, and it makes use of many operations applied to arrangements in the corresponding representations. The first method uses the traditional (spherical) Gaussian map. The map is represented as an arrangement of geodesic arcs embedded on the unit sphere. The second method uses a data structure called *Cubical Gaussian Map* . It consists of six arrangements induced by linear segments embedded in the plane. The six arrangements correspond to the six faces of the unit cube — the parallel-axis cube circumscribing the unit sphere.

A simple method to compute the Minkowski sum of two polytopes is to compute the convex hull of the pairwise sum of the vertices of the two polytopes. Although there are many implementations of various algorithms to compute Minkowski sums and answer proximity queries, we are unaware of the existence of complete implementations of methods to compute exact Minkowski sums other than (i) the naive method above, (ii) a method based on Nef polyhedra embedded on the sphere [HKM07], and (iii) an implementation by Weibel [28] of Fukuda's algorithm [Fuk04]. Both our methods exhibit much better performance than the other methods in all cases, as demonstrated by the experiments reported in Table 3.5. Our methods well handle degenerate cases that require special treatment when alternative representations are used. For example, the case of two parallel facets facing the same direction, one from each polytope, does not bear any burden on our methods, and neither does the

extreme case of two polytopes with identical sets of facet normals.

The results of experimentation with a broad family of convex polyhedra are reported. The relevant programs, source code, data sets, and documentation are available at `http://www.cs.tau.ac.il/~efif/CD`. A short movie [FH05] that describes some of the concepts of the cubical Gaussian-map method can be downloaded from `http://acg.cs.tau.ac.il/projects/internal-projects/gaussian-map-cubical/Mink3d.avi`. Another short movie [FSH08b] that describes some of the concepts of the (spherical) Gaussian map method among the other can be downloaded from `http://acg.cs.tau.ac.il/projects/internal-projects/arr-geodesic-sphere/movie/aos-xvid.avi`.

Both methods are implemented on top of CGAL, and are mainly based on the arrangement package of the library (see Chapter 2 and [FWH04, WFZH07b]), although other parts, such as the polyhedral-surface package developed by L. Kettner [Ket99], are used as well. In some cases it is sufficient to build only portions of the boundary of the Minkowski sum of two given polytopes to answer collision and proximity queries efficiently. This requires locating the corresponding features that contribute to the sought portion of the boundary. As both methods we have developed employ two-dimensional arrangements implemented on top of the CGAL arrangement package, we harness the ability to answer point-location queries efficiently that comes along, to locate corresponding features of two given polytopes.

The rest of this chapter is organized as follows. The *Gaussian maps* dual representations of polytopes in $\mathbb{R}^3$ are described in Section 3.1 along with some of their properties. In Sections 3.2 and 3.3 we show how 3D Minkowski sums can be computed efficiently, after the summands are converted to (spherical) Gaussian maps and cubical Gaussian maps, respectively. Section 3.4 presents an exact implementation of an efficient collision-detection algorithm under translation based on either of the dual representations. In the last section, dedicated to experimental results, we highlight the performance of our methods on various benchmarks. Suggestions for future directions are provided in the conclusion chapter in Section 6.4. The software access-information along with some further design details are provided in the Appendix.

## 3.1 Gaussian Maps

The *Gaussian map* $G = G(P)$ of a compact convex polyhedron $P$ in Euclidean three-dimensional space $\mathbb{R}^3$ is a set-valued function from $P$ to the unit sphere $\mathbb{S}^2$, which assigns to each point $p$ on the boundary of $P$ the set of outward unit normals to support planes to $P$ at $p$. Thus, the whole of a facet $f$ of $P$ is mapped under $G$ to a single point, representing the outward unit normal to $f$. An edge $e$ of $P$ is mapped to

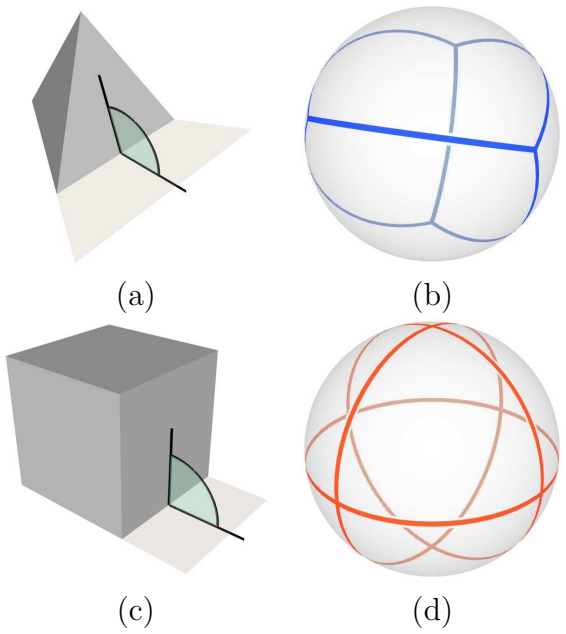


Figure 3.1: (a) A tetrahedron, (b) the Gaussian map of the tetrahedron, (c) a cube, and (d) the Gaussian map of the cube.

a (geodesic) segment $G(e)$ on $\mathbb{S}^2$, whose length is easily seen to be the exterior dihedral angle at $e$. A vertex $v$ of $P$ is mapped by $G$ to a spherical polygon $G(v)$, whose sides are the image under $G$ of edges incident to $v$, and whose angles are the angles supplementary to the planar angles of the facets incident to $v$; that is, $G(e_1)$ and $G(e_2)$ meet at angle $\pi - \alpha$ whenever $e_1$ and $e_2$ meet at angle $\alpha$. In other words, $G(v)$ is exactly the "spherical polar" of the link of $v$ in $P$. (The link of a vertex is the intersection of an infinitesimal sphere centered at $v$ with $P$, rescaled, so that the radius is 1.) The above implies that $G(P)$ is combinatorially dual to $P$ and an arrangement embedded on the unit sphere [HRS92]. Extending the mapping above, by marking each face $f = G(v)$ of the arrangement with its dual vertex $v$, enables a unique inverse Gaussian mapping, denoted by $G^{-1}$, which maps an extended arrangement embedded on the unit sphere back to a polytope boundary.

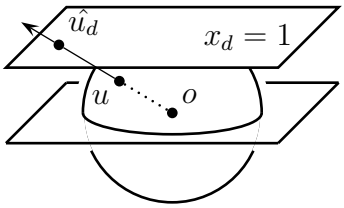


An alternative and practical definition follows. A direction in $\mathbb{R}^3$ can be represented by a point $u \in \mathbb{S}^2$. Let $P$ be a polytope in $\mathbb{R}^3$, and let $V$ denote the set of its boundary vertices. For a direction $u$, we define the *extremal point* in direction $u$ to be $\lambda_V(u) = \arg\max_{p \in V} \langle u, p \rangle$, where $\langle \cdot, \cdot \rangle$ denotes the inner product. The decomposition of $\mathbb{S}^2$ into maximal connected regions, so that the extremal point is the same for all directions within any region forms the Gaussian map of $P$. For some $u \in \mathbb{S}^2$ the intersection point of the ray $\vec{ou}$ emanating from the origin with one of the planes listed below is a *central projection* of $u$ denoted as $\hat{u_d}$, and illustrated on the right. The relevant planes are $x_d = 1$, $d = 1, 2, 3$, if $u$ lies in the positive respective hemisphere, and $x_d = -1$, $d = 1, 2, 3$ otherwise.

Similar to the Gaussian map, the *Cubical Gaussian Map* (CGM) $C = C(P)$ of a polytope $P$ in $\mathbb{R}^3$ is a set-valued function from $P$ to the six faces of the unit cube whose edges are parallel to the major axes and are of length two. A facet $f$ of $P$ is mapped under $C$ to a central projection of the outward unit normal to $f$ onto one of the cube faces. Observe that, a single edge $e$ of $P$ is mapped to a chain of at most four connected segments that lie in four adjacent cube-faces respectively, and a vertex $v$ of $P$ is mapped to at most five abutting convex dual faces that lie in five adjacent cube-faces, respectively. The decomposition of the unit-cube faces into maximal connected regions, so that the extremal point is the same for all directions within any region forms the CGM of $P$. Likewise, the inverse CGM, denoted by $C^{-1}$, maps the six extended arrangement embedded on the six faces of the unit cube to the polytope boundary. Figure 3.2 shows the CGM of a tetrahedron.

## 3.2 The (Spherical) Gaussian-Map Method

Armed with the geometry-traits class for geodesic arcs on the sphere (see Section 2.6), we compute Minkowski sums of convex polyhedra, by overlaying their respective Gaussian maps represented as arrangements of geodesics on the sphere. Each face $f$ of the Gaussian map is extended with the coordinates of its dual vertex $v = G^{-1}(f)$, resulting with a unique representation.

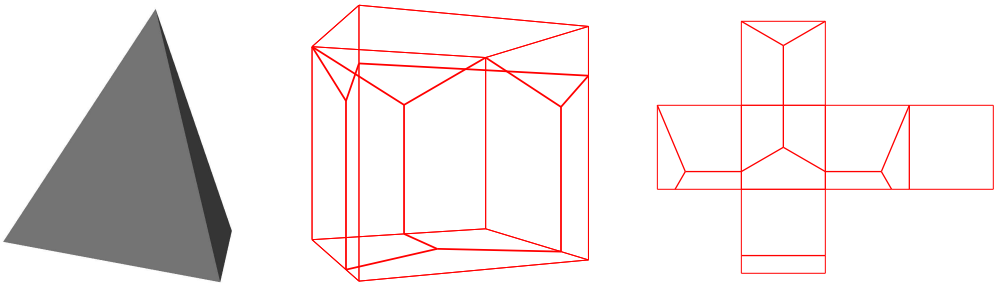

(a) (b) (c)

Figure 3.2: (a) A tetrahedron, (b) the CGM of the tetrahedron, and (c) the CGM unfolded. Thick lines indicate real edges.

### 3.2.1 The Representation

An input model of a polytope is provided as a polyhedral mesh in $\mathbb{R}^3$. A polyhedral mesh representation consists of an array of boundary vertices and the set of boundary facets, where each facet is described by an array of indices into the vertex array. Constructing the Gaussian map of a model given in this representation is done indirectly. First, the CGAL `Polyhedron_3` [Ket99] data-structure that represents the model is constructed. This data structure provides quick access to the incidence relations on the polytope features. Then, the Gaussian map is constructed from the accessible information stored in the `Polyhedron_3` data-structure. Once the construction of the Gaussian map is complete, the `Polyhedron_3` intermediate representation is discarded.

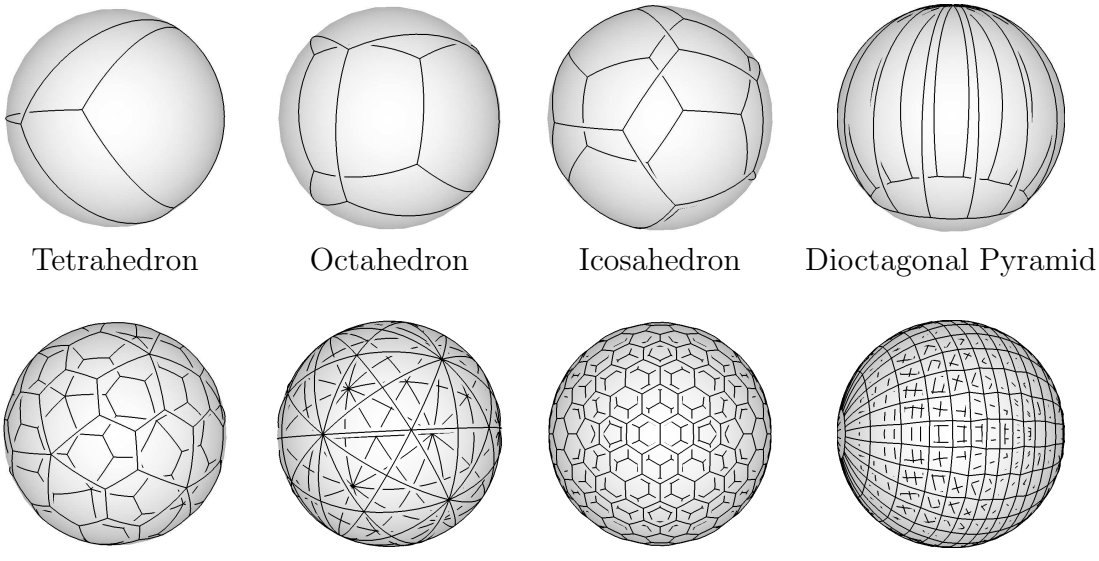


Figure 3.3: Gaussian maps of various polytopes.

The `Polyhedron_3` data-structure, like the arrangement DCEL, is based on the implementation of an HDS; see Section 2.3. It consists of extendible vertices, halfedges, and facets

and incidence relations on them. It provides methods to traverse all vertices, halfedges, and facets, and for local traversals, such as traversing all halfedges incident to a specific vertex. It also provides quick access from one halfedge to its twin, and to the incident facet to its left. Each vertex and halfedge of the `Polyhedron_3` data-structure is extended with a Boolean flag that indicates whether the vertex or the halfedge respectively have already been processed during the construction of the arrangement that represents the Gaussian map. Each facet is extended with the handle of an arrangement vertex. The handle extension of a facet $f$ that has already been processed points to the dual vertex $v = G(f)$. The procedure that converts an (extended) `Polyhedron_3` data-structure $P$ representing a polytope to an (extended) `Arrangement_on_surface_2` data-structure $G(P)$ consists of two steps. First all field extensions of all vertices, halfedges, and facets of $P$ are cleared. Then, a recursive function provided with an arbitrary vertex $v$ of $P$ as a single parameter is invoked. This function traverses the halfedges incident to $v$. When it encounters an unprocessed halfedge $e$, it obtains the normal $n_1$ and the vertex-handle extension $h(v_1)$ of the facet $f_1$ adjacent to the left of $e$ and the normal $n_2$ and the vertex-handle extension $h(v_2)$ of the facet $f_2$ adjacent to the left of the next halfedge in the cyclic chain of halfedges incident to $v$. Finally, the geodesic short arc between $n_1$ and $n_2$ is constructed and inserted into the arrangement $G(P)$, as explained below, using one of the efficient insertion member-functions of `Arrangement_on_surface_2`; see Section 2.3.2. Once the insertion is complete, the halfedge $e$ is marked as processed. $v$ is marked as processed once all its incident halfedges are processed. The function recursively invokes itself providing an unprocessed vertex adjacent to $v$, and terminates when no such vertex is found.

Let $C$ indicate the new geodesic arc to be inserted into the arrangement representing the Gaussian map. Assume that $C$ is $u$-monotone with respect to the parameterization defined by the geometry-traits class; see Section 2.6. That is, it does not intersect the identification arc. Let $v_1$, $v_2$, $f_1$, and $f_2$ be the two vertices and two facets as described above. There are four cases to handle as follows.

1. If $v_1$ and $v_2$ are both null, it implies that this is the first attempt to insert a geodesic arc into the arrangement. In this case we call `insert_in_face_interior(`$C$`,`$f$`)`, where $f$ is the single face the Dcel was initialized with; see Section 2.6. The handle of the two new vertices associated with the endpoints of the newly created geodesic arc $C$ are stored in the records of the corresponding facets $f_1$ and $f_2$ of $P$ respectively for later use.
2. If $v_1$ is null but $v_2$ is not, we call either `insert_from_left_vertex(`$C$`,`$v_2$`)` or `insert_from_right_vertex(`$C$`,`$v_2$`)` depending on whether the existing vertex $v_2$ is to the right or to the left of $C$, and update the vertex-handle field of the corresponding facet $f_1$ with the new vertex $v_1$.
3. We handle the analogous case where $v_2$ is null but $v_1$ is not similarly.
4. If both $v_1$ and $v_2$ are not null, we call `insert_at_vertices(`$C$`,`$v_1$`,`$v_2$`)`. In this case no vertex-handle field needs to be updated.

If $C$ intersects the identification arc, it is first split at the intersection point into two $u$-monotone arcs $C_1$ and $C_2$. Then, $C_1$ and $C_2$ are inserted according to four cases similar to the above. The handling is a bit more intricate. For example, consider the case where $v_1$ is null but $v_2$ already exists. Assume that $C_1$ reaches the right boundary of the parameter

space and $C_2$ reaches the left boundary (they both meet at an identified point). If $v_2$ is associated with the left endpoint of $C_1$, we first call `insert_from_left_vertex`$(C_1, v_2)$, and then `insert_from_left_vertex`$(C_2, v')$, where $v'$ is the new vertex associated with the right endpoint of $C_1$ introduced while $C_1$ is inserted. Otherwise, $v_2$ must be associated with the right endpoint of $C_2$. In this case we first call `insert_from_right_vertex`$(C_2, v_2)$, and then `insert_from_right_vertex`$(C_1, v')$, where $v'$ is the new vertex associated with the right endpoint of $C_2$ introduced while $C_2$ is inserted. The other three cases are handled similarly.

We have created a large database of models of polytopes. Table 3.3 lists, for a small subset of our polytope collection, the number of features in the arrangement of geodesic arcs embedded on the sphere that represents the Gaussian map of each polytope. Recall that the number of faces (**F**) of the Gaussian map is always equal to the number of vertices of the polytope. However, the number of vertices (**V**) of the Gaussian map is either equall to, or greater than, the number of facets of the primal representation due to intersections between Gaussian-map edges and the identification arc. A similar argument holds for the edges. That is, the number of halfedges (**HE**) of the Gaussian map is either equall to, or greater than, twice the number of edges of the primal representation. An edge of the Gaussian map that intersects the identification arc must be split at the intersection point into two $u$-monotone geodesic arcs. The table also lists the time in seconds (**t**) it takes to construct the arrangement once the intermediate polyhedron is in place, on a Pentium PC clocked at 1.7 GHz.

### 3.2.2 Exact Minkowski Sums

The overlay (see Section 2.4.2 for the exact definition) of the Gaussian maps of two polytopes $P$ and $Q$ respectively identifies all pairs of features of $P$ and $Q$ that have parallel supporting planes, as they occupy the same space on the unit sphere, thus, identifying all the pairwise features that contribute to the boundary of the Minkowski sum of $P$ and $Q$. A facet of the Minkowski sum is either a facet $f$ of $Q$ translated by a vertex of $P$ supported by a plane parallel to $f$, or vice versa, or it is a facet parallel to two parallel planes supporting an edge of $P$ and an edge of $Q$, respectively. A vertex of the Minkowski sum is the sum of two vertices of $P$ and $Q$ respectively supported by parallel planes.

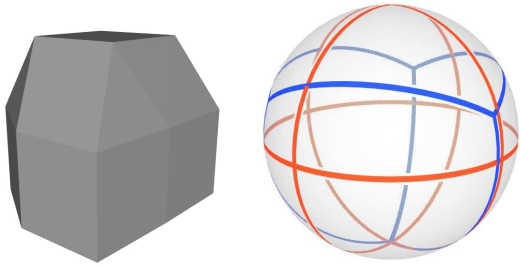

(a) (b)

Figure 3.4: (a) The Minkowski sum of a tetrahedron and a cube and (b) the Gaussian map of the Minkowski sum.

When the overlay operation progresses, new vertices, edges, and faces of the resulting arrangement are created based on features of the two operands. When a new feature is created its attributes are updated. There are ten cases that arise and must be handled; see Section 2.4.2 for the precise enumeration of the various cases. For example, a new face $f$ is induced by the overlap of two faces $f_1$ and $f_2$ of the two summands, respectively. The primal vertex associated with $f$ is set to be the sum of the primal vertices associated with $f_1$ and $f_2$, respectively.

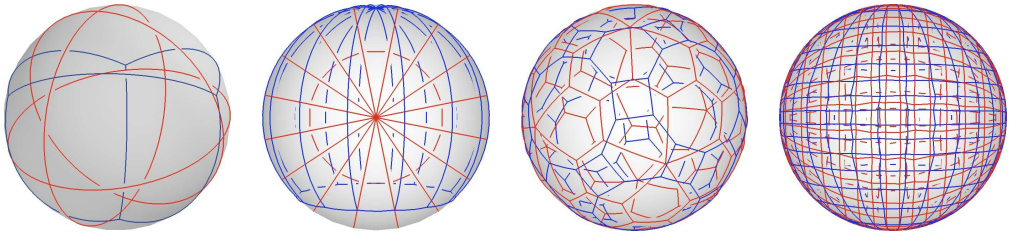


Figure 3.5: Gaussian maps of Minkowski sums. DP — Dioctagonal Pyramid, PH — Pentagonal Hexecontahedron, TI — Truncated Icosidodecahedron, GS4 — Geodesic Sphere level 4, El16 — Ellipsoid-like polyhedron made of 16 latitudes and 32 longitudes.

Table 3.4 lists the number of features (**V**, **HE**, **F**) in the arrangement that represents the Gaussian map of the respective Minkowski sums. Table 3.5 shows the time in seconds (**t**) it takes to construct the arrangement once the Gaussian maps of the summands are in place.

## 3.3 The Cubical Gaussian-Map Method

While using the CGM increases the overhead of some operations sixfold, and introduces degeneracies that are not present in the case of alternative representations, it simplifies the construction and manipulation of the representation, as the partition of each cube face is a planar map of segments, a well known concept that has been intensively experimented with during recent years. Indeed, all the basic software components that the CGM layer depends on are available in CGAL version 3.3 and higher, while many of the software components required by the (spherical) Gaussian map method are expected to appear only in a future release of CGAL. The CGM method, being more mature, exhibits better performance than the (spherical) Gaussian map method. One of the reasons for the performance gap is the lack of optimized primitives that operate on unnormalized vectors in $\mathbb{R}^3$ in case of the (spherical) Gaussian map method. Evidently, most of the methods of the geometry-traits class that handle geodesic arcs embedded on the sphere project their input $u$-monotone curves and points onto one of the axis-aligned planes every time they are invoked, while all geometric objects in case of the CGM method are projected onto the plane *a priori*. This creates an opportunity for optimization; see Section 6.1.4. In addition, the CGM data structure, being based on components confined to the plane, has a broader recognition, as it can be used in restricted environments, e.g., 3D hardware accelerators; see Section 6.5.

### 3.3.1 The Representation

We use the CGAL `Arrangement_2` data-structure to maintain the planar maps. The construction of the six planar maps from the polytope features and their incident relations is similar to the construction of the arrangement of geodesic arcs that represents the Gaussian map; see Section 3.2.1. As in the case of the (spherical) Gaussian map, the `Polyhedron_3` intermediate representation is discarded once the construction of the CGM is complete. However,

while a single edge of $P$ is mapped to at most two $u$-monotone geodesic arcs in case of the (spherical) Gaussian map, it can be mapped to a chain of at most four connected segments that lie in four adjacent cube-faces, respectively. In any case the constructions of the Gaussian maps of both methods respectively amount to the insertion of curves that are pairwise disjoint in their interior into the arrangement, an operation that is carried out efficiently, especially when one or both endpoints are known. The construction of the Minkowski sum, described in Section 3.3.2, amounts to the computation of the six overlays of six pairs of planar maps, respectively, an operation well supported by the data structure as well.

A related dual representation had been considered and discarded before the CGM representation was chosen. It uses only two planar maps that partition two parallel planes respectively instead of six, but each planar map partitions the entire plane.[1] In this 2-map representation facets that are near orthogonal to the parallel planes are mapped to points that are far away from the origin. The exact representation of such points requires coordinates with large bit-lengths, which increases significantly the time it takes to perform exact arithmetic operations on them. Moreover, facets exactly orthogonal to the parallel planes are mapped to points at infinity, and require special handling all together.

Features that are not in general position, such as two parallel facets facing the same direction, one from each polytope, or worse yet, two identical polytopes, typically require special treatment. Still, the handling of many of these problematic cases falls under the "general" case, and becomes transparent to the Gaussian-map layer (either cubical or spherical). Consider for example the case of two neighboring facets in one polytope that have parallel neighboring facets in the other. This translates to overlapping segments in case of the CGM method and overlapping geodesic arcs in case of the (spherical) Gaussian-map method, one from each Gaussian map of the two polytopes,[2] that appear during the Minkowski sum computation. The algorithm that computes it is oblivious to this condition, as the underlying arrangement data structure, either embedded in the plane or on the sphere, is perfectly capable of handling overlapping curves. However, as mentioned above, other degeneracies do emerge, and are handled successfully. One example, in case of the CGM, is a facet $f$ mapped to a point that lies on an edge of the unit cube, or even worse, coincides with one of the eight corners of the cube. Figure 3.7(a,b,c) depicts an extreme degenerate case of an octahedron oriented in such a way that its eight facets are mapped to the eight vertices of the unit cube, respectively. The (spherical) Gaussian map method is not free of degenerate conditions. For example, a facet mapped to a point that lies on the identification arc, or worse yet, coincides with one of the two poles.

The dual representation is extended further, in order to handle all these degeneracies and perform all the necessary operations as efficiently as possible. Each planar map is initialized with four edges and four vertices that define the unit square — the parallel-axis square circumscribing the unit circle. During construction, some of these edges or portions of them along with some of these vertices may turn into real elements of the CGM. The introduction

[1] Each planar map that corresponds to one of the six unit-cube faces in the CGM representation also partitions the entire plane, but only the $[-1,-1] \times [1,1]$ square is relevant. The unbounded face, which comprises all the rest, is irrelevant.

[2] Other conditions translate to overlapping segments in case of the CGM or geodesic arcs in case of the (spherical) Gaussian map method as well.

of these artificial elements not only expedites the traversals below, but is also necessary for handling degenerate cases, such as an empty cube face that appears in the representation of the tetrahedron and depicted in Figure 3.2(c). The global data consists of the six planar maps and 24 references to the planar vertices that coincide with the unit-cube corners.

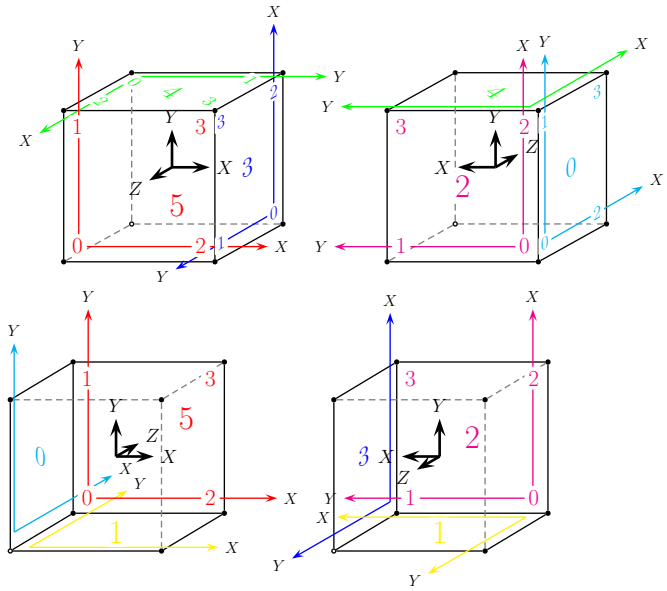

Figure 3.6: The data structure. Large-font numbers indicate plane ids. Small-font numbers indicate corner ids. $X$ and $Y$ axes in different 2D coordinate systems are rendered in different colors.

The exact mapping from a facet normal in the 3D coordinate-system to a pair that consists of a planar map and a planar point in the 2D coordinate-system is defined precisely through the indexing and ordering system, illustrated in Figure 3.6. Now before your eyes cross permanently, we advise you to keep reading the next few lines, as they reveal the meaning of some of the enigmatic numbers that appear in the figure. The six planar maps are given unique ids from 0 through 5. Ids 0, 1, and 2 are associated with the planes $x = -1$, $y = -1$, and $z = -1$, respectively, and ids 3, 4, and 5 are associated with the planes $x = 1$, $y = 1$, and $z = 1$, respectively. The major axes in the 2D Cartesian coordinate-system of each planar map are determined by the 3D coordinate-system. The four corner vertices of each planar map are also given unique ids from 0 through 3 in lexicographic order in their respective 2D coordinate-system, see Table 3.1 columns titled **Underlying Plane** and **2D Axes**.

Table 3.1: The coordinate systems and the cyclic chains of corner vertices. **PM** stands for **Planar Map**, and **Cr** stands for **Corner**.

| **Underlying Plane** | | **2D Axes** | | **Corner** | | | | | | | |
|---|---|---|---|---|---|---|---|---|---|---|---|
| | | | | **0** (0,0) | | **1** (0,1) | | **2** (1,0) | | **3** (1,1) | |
| **Id** | **Eq** | ***X*** | ***Y*** | **PM** | **Cr** | **PM** | **Cr** | **PM** | **Cr** | **PM** | **Cr** |
| 0 | $x = -1$ | $Z$ | $Y$ | 1 | 0 | 2 | 2 | 5 | 0 | 4 | 2 |
| 1 | $y = -1$ | $X$ | $Z$ | 2 | 0 | 0 | 2 | 3 | 0 | 5 | 2 |
| 2 | $z = -1$ | $Y$ | $X$ | 0 | 0 | 1 | 2 | 4 | 0 | 3 | 2 |
| 3 | $x = 1$ | $Y$ | $Z$ | 2 | 1 | 1 | 3 | 4 | 1 | 5 | 3 |
| 4 | $y = 1$ | $Z$ | $X$ | 0 | 1 | 2 | 3 | 5 | 1 | 3 | 3 |
| 5 | $z = 1$ | $X$ | $Y$ | 1 | 1 | 0 | 3 | 3 | 1 | 4 | 3 |

Each feature type of the DCEL used to maintain the incidence relations of the vertices, halfedges, and faces of the `Arrangement_2` data structure (see Section 2.3) is extended to hold additional attributes. Some of the attributes are introduced only in order to expedite the computation of certain operations, but most of them are necessary to handle degenerate cases such as a planar vertex lying on the unit-square boundary. Each planar-map vertex

$v$ is extended with (i) the coefficients of the plane containing the polygonal facet $C^{-1}(v)$ (see Section 3.1 for the definition of $C$ and $C^{-1}$), (ii) the location of the vertex — an enumeration indicating whether the vertex coincides with a cube corner, or lies on a cube edge, or contained in a cube face, (iii) a Boolean flag indicating whether it is non-artificial (there exists a facet that maps to it), and (iv) a pointer to a vertex of a planar map associated with an adjacent cube-face that represents the same central projection for vertices that coincide with a cube corner or lie on a cube edge. Each planar-map halfedge $e$ is extended with a Boolean flag indicating whether it is non-artificial (there exists a polytope edge that maps to it). Each planar-map face $f$ is extended with the polytope vertex that maps to it $v = C^{-1}(f)$.

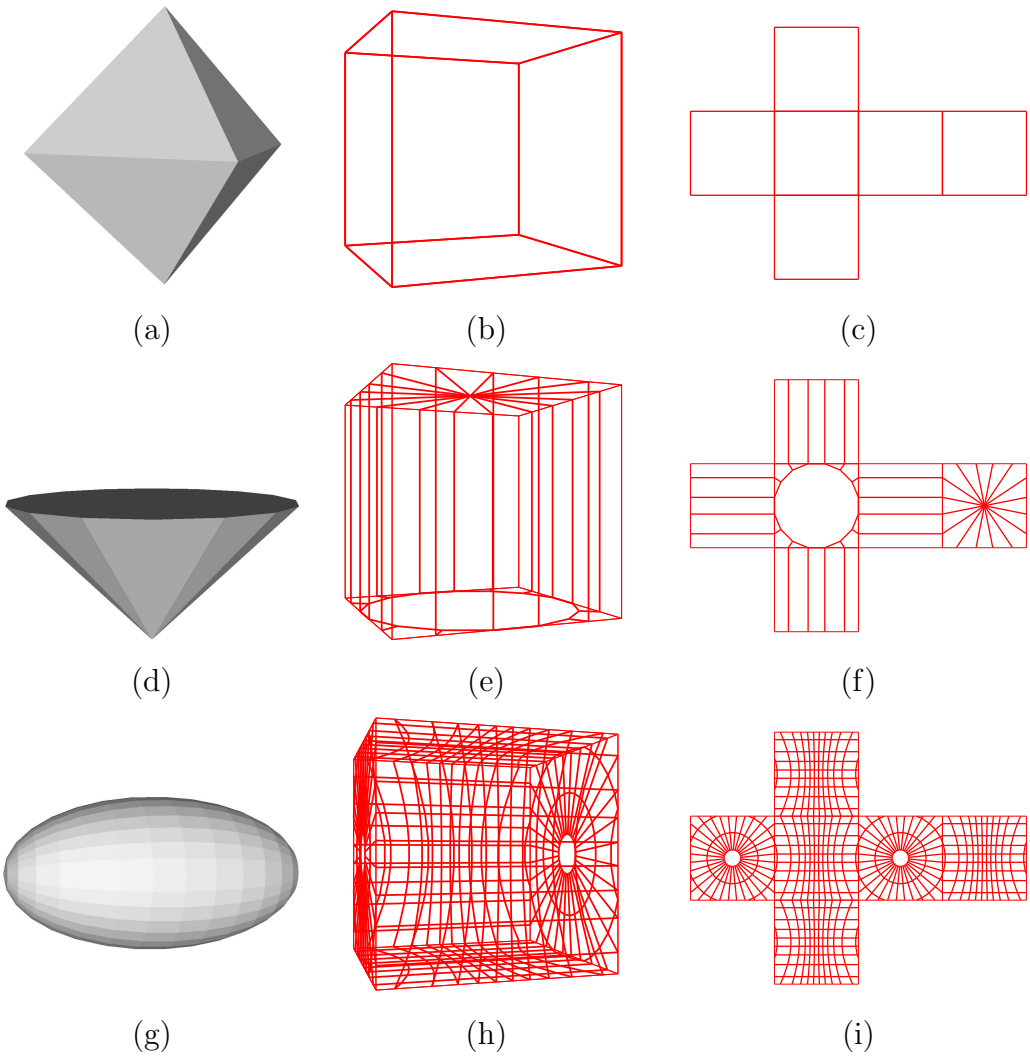


Figure 3.7: (a) An octahedron, (d) a dioctagonal pyramid, (g) an ellipsoid-like polyhedron level 16, (b,e,h) the CGM of the respective polytope, and (c,f,i) the CGM unfolded.

Each vertex that coincides with a unit-cube corner or lies on a unit-cube edge contains a pointer to a vertex of a planar map associated with an adjacent cube face that represents the same central projection. Vertices that lie on a unit-cube edge (but do not coincide with

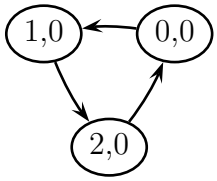


unit-cube corners) come in pairs. Two vertices that form such a pair lie on the unit-square boundary of planar maps associated with adjacent cube faces, and they point to each other. Vertices that coincide with unit-cube corners come in triplets and form cyclic chains ordered clockwise around the respective vertices. The diagram on the right specifies one of the eight cyclic chains. The left and right indices of each pair specify a planar-map id and a corner id, respectively. All specific connections are listed in Table 3.1. Recall that all maps are facing outwards. As a convention, edges incident to a vertex are ordered clockwise around the vertex, and edges that form the boundary of a face are ordered counterclockwise. The `Polyhedron_3` and `Arrangement_2` data structures for example both use a DCEL data structure that follows the convention above.

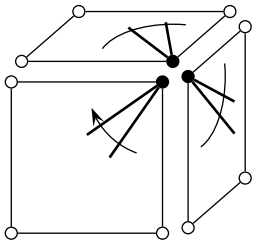

We provide a fast clockwise traversal of the faces incident to any given vertex $v$. Clockwise traversals around internal vertices are immediately available by the DCEL. Clockwise traversals around boundary vertices are enabled by the cyclic chains above. This traversal is used to calculate the normal to the (primary) polytope-facet $f = C^{-1}(v)$ and to render the facet. Fortunately, rendering systems are capable of handling a sequence of vertices that define a polygon in clockwise order as well, an order opposite to the conventional ordering above.

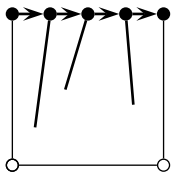

The data structure also supports a fast traversal over the planar-map halfedges that form each one of the four unit-square edges. This traversal is used during construction to quickly locate a vertex that coincides with a cube corner or lies on a cube edge. It is also used to update the cyclic chains of pointers mentioned above; see Section 3.3.2.

We maintain a flag that indicates whether a planar vertex coincides with a cube corner, a cube edge, or a cube face. At first glance this looks redundant. After all, this information could be derived by comparing the $x$ and $y$ coordinates to $-1$ and $+1$. However, it has a good reason as explained next. Using exact number-types often leads to representations of the geometric objects with large bit-lengths. Even though we use various techniques to prevent the length from growing exponentially [FWH04], we cannot prevent the length from growing at all. Even the computation of a single intersection requires a few multiplications and additions. Cached information computed once and stored at the features of the planar map avoids unnecessary processing of potentially long representations.

The table to the right shows the number of vertices (**V**), halfedges (**HE**), and faces (**F**) of the six planar maps that comprise the CGM of the dioctagonal pyramid shown in Figure 3.7 (d,e,f). The number of faces of each planar map include the unbounded face. Table 3.3 shows the number of features in the primal and dual representations of a small subset of our polytopes collection, on which we report the results of experiments below. The number of planar features is the total number of features of the six planar maps.

Table 3.2: The number of features of the six planar maps of the CGM of the dioctagonal pyramid.

| **Planar map** | **V** | **HE** | **F** |
|---|---|---|---|
| 0, $(x = -1)$ | 12 | 32 | 6 |
| 1, $(y = -1)$ | 28 | 80 | 14 |
| 2, $(z = -1)$ | 12 | 32 | 6 |
| 3, $(x = 1)$ | 12 | 32 | 6 |
| 4, $(y = 1)$ | 21 | 72 | 17 |
| 5, $(z = 1)$ | 12 | 32 | 6 |
| **Total** | 97 | 280 | 55 |

### 3.3.2 Exact Minkowski Sums

A similar argument regarding the representation of Minkowski sums using Gaussian maps mentioned in Section 3.2 holds for the cubical Gaussian maps with the unit cube replacing the unit sphere. More precisely, a single map that subdivides the unit sphere is replaced by six planar maps, and the computation of a single overlay is replaced by the computation of six overlays of corresponding pairs of planar maps. Recall that each (primal) vertex is associated with a planar-map face, and is the sum of two vertices associated with the two overlapping faces of the two CGM's of the two input polytopes, respectively.

Each planar map in a CGM is a convex subdivision. Finke and Hinrichs [FH95] describe how to compute the overlay of such special subdivisions optimally in linear time. However, a preliminary investigation shows that a large constant governs the linear complexity, which renders this choice less attractive. Instead, we resort to a sweep-line based algorithm that exhibits good practical performance, and incurs a mere logarithmic factor over the optimal computing time. In particular we use the overlay operation supported by the Arrangement package. It requires the provision of a complementary component that is responsible for updating the attributes of the DCEL features of the resulting six planar maps; see Section 2.4.2.

The overlay operates on two instances of `Arrangement_2`. In the description below $v_1$, $e_1$, and $f_1$ denote a vertex, a halfedge, and a face of the first operand respectively, and $v_2$, $e_2$, and $f_2$ denote the same feature types of the second operand, respectively. When the overlay operation progresses, new vertices, halfedges, and faces of the resulting planar map are created based on features of the two operands. Exactly ten cases described below arise and must be handled. When a new feature is created its attributes are updated. The updates performed in all cases except for case (1) are simple and require constant time.

1. A new vertex $v$ is induced by coinciding vertices $v_1$ and $v_2$.
   The location of the vertex $v$ is set to be the same as the location of the vertex $v_1$ (the locations of $v_2$ and $v_1$ must be identical). The induced vertex is not artificial if and only if (i) at least one of the vertices $v_1$ or $v_2$ is not artificial, or (ii) the vertex lies on a cube edge or coincides with a cube corner, and both vertices $v_1$ and $v_2$ have

Table 3.3: Complexities of the primal and dual representations. DP — Dioctagonal Pyramid, PH — Pentagonal Hexecontahedron, TI — Truncated Icosidodecahedron, GS4 — Geodesic Sphere level 4, El16 — Ellipsoid-like polyhedron made of 16 latitudes and 32 longitudes, t - time consumption in seconds.

| Object Type | Primal | | | SGM | | | | CGM | | | |
|---|---|---|---|---|---|---|---|---|---|---|---|
| | V | E | F | V | HE | F | t | V | HE | F | t |
| Tetrahedron | 4 | 6 | 4 | 4 | 12 | 4 | 0.01 | 42 | 102 | 21 | 0.01 |
| Octahedron | 6 | 12 | 8 | 10 | 28 | 6 | 0.01 | 24 | 48 | 12 | 0.01 |
| Icosahedron | 12 | 30 | 20 | 21 | 62 | 12 | 0.01 | 72 | 192 | 36 | 0.01 |
| DP | 17 | 32 | 17 | 25 | 80 | 17 | 0.01 | 97 | 280 | 55 | 0.01 |
| PH | 60 | 150 | 92 | 101 | 318 | 60 | 0.03 | 200 | 600 | 112 | 0.02 |
| TI | 120 | 180 | 62 | 77 | 390 | 120 | 0.05 | 230 | 840 | 202 | 0.03 |
| GS4 | 252 | 750 | 500 | 506 | 1512 | 252 | 0.08 | 708 | 2124 | 366 | 0.07 |
| El16 | 482 | 992 | 512 | 528 | 2016 | 482 | 0.11 | 776 | 2752 | 612 | 0.06 |

non-artificial incident halfedges that do not overlap.

2. A new vertex $v$ is induced by a vertex $v_1$ that lies on an edge $e_2$.
   The location of the vertex $v$ is set to be the same as the location of the vertex $v_1$. $v$ is not artificial if and only if $v_1$ is not artificial or $e_2$ is not artificial.
3. An analogous case of a vertex $v_2$ that lies on an edge $e_1$.
4. A new vertex $v$ is induced by a vertex $v_1$ that is contained in a face $f_2$.
   The attributes of the vertex $v$ are set to be the same as the attributes of the vertex $v_1$.
5. An analogous case of a vertex $v_2$ contained in a face $f_1$.
6. A new vertex $v$ is induced by the intersection of two edges $e_1$ and $e_2$.
   The vertex $v$ cannot lie on a cube edge and cannot coincide with a cube corner. Thus, it is necessarily not artificial.
7. A new edge $e$ is induced by the overlap of two edges $e_1$ and $e_2$.
   The edge $e$ is not artificial if at least one of $e_1$ or $e_2$ is not artificial.
8. A new edge $e$ is induced by an edge $e_1$ that is contained in a face $f_2$.
   The edge $e$ is not artificial if $e_1$ is not artificial.
9. An analogous case of an edge $e_2$ contained in a face $f_1$.
10. A new face $f$ is induced by the overlap of two faces $f_1$ and $f_2$.
    The primal vertex associated with $f$ is set to be the sum of the primal vertices associated with $f_1$ and $f_2$, respectively.

After the six map overlays are computed, some maintenance operations must be performed to obtain a valid CGM representation. As mentioned above, the global data consists of the six planar maps and 24 references to vertices that coincide with the unit-cube corners. For each planar map we traverse its vertices, obtain the four vertices that coincide with the unit-cube corners, and initialize the global data. We also update the cyclic chains of pointers to vertices that represent identical central projections. To this end, we exploit the fast traversal over the halfedges that coincide with the unit-cube edges mentioned in Section 3.3.1.

The complexity of a single overlay operation is $O(k \log n)$, where $n$ is the total number of vertices in the input planar maps, and $k$ is the number of vertices in the resulting planar map. The total number of vertices in all the six planar maps in a CGM that represents a polytope $P$ is of the same order as the number of facets in the primary polytope $P$. Thus, the complexity of the entire overlay operation is $O(F \log(F_1 + F_2))$, where $F_1$ and $F_2$ are the number of facets in the input polytopes respectively, and $F$ is the number of facets in the Minkowski sum.

## 3.4 Exact Collision Detection

Computing the separation distance between two polytopes with $m$ and $n$ features respectively can be done in $O(\log m \log n)$ time, after an investment of at most linear time in preprocessing [DK90]. Many practical algorithms that exploit spatial and temporal coherence between successive queries have been developed, some of which became classic, such as the GJK algorithm [GJK88] and its improvement [Cam97], and the LC algorithm [LC91] and its optimized variations [EL00, GHZ99, Mir98]. Several general-purpose software libraries

that offer practical solutions are available today, such as the SOLID library [24] based on the improved GJK algorithm, the SWIFT library [26] based on an advanced version of the LC algorithm, the QuickCD library [21], and more. For an extensive review of methods and libraries see the survey [LM04].

Given two polytopes $P$ and $Q$, detecting collision between them and computing their relative placement can be conveniently done in the configuration space, where their Minkowski sum $M = P \oplus (-Q)$ resides. These problems can be solved in many ways, and not all require the explicit representation of the Minkowski sum $M$. However, having it available is attractive, especially when the polytopes are restricted to translations only, as the combinatorial structure of the Minkowski sum $M$ is invariant to translations of $P$ or $Q$. The algorithms described below are based on the following well known observations (see Chapter 1 for definitions):

$$\begin{aligned} P^u \cap Q^w \neq \emptyset &\Leftrightarrow w - u \in M = P \oplus (-Q) \ , \\ \pi(P^u, Q^w) &= \min\{\|t\| \mid (w - u + t) \in M, t \in \mathbb{R}^3\} \ , \\ \delta_r(P^u, Q^w) &= \inf\{\alpha \mid (w - u + \alpha\vec{r}) \notin M, \alpha \in \mathbb{R}\} \ . \end{aligned}$$

Given two polytopes $P$ and $Q$ in either (spherical) Gaussian map or CGM representation respectively, we reflect $Q$ through the origin to obtain $-Q$, compute the Minkowski sum $M = P \oplus (-Q)$, and retain it in the respective Gaussian-map representation $G(M)$. Then, each time $P$ or $Q$ or both translate by two vectors $u$ and $w$ in $\mathbb{R}^3$ respectively, we apply a procedure that determines whether the query point $s = w - u$ is inside, on the boundary of, or outside $M$. In addition to an enumeration of one of the three conditions above, the procedure returns a witness of the respective relative placement. Let $r$ be a ray emanating from an internal point $c \in M$ and going through $s$. If the (spherical) Gaussian map representation is used, the witness data is the vertex $v = G(f)$ — a mapping of a facet $f$ of $M$ embedded on the sphere and stabbed by the ray $r$. If the CGM representation is used, the witness data is a pair that consists of a vertex $v = G(f)$ — a mapping of a facet $f$ of $M$ embedded in a unit cube face, and the planar map $\mathcal{P}$ containing $v$. This information is used as a hint in consecutive invocations. The internal point $c$ could be the average of all vertices of $M$ computed once and retained along $M$, or just the midpoint of two vertices that have supporting planes with opposite normals easily extracted from either map representation. Once $f$ is obtained, determining whether $P^u$ and $Q^w$ collide is trivial, according to the first formula (of the three) above. The query point $s$ is contained in the open half-space defined by the supporting plane to $f$ if and only if $s$ is outside of $M$, this occurs if and only if $P^u$ does not collide with $Q^w$.

The collision-detection procedure applies a local walk on the respective Gaussian map faces. It starts with some vertex $v_0$, and then performs a loop moving from the current vertex to a neighboring vertex, until it reaches the final vertex. If the CGM representation is used, the procedure may jump from a planar map associated with one cube-face to a different one associated with an adjacent cube-face. The first time the procedure is invoked, $v_0$ is chosen to be a vertex that lies on the central projection of

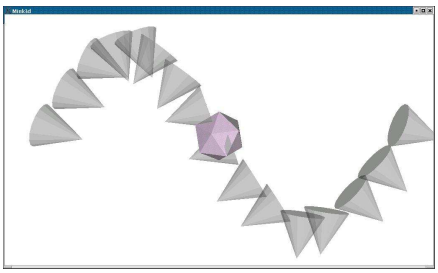

Figure 3.8: Simulation of motion.

the normal directed in the same direction as the ray $r$. In consecutive calls, $v_0$ is chosen to be the final vertex of the previous call exploiting spatial and temporal coherence. The figure above is a snapshot of a simulation program that detects collision between a static obstacle and a moving robot, and draws the obstacle and the trail of the robot; instructions to obtain, install, and execute the program appear in the Appendix. The Minkowski sum is recomputed only when the robot is rotated, which occurs every other frame. The program has the distinctive feature of being able to identify the case where the robot grazes the obstacle, but does not penetrate it, since it produces exact results. The computation takes just a fraction of a second on a Pentium PC clocked at 1.7 GHz using either representation. Similar procedures that compute the directional penetration-depth and minimum distance are available as well.

## 3.5 Minkowski Sum Complexity

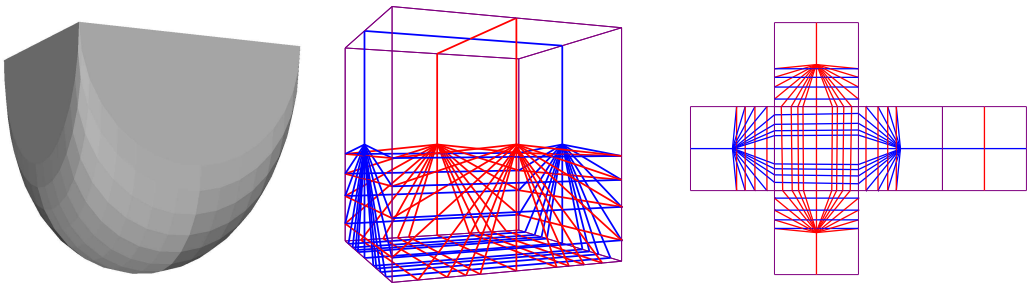

(a) (b) (c)

Figure 3.9: (a) The Minkowski sum (of two polytopes) the complexity of which is maximal, (b) the CGM of the Minkowski sum, and (c) the CGM unfolded. Red lines are graphs of edges that originate from one polytope and blue lines are graphs of edges that originate from the other.

In Chapter 4 we show that the exact maximum number of facets of Minkowski sums of two polytopes is $4mn - 9m - 9n + 26$, where $m$ and $n$ are the number of facets of the two summands, respectively. This bound is tight [FHW07]. The example depicted in Figure 3.9 shows a Minkowski sum that reaches this maximum complexity. It is the sum of two identical polytopes, each containing $n$ faces ($n = 11$ in Figure 3.9), but one is rotated about the vertical axis approximately[3] 90° relative to the other. The polytopes are specifically shaped to ensure that the number of intersections between dual edges, which are the mappings of the polytope edges, is maximal. A careful counting reveals that the number of vertices in the dual representation excluding the artificial vertices reaches $4 \cdot 11 \cdot 11 - 9 \cdot 11 - 9 \cdot 11 + 26 = 312$, which is the number of facets of the Minkowski sum.

Not every pair of polytopes yields a Minkowski sum proportional to $mn$. As a matter of fact, it can be as low as $n$ in the extremely-degenerate case of two identical polytopes variant under scaling. Even if no degeneracies exist, the complexity can be proportional to

[3]The results of all rotations are approximate, as we have not yet dealt with exact rotation. One of our future goals is the handling of exact rotations.

only $m + n$, as in the case of two geodesic spheres[4] level $l = 2$ slightly rotated with respect to each other, depicted in Figure 3.10. Naturally, an algorithm that accounts for all pairs of vertices, one from each polytope, is rendered inferior compared to an output-sensitive algorithm like ours in such cases, as we demonstrate in the next section.

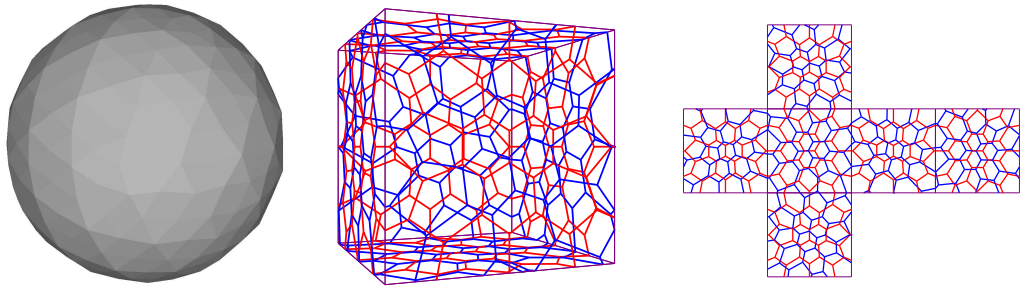

(a) (b) (c)

Figure 3.10: (a) The Minkowski sum of two geodesic spheres level 2 slightly rotated with respect to each other, (b) the CGM of the Minkowski sum, and (c) the CGM unfolded.

## 3.6 Experimental Results

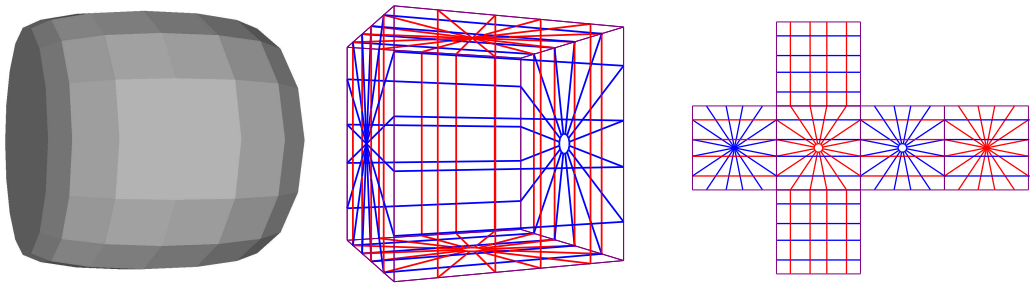

(a) (b) (c)

Figure 3.11: (a) The Minkowski sum of two approximately orthogonal squashed dioctagonal pyramids, (b) the CGM, and (c) the CGM unfolded.

As mentioned above, the Minkowski sum of two polytopes is the convex hull of the pairwise sum of the vertices of the two polytopes. We have implemented this straightforward method using the CGAL `convex_hull_3` function, which uses the `Polyhedron_3` data structure to represent the resulting polytope, and used it to verify the correctness of our two methods. We compared the time it took to compute exact Minkowski sums using our two methods, a third method implemented by Hachenberger based on Nef polyhedra embedded on the sphere [HKM07], a fourth method implemented by Weibel [28], based on an output-sensitive algorithm designed by Fukuda [Fuk04], and the naive convex-hull method.

[4] An icosahedron, every triangle of which is divided into $4^l$ triangles using class I aperture 4 partition method, whose vertices are elevated to the circumscribing sphere [SWK03].

The Nef-based method is not specialized for Minkowski sums. It can compute the overlay of two arbitrary Nef polyhedra embedded on the sphere, which can have open and closed boundaries, facets with holes, and lower dimensional features. The overlay is computed by two separate hemisphere-sweeps.

Fukuda's algorithm relies on linear programming. Its complexity is $O(\delta LP(3,\delta)V)$, where $\delta = \delta_1 + \delta_2$ is the sum of the maximal degrees of vertices, $\delta_1$ and $\delta_2$, in the two input polytopes respectively, $V$ is the number of vertices of the resulting Minkowski sum, and $LP(d,m)$ is the time required to solve a linear programming in $d$ variables and $m$ inequalities. Note that Fukuda's algorithm is more general, as it can be used to compute the Minkowski sum of polytopes in an arbitrary dimension $d$, and as far as we know, it has not been optimized specifically for $d = 3$.

Table 3.4: Complexities of primal and dual Minkowski-sum representations. DP — Dioctagonal Pyramid, ODP — Dioctagonal Pyramid orthogonal to DP, PH — Pentagonal Hexecontahedron, TI — Truncated Icosidodecahedron, GS4 — Geodesic Sphere level 4, RGS4 — Rotated Geodesic Sphere level 4, El16 — Ellipsoid-like polyhedron made of 16 latitudes and 32 longitudes, OEl16 — Ellipsoid-like polyhedron made of 16 latitudes and 32 longitudes orthogonal to El16.

| **Summand 1** | **Summand 2** | **Minkowski Sum** | | | | | | | | |
|---|---|---|---|---|---|---|---|---|---|---|
| | | **Primal** | | | **SGM** | | | **CGM** | | |
| | | **V** | **E** | **F** | **V** | **HE** | **F** | **V** | **HE** | **F** |
| Icosahedron | Icosahedron | 12 | 30 | 20 | 21 | 62 | 12 | 72 | 192 | 36 |
| DP | ODP | 131 | 261 | 132 | 141 | 540 | 131 | 242 | 832 | 186 |
| PH | TI | 248 | 586 | 340 | 429 | 1712 | 429 | 514 | 1670 | 333 |
| GS4 | RGS4 | 1048 | 2582 | 1536 | 1564 | 5220 | 1048 | 1906 | 6288 | 1250 |
| El16 | OEl16 | 2260 | 4580 | 2322 | 2354 | 9224 | 2260 | 2826 | 10648 | 2510 |

Table 3.5: Time consumption (in seconds) of the Minkowski-sum computation. **CH** — the Convex Hull method, **SGM**— the (spherical) Gaussian map based method, **CGM**— the cubical Gaussian-map based method, **NGM**— the Nef based method, **Fuk**— Fukuda's Linear-Programming based algorithm, $\frac{F_1 F_2}{F}$ — the ratio between the product of the number of input facets and the number of output facets.

| **Summand 1** | **Summand 2** | **SGM** | **CGM** | **NGM** | **Fuk** | **CH** | $\frac{F_1 F_2}{F}$ |
|---|---|---|---|---|---|---|---|
| Icosahedron | Icosahedron | 0.01 | **0.01** | 0.12 | 0.01 | 0.01 | 20.0 |
| DP | ODP | 0.04 | **0.02** | 0.33 | 0.35 | 0.05 | 2.2 |
| PH | TI | 0.13 | **0.03** | 0.84 | 1.55 | 0.20 | 10.9 |
| GS4 | RGS4 | 0.71 | **0.12** | 6.81 | 5.80 | 1.89 | 163.3 |
| El16 | OEl16 | 1.01 | **0.14** | 7.06 | 13.04 | 6.91 | 161.3 |

The results listed in Table 3.5, produced by experiments conducted on a Pentium PC clocked at 1.7 GHz, show that our methods are much more efficient in all cases, and the CGM method in particular is more than fifty times faster than the convex-hull method in one case. The number of models used as summands in the listed experiments is just a small fraction of the total number of models in our collection, which contains hundreds of models of polytopes; see Section A.2 for instructions how to download the corresponding files. The

listed experiments are just a small sample of all the experiments we have conducted. The last column of the table indicates the ratio $\frac{F_1 F_2}{F}$, where $F_1$ and $F_2$ are the number of facets of the input polytopes respectively, and $F$ is the number of facets of the Minkowski sum. As this ratio increases, the relative performance of the output-sensitive algorithms compared to the convex-hull method improves as expected. Figure 3.12 illustrates some of the resulting Minkowski sums listed in Table 3.5.

The **SGM**, **CGM**, **NGM**, and **CH** methods are all based on CGAL. As the implementation of these methods and of CGAL is generic, it is possible to instantiate specific components, such as the number type, the geometric kernel, and the segment-handling traits class with the model of the respective concept that achieves the best result. The code of the programs used to obtain the results listed in Table 3.5 are instantiated with the `CGAL::Gmpq` exact rational number-type, the `Simple_cartesian` geometric kernel, and the `Lazy_kernel` kernel adaptor, which performs lazy exact computations [PF06]. The computation is delayed until a point where the approximation with interval arithmetic is not precise enough to perform safe comparisons. In other words, these programs need only to compute to sufficient precision to evaluate predicates correctly, exploiting a significant relaxation of the naive concept of numerical exactness.

We experimented with two different exact number types: One provided by LEDA 4.4.1, namely `leda::rational`, and another based on GMP 4.1.2, namely `CGAL::Gmpq`. The former does not normalize the rational numbers automatically. Therefore, we had to initiate normalization operations to contain their bit-length growth. In case of the CGM method, for example, we chose to do it right after the central projections of the facet-normals are calculated, and before the chains of segments, which are the mapping of facet-edges, are inserted into the planar maps. Our experience shows that indiscriminate normalization considerably slows down the planar-map construction, and the choice of number type may have a drastic impact on the performance of the code overall.

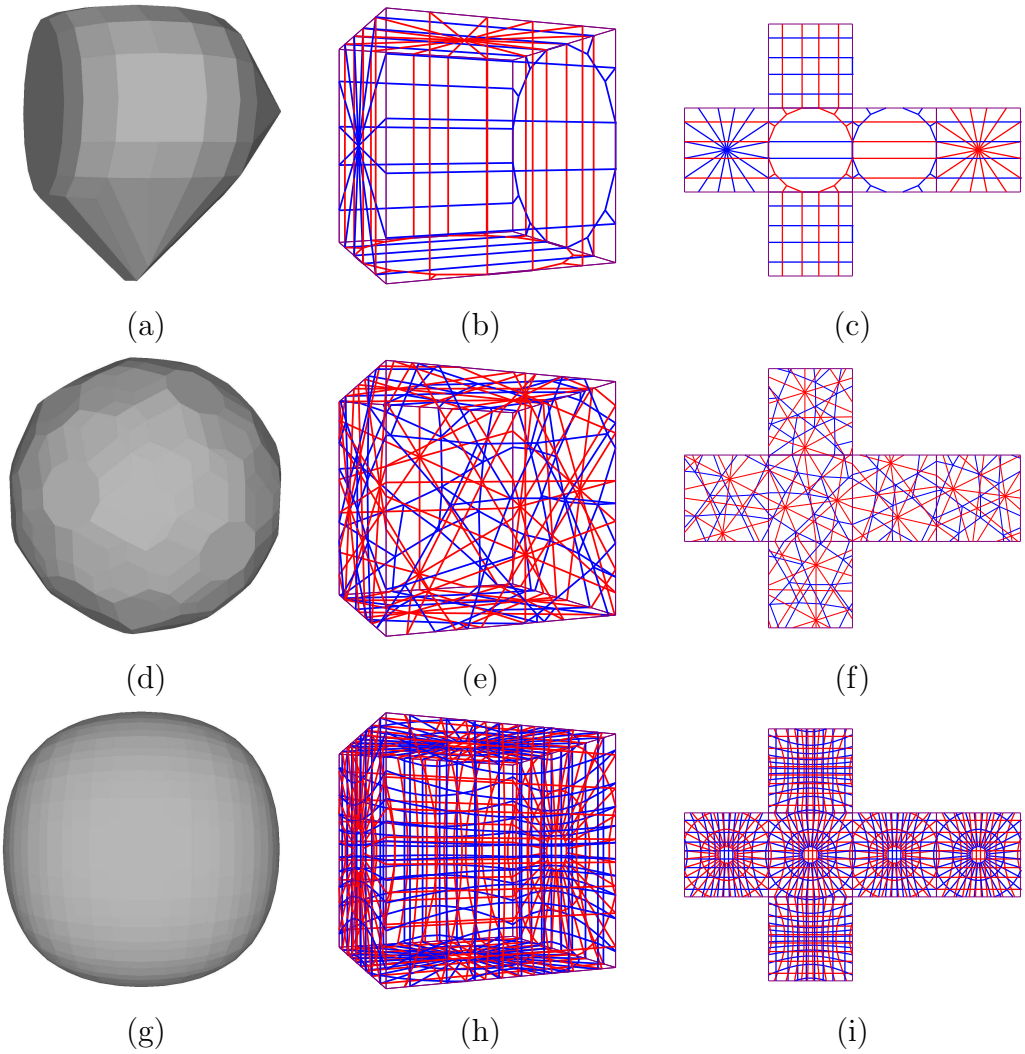


Figure 3.12: (a) The Minkowski sum of two approximately orthogonal dioctagonal pyramids, (d) the Minkowski sum of a Pentagonal Hexecontahedron and a Truncated Icosidodecahedron, (g) the Minkowski sum of two approximately orthogonal ellipsoid-like polyhedra, (b,e,h) the CGM of the respective polytope, and (c,f,i) the CGM unfolded.

*I was working on the proof of one of my poems all the morning, and took out a comma. In the afternoon I put it back again.*

Oscar Wilde

# 4

# Exact Complexity of Minkowski Sums

We present a tight bound on the exact maximum complexity of Minkowski sums of polytopes in $\mathbb{R}^3$. In particular, we prove that the maximum number of facets of the Minkowski sum of $k$ polytopes with $m_1, m_2, \ldots, m_k$ facets respectively is bounded from above by $\sum_{1\leq i<j\leq k}(2m_i - 5)(2m_j - 5) + \sum_{1\leq i\leq k} m_i + \binom{k}{2}$. Given $k$ positive integers $m_1, m_2, \ldots, m_k$, we describe how to construct two polytopes with corresponding number of facets, such that the number of facets of their Minkowski sum is exactly $\sum_{1\leq i<j\leq k}(2m_i - 5)(2m_j - 5) + \sum_{1\leq i\leq k} m_i + \binom{k}{2}$. When $k = 2$, for example, the expression above reduces to $4m_1m_2 - 9m_1 - 9m_2 + 26$. Figure 4.1 illustrates some polytopes that when rotated properly and used as summand, the number of facets of the resulting Minkowski sums is maximal.

Various methods to compute the Minkowski sum of two polyhedra in $\mathbb{R}^3$ have been proposed; see Section 1.2 for details about these methods and about the combinatorial complexity of the sum. Recall, that (i) a common approach for computing Minkowski sums

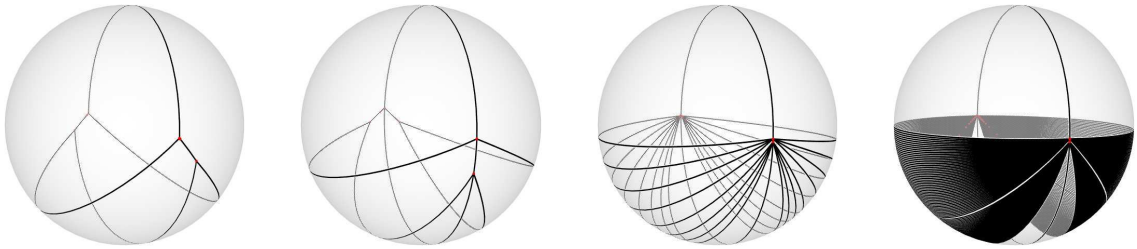

(a) (b) (c) (d)

Figure 4.1: Gaussian maps of summands of Minkowski sums with maximal number of facets. The polytopes represented by the Gaussian maps (a), (b), (c), and (d) consist of 4, 5, 11, and 101 facets, respectively.

of non-convex polyhedra decomposes each polyhedron into convex pieces, and computes pairwise Minkowski sums of the convex pieces, and (ii) all the efficient methods are output sensitive. Thus, the exact maximum complexity of the Minkowski sum structure has practical implications.

One method to compute the Minkowski sum of two polytopes is to compute the convex hull of the pairwise sum of the vertices of the two polytopes. While being simple and easy to implement, the time complexity of this method is $\Omega(mn)$ regardless of the size of the resulting sum, which can be as low as $(m+n)$ (counting facets) for degenerate cases.[1] In Chapter 3 we describe several complete implementations of output-sensitive methods for computing exact Minkowski sums (beyond the naive method mentioned above), including two methods that we introduce. These methods exploit efficient innovative techniques in the area of exact geometric computing to minimize the time it takes to ensure exact results. However, even with the use of these techniques, the amortized time of a single arithmetic operation is larger than the time it takes to carry out a single arithmetic operation on native number types, such as floating point. Thus, the constant that scales the dominant element in the expression of the time complexity of these algorithms increases, which makes the question this chapter attempts to answer, "What is the exact maximum complexity of Minkowski sums of polytopes in $\mathbb{R}^3$?", even more relevant.

Gritzmann and Sturmfels [GS93] formulated an upper bound on the number of features $f_i^d$ of any given dimension $i$ of the Minkowski sum of many polytopes in $d$ dimensions: $f_i^d(P_1 \oplus P_2 \oplus \ldots \oplus P_k) \leq 2\binom{j}{i} \sum_{h=0}^{d-i-1} \binom{j-i-1}{h}$ for $i = 0, 1, \ldots d-1$, where $j$ denotes the number of non-parallel edges of $P_1, P_2, \ldots, P_k$. According to this expression, the number of facets $f_2^3$ of the Minkowski sum of two polytopes in $\mathbb{R}^3$ is bounded from above by $j(j-1)$. Fukuda and Weibel [FW07] obtained upper bounds on the number of edges and facets of the Minkowski sum of two polytopes in $\mathbb{R}^3$ in terms of the number of vertices of the summands: $f_2^3(P_1 \oplus P_2) \leq f_0^3(P_1)f_0^3(P_2) + f_0^3(P_1) + f_0^3(P_2) - 6$. They also studied the properties of Minkowski sums of perfectly centered polytopes and their polars, and provided a tight bound on the number of vertices of the sum of polytopes in any given dimension.

The main result presented in this chapter concerning two polytopes follows.

**Theorem 4.1.** *Let $P_1, P_2, \ldots, P_k$ be a set of $k$ polytopes in $\mathbb{R}^3$, such that the number of facets of $P_i$ is $m_i$ for $i = 1, 2, \ldots, k$. The number of facets of the Minkowski sum $P_1 \oplus P_2 \oplus \ldots \oplus P_k$ cannot exceed $\sum_{1 \leq i < j \leq k} (2m_i - 5)(2m_j - 5) + \sum_{i=1}^{k} m_i + \binom{k}{2}$. This bound is tight. Namely, given $k$ integers $m_1, m_2, \ldots, m_k$, such that $m_i \geq 4$ for $i = 1, 2, \ldots, k$, it is possible to construct $k$ polytopes in $\mathbb{R}^3$ with corresponding number of facets, such that the number of facets of their Minkowski sum is exactly the expression above.*

The rest of this chapter is organized as follows. The upper bound on the number of facets of Minkowski sums for the special case of two polytopes in $\mathbb{R}^3$ is derived in Section 4.1. In Section 4.2 we describe how to construct two polytopes, the number of facets of which is given, such that the number of facets of their Minkowski sum is identical to the bound derived in Section 4.1. The bounds for the general case of $k$ polytopes is proved in Section 4.3.

[1] It can be as low as $m(=n)$ in the extremely-degenerate case of two similar polytopes with parallel facets.

Information about the polyhedra models and the interactive program that computes their Minkowski sums and visualizes them, used to verify the results and generate the figures in this chapter are provided in the Appendix.

## 4.1 The Upper Bound for $k = 2$

The overlay (see Section 2.4.2 for the exact definition) of the Gaussian maps (see Section 3.1 for the exact definition) of two polytopes $P$ and $Q$ respectively is the Gaussian map of the Minkowski sum of $P$ and $Q$; see Section 3.2.2 for a detailed explanation.

The number of facets of the Minkowski sum $M$ of two polytopes $P$ and $Q$ with $m$ and $n$ facets respectively is equal to the number of vertices of the Gaussian map $G(M)$ of $M$. A vertex in $G(M)$ is either due to a vertex in the Gaussian map of $P$, or due to a vertex in the Gaussian map of $Q$, or due to an intersection of exactly two edges, one of the Gaussian map of $P$ and the other of the Gaussian map of $Q$. Thus, the number of facets of $M$ cannot exceed $m+n+g(M)$, where $g(M)$ is the number of intersections of edges of $G(P)$ with edges of $G(Q)$ in $G(M)$.[2]

**Observation 4.2.** *The maximum exact number of edges in a Gaussian map $G(P)$ of a polytope $P$ with $m$ facets is $3m-6$. The maximum exact number of faces is $2m-4$. Both maxima occur at the same Gaussian maps.*

The above can be obtained by a simple application of Euler's formula for planar graphs to the Gaussian map $G(P)$. It can be used to trivially bound the exact maximum number of facets of the Minkowski sum of two polytopes defined as $f(m,n) = \max\{f(P \oplus Q) \mid f(P) = m, f(Q) = n\}$, where $f(P)$ is the number of facets of a polytope $P$. First, we can use the bound on the number of edges to obtain: $f(m,n) \leq m + n + (3m-6)\cdot(3n-6) = 9mn - 17m - 17n + 36$. Better yet, we can plug the bound on the number of dual faces, which is the number of primal vertices, in the expression introduced by Fukuda and Weibel, see above, to obtain: $f(m,n) \leq (2m-4)\cdot(2n-4)+(2m-4)+(2n-4)-6 = 4mn-6m-6n+2$. Still, we can improve the bound even further, but first we need to bound the number of faces in $G(M)$.

**Lemma 4.3.** *Let $G_1$ and $G_2$ be two Gaussian maps of convex polytopes, and let $G$ be their overlay. Let $f_1$, $f_2$, and $f$ denote the number of faces of $G_1$, $G_2$, and $G$, respectively. Then, $f \leq f_1 \cdot f_2$.*

Each face in the overlay is an intersection of a face of each map. Since these faces are spherically convex (and smaller than hemispheres), the intersection is also spherically convex (and thus connected). This lemma is similar to the one where convex planar maps replace the Gaussian maps. Nevertheless, we provide a formal proof directly applied to the spherical case.

*Proof.* We label each face in $G$ by a pair of indices of the originating overlaid faces in $G_1$ and $G_2$ respectively, and argue that no two faces in $G$ can have the same label. Assume to

[2]The number of facets is strictly equal to the given expression, only when no degeneracies occur.

the contrary that there exist two faces $h_a$ and $h_b$ in $G$ that have the same label, say $\langle i, j\rangle$. That is, the faces $h_1^i$ in $G_1$ and $h_2^j$ in $G_2$ induce the two distinct faces $h_a$ and $h_b$. Pick two points $a \in h_a$ and $b \in h_b$. There must be a geodesic segment between $a$ and $b$ that is entirely contained in $h_1^i$ and also in $h_2^j$, as both maps are spherically convex. This implies that none of the edges in $G_1$ and $G_2$ split this geodesic segment, contradicting the fact that they reside in two different faces of $G$. □

We are ready to tackle the upper bound of Theorem 4.1 for the special case $k = 2$, that is, prove that the number of facets of the Minkowski sum $P \oplus Q$ of two polytopes $P$ and $Q$ with $m$ and $n$ facets respectively cannot exceed $4mn - 9m - 9n + 26$; see Page 66.

*Proof.* Let $v_1, e_1, f_1$ and $v_2, e_2, f_2$ denote the number of vertices, edges, and faces of $G(P)$ and $G(Q)$, respectively. The number of vertices, edges, and faces of $G(M)$ is denoted as $v$, $e$, and $f$, respectively. Assume that $P$ and $Q$ are two polytopes, such that the number of facets of their Minkowski sum is maximal. Recall that the number of facets of a polytope is equal to the number of vertices of its Gaussian map. Thus, we have $v_1 = m$, $v_2 = n$, and $v = f(m, n)$. First, we need to show that vertices of $G(P)$, vertices of $G(Q)$, and intersections between edges of $G(P)$ and edges of $G(Q)$ do not coincide. Assume to the contrary that some do. Then, one of the polytopes $P$ or $Q$ or both can be slightly rotated to escape this degeneracy, but this would increase the number of vertices $v = f(m, n)$, contradicting the fact that $f(m, n)$ is maximal. Therefore, the number of vertices $v$ is exactly equal to $v_1 + v_2 + v_x$, where $v_x$ denotes the number of intersections of edges of $G(P)$ and edges of $G(Q)$ in $G(M)$. Counting the degrees of all vertices in $G(M)$ implies that $2e_1 + 2e_2 + 4v_x = 2e$. Using Euler's formula, we get $e_1 + e_2 + 2v_x = f + v_1 + v_2 + v_x - 2$. Applying Lemma 4.3, we can bound $v_x$ from above $v_x \leq f_1 f_2 + v_1 + v_2 - 2 - e_1 - e_2$.

Observation 4.2 sets an upper bound on the number of edges $e_1$. Thus, $e_1$ can be expressed in terms of $\ell_1$, a non-negative integer, as follows: $e_1 = 3v_1 - 6 - \ell_1$. Applying Euler's formula, the number of facets can be expressed in terms of $\ell_1$ as well: $f_1 = e_1 + 2 - v_1 = 2v_1 - 4 - \ell_1$. Similarly, we have $e_2 = 3v_2 - 6 - \ell_2$ and $f_2 = 2v_2 - 4 - \ell_2$ for some non-negative integer $\ell_2$.

$$\begin{aligned} v_x &\leq (2v_1 - 4 - \ell_1)(2v_2 - 4 - \ell_2) + v_1 + v_2 - 2 - (3v_1 - 6 - \ell_1) - (3v_2 - 6 - \ell_2) \\ &\leq 4v_1v_2 - 10v_1 - 10v_2 + 26 + h(\ell_1, \ell_2) \ , \end{aligned} \tag{4.1}$$

where $h(\ell_1, \ell_2) = \ell_1\ell_2 + 5\ell_1 + 5\ell_2 - 2v_1\ell_2 - 2v_2\ell_1$.

$G(P)$ consists of a single connected component. Therefore, the number of edges $e_1$ must be at least $v_1 - 1$. This is used to obtain an upper bound on $\ell_1$ as follows: $v_1 - 1 \leq e_1 = 3v_1 - 6 - \ell_1$, which implies $\ell_1 \leq 2v_1 - 5$, and similarly $\ell_2 \leq 2v_2 - 5$. Thus, we have:

$$\begin{aligned} h(\ell_1, \ell_2) &= \ell_1\ell_2 + 5\ell_1 + 5\ell_2 - 2v_1\ell_2 - 2v_2\ell_1 \\ &= \ell_1\left(\frac{\ell_2}{2} - (2v_2 - 5)\right) + \ell_2\left(\frac{\ell_1}{2} - (2v_1 - 5)\right) \leq 0 \ . \end{aligned}$$

From Equation (4.1) we get that $v_x \leq 4v_1v_2 - 10v_1 - 10v_2 + 26$, and since $f(m, n) = v_1 + v_2 + v_x$, we conclude that $f(m, n) \leq 4v_1v_2 - 9v_1 - 9v_2 + 26$. The maximum number of facets can be reached when $h(\ell_1, \ell_2)$ vanishes. This occurs when $\ell_1 = \ell_2 = 0$. That is, when

the number of edges of $G(P)$ and $G(Q)$ is maximal. This concludes the proof of the upper bound of Theorem 4.1 for the special case $k = 2$. □

**Corollary 4.4.** *The maximum number of facets can be attained only when the number of edges of each of $P$ and $Q$ is maximal for the given number of facets.*

## 4.2 The Lower Bound for $k = 2$

Given two integers $m \geq 4$ and $n \geq 4$, we describe how to construct two polytopes in $\mathbb{R}^3$ with $m$ and $n$ facets respectively, such that the number of facets of their Minkowski sum is exactly $4mn - 9m - 9n + 26$, establishing the lower bound of Theorem 4.1 for the special case $k = 2$. More precisely, given $i$, we describe how to construct a skeleton of a polytope $P_i$ with $i$ facets, $3i - 6$ edges, and $2i - 4$ vertices, and prove that the number of facets of the Minkowski sum of $P_m$ and $P_n$, properly adjusted and oriented, is exactly $4mn-9m-9n+26$. As in the previous sections we mainly operate in the dual space of Gaussian maps. However, the construction of the desired Gaussian maps described below is an involved task, since not every arrangement of arcs of great circles embedded on the unit sphere, the faces of which are convex and the edges of which are strictly less than $\pi$ long constitutes a valid Gaussian map.

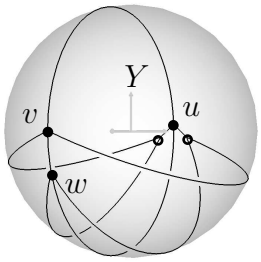


We defer the treatment of the special case $i = 4$ to the sequel, and start with the general case $i \geq 5$. The figure to the right depicts the Gaussian map of $P_5$. We use the subscript letter $i$ in all notations $X_i$ to identify some object $X$ with the polytope $P_i$. For example, we give the Gaussian map $G(P_i)$ of $P_i$ a shorter notation $G_i$, but in this paragraph we omit the subscript letter in all notations for clarity. First, we examine the structure of the Gaussian map $G$ of $P$ to better understand the structure of $P$. Let $V$ and $E$ denote the set of vertices and edges of $G$, respectively. Recall that the number of vertices, edges, and faces of $G$ is $i$, $3i - 6$, and $2i - 4$, respectively. The unit sphere, where $G$ is embedded on, is divided by the plane $y = 0$ into two hemispheres $H^- \subset \{(x, y, z) \,|\, y \leq 0\}$ and $H^+ \subset \{(x, y, z) \,|\, y > 0\}$. Three vertices, namely $u$, $v$, and $w$, lie in the plane $x = 0$. $u$ is located very close to the pole $(0, 0, -1)$. It is the only vertex (out of the $i$ vertices) that lies in $H^+$. $v$ is located exactly at the opposite pole $(0, 0, 1)$, and $w$ lies in $H^-$ very close to $v$. None of the remaining $i - 3$ vertices in $V \setminus \{u, v, w\}$ lie in the plane $x = 0$; they are all concentrated near the pole $(0, 0, -1)$ and lie in $H^-$. The edge $\overline{uv}$, which is contained in the plane $x = 0$, is the only edge whose interior is entirely contained in $H^+$. Every vertex in $V \setminus \{u, v, w\}$ is connected by two edges to $v$ and $w$, respectively. These edges together with the edge $\overline{uw}$, contained in the plane $x = 0$, form a set of $2i - 5$ edges, denoted as $E' = E \setminus \{\overline{uv}\}$. The length of each of the edges in $E'$ is almost $\pi$, due to the near proximity of $u$, $v$, and $w$ to the respective poles.

It is easy to verify that if the polytope $P$ is not degenerate, namely, its affine hull is 3-space, then any edge of $G(P)$ is strictly less than $\pi$ long. Bearing this in mind, the main difficulty in arriving at a tight-bound construction is forcing sufficient edges of the set $E'$ of the Gaussian map of one polytope to intersect sufficient edges of the set $E'$ of the Gaussian map of the other polytope. The remaining pair of edges, one from each Gaussian map,

contributes a single intersection to the total count. As shown below, this is the best one can do in terms of intersections.

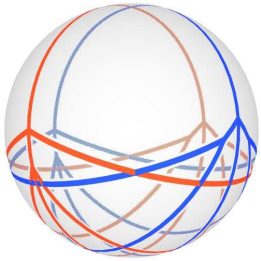

Figure 4.2: The overlay of $G_5$ and $G'_5$, where $G'_5$ is $G_5$ rotated 90° about the $Y$ axis.

The number of facets of the Minkowski sum of $P_m$ and $P_n$ is maximal, when the number of vertices in the overlay of $G_m$ and $G_n$ is maximal. This occurs, for example, when one of them is rotated 90° about the $Y$ axis, as depicted on the left for the case of $m = n = 5$. In this configuration, all the $2m - 5$ edges in $E'_m$ intersect all the $2n - 5$ edges in $E'_n$. All intersections occur in $H^-$. In addition, the edge $\overline{uv}_m$ intersects the edge $\overline{uv}_n$. The intersection point lies in $H^+$ exactly at the pole $(0, 1, 0)$. Counting all these intersections results with $(2m - 5)(2n - 5) + 1 = 4mn - 10m - 10n + 26$. Adding the original vertices of $G(P_m)$ and $G(P_n)$, yields the desired result.

Next, we explain how $P_i, i \geq 5$ is constructed to match the description of $G_i$ above. The construction of $P_i$ is guided by a cylinder. All the vertices of $P_i$ lie on the boundary of a cylinder the axis of which coincides with the $Z$ axis. We start with the case $i = 5$, and show how to generalize the construction for $i > 5$. The special case $i = 4$ is explained last.

### 4.2.1 Constructing $P_5$

Figure 4.3 shows various views of $P_5$. Recall that $P_5$ has 6 vertices, denoted as $v_0, v_1, \ldots, v_5$, and 9 edges. We omit the subscript digit 5 in all the notations through the rest of this subsection for clarity. Let $\overline{v_1 v_2 \ldots v_n}$ denote the face defined by the sequence of vertices $v_1, v_2, \ldots, v_n$ on the face boundary. The projection of all vertices onto the plane $z = 0$ lie on the unit circle. As a matter of fact, the entire face $f^v = \overline{v_0 v_1 v_2 v_3}$ lies in the plane $z = 0$. It is mapped under $G$ to the vertex $v = G(f^v)$. Similarly, the faces $f^u = \overline{v_5 v_4 v_2 v_1}$ and $f^w = \overline{v_3 v_4 v_5 v_0}$ are mapped under $G$ to the vertices $u = G(f^u)$ and $w = G(f^w)$, respectively. Consider the projection of the vertices onto the plane $z = 0$ best seen in Figure 4.3(b). Once the projection $v'_5$ of $v_5$ is determined as explained below, $v_0$ is placed exactly on the bisector of $\angle v'_5 o v_1$. The vertices $v_4$, $v_3$, and $v_2$ are the reflection of the vertices $v_5$, $v_0$, and $v_1$ respectively through the plane $x = 0$.

Two parameters govern the exact placement of $v_5$ (and $v_4$). One is the size of the exterior-dihedral angle at the edge $\overline{v_0 v_3}$, denoted as $\alpha$, that is, the length of the geodesic-segment that is the mapping of the edge $\overline{vw}$ of $G$. This angle is best seen in Figure 4.3(c). Notice, that the $Z$ axis is scaled up for clarity, and the angle in practice is much smaller. The other parameter is the size of the angle $\beta = \angle v'_4 o v'_5$, where $v'_4$ and $v'_5$ are the projections of $v_4$ and $v_5$ respectively onto the plane $z = 0$. This is best seen in Figures 4.3(b) and (e). Given $m$ and $n$, these angles for each of $P_m$ and $P_n$ depend on both $m$ and $n$. For large values of $m$ and $n$ the values of $\alpha$ and $\beta$ should be small. For example, setting $\alpha = \beta = 10°$ is sufficient for the case $m = n = 5$ depicted in Figure 4.2. The actual setting is discussed below after the description of the general case $i > 5$.

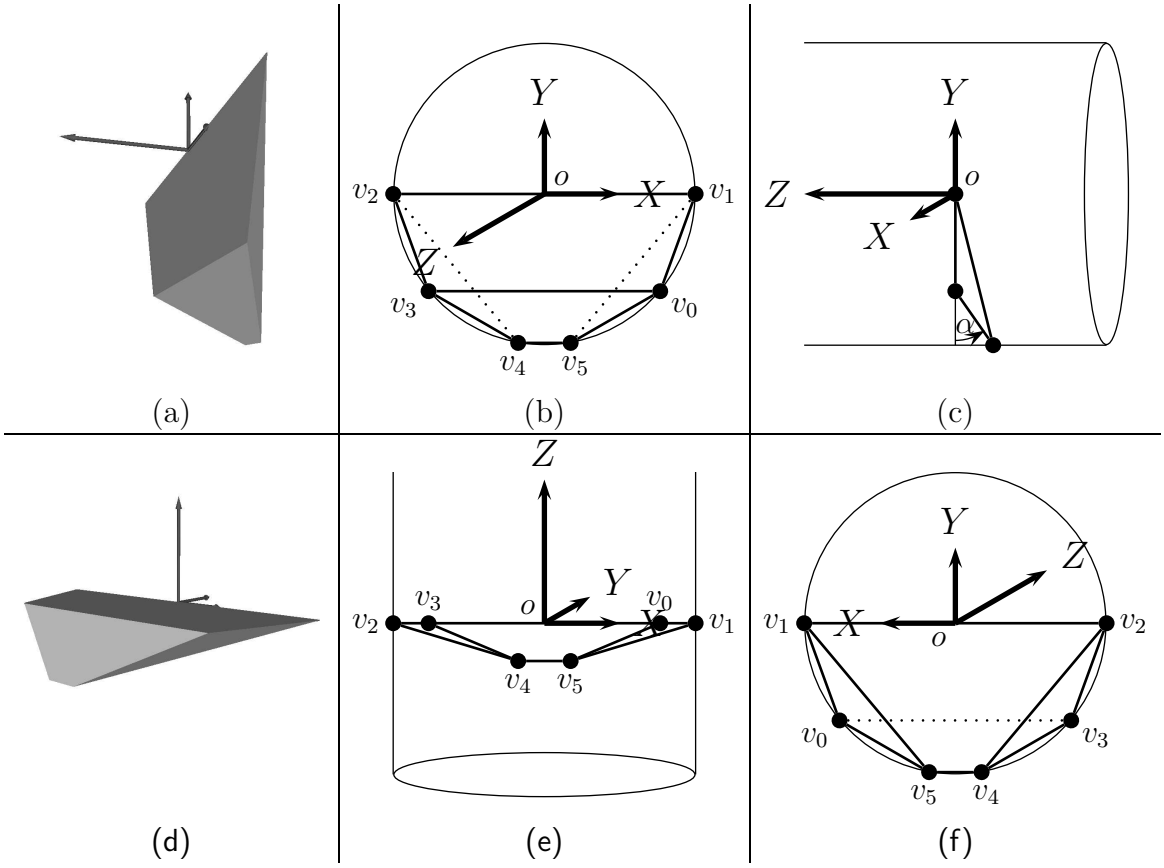


Figure 4.3: Different views of $P_5$. (a) and (d) are perspective views, while (b), (c), (e), and (f) are orthogonal views. Notice that the $Z$ axis is scaled up for clarity.

### 4.2.2 Constructing $P_i, i \geq 5$

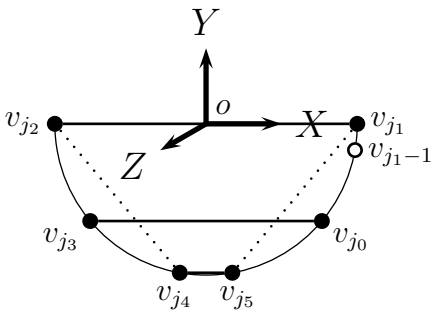


We construct a polytope, such that two facets are visible when looked at from $z = \infty$, and $i-2$ facets are visible when looked at from $z = -\infty$. First, we place the projection of all vertices onto the plane $z = 0$ along the unit circle, and denote the projection of a vertex $v$ as $v'$. The projection of the vertices $v_{j_0}$, $v_{j_1}$, $v_{j_2}$, $v_{j_3}$, $v_{j_4}$, and $v_{j_5}$, where $j_0 = 0$, $j_1 = \lfloor (i-2)/2 \rfloor$, $j_2 = \lfloor (i-2)/2 \rfloor + 1$, $j_3 = i-2$, $j_4 = \lfloor (3i-7)/2 \rfloor$, and $j_5 = \lfloor (3i-7)/2 \rfloor + 1$, are placed at the same locations as those of the corresponding vertices of $P_5$, as depicted on the right. The projection of the remaining vertices are placed on the arcs $\widehat{v'_{j_5}, v_{j_0}}$, $\widehat{v_{j_0}, v_{j_1}}$, $\widehat{v_{j_2}, v_{j_3}}$, and $\widehat{v_{j_3}, v'_{j_4}}$ in cyclic order.

The angle $\gamma = \angle v_{j_0} o v_{j_1-1}$ is another parameter that governs the final configuration of $P_i$. Once the placement of the projection of $v_{j_1-1}$ is determined, the projections of the vertices $v_{j_0+1}, v_{j_0+2}, \ldots, v_{j_1-2}$ are arbitrarily spread along the open arc $\widehat{v_{j_0}, v_{j_1-1}}$. The vertex placement along the arc $\widehat{v'_{j_5}, v_{j_0}}$ must be a symmetric reflection of the vertex placement along the arc $\widehat{v_{j_0}, v_{j_1}}$. This guarantees that all the quadrilateral facets are planar. Similarly, the

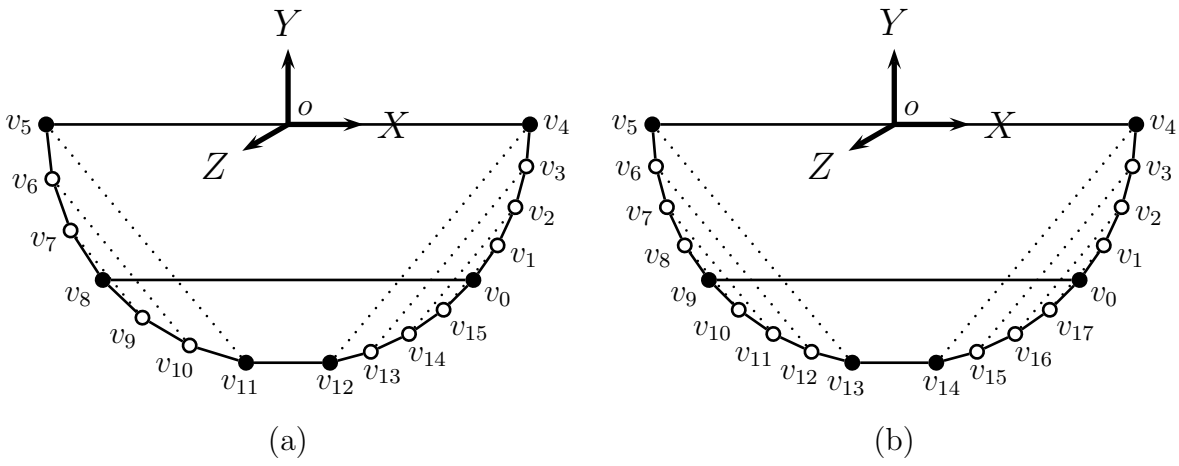


Figure 4.4: (a) An orthogonal view of $P_{10}$. (b) An orthogonal view of $P_{11}$.

vertex placement along the arc $\widehat{v_{j_2}, v_{j_3}}$ is a symmetric reflection of the vertex placement along the arc $\widehat{v_{j_3}, v'_{j_4}}$. For large values of $m$ and $n$ the angle $\gamma$ should be small as explained below, implying that the projection of the vertices are concentrated near $v_{j_0}$ and $v_{j_3}$, (which lie on the bisectors of $\angle v_{j_1} o v'_{j_5}$ and $\angle v_{j_2} o v'_{j_4}$, respectively). Figure 4.4 depicts the cases $i = 10$, and $i = 11$. In these examples we force a regular placement, which is sufficient in many cases. As in the case of $i = 5$, the face $f_i^v = \overline{v_0, v_1, \ldots, v_{i-2}}$, represented by the vertex $v_i$ of $G_i$, lies in the plane $z = 0$. The exterior-dihedral angle $\alpha$ at the edge $\overline{v_{j_0} v_{j_3}}$ is made small, so that the vertex $w_i$ of $G_i$ representing the adjacent face $f_i^w = \overline{v_{j_3}, v_{j_3+1}, \ldots, v_{2i-5}, v_0}$, is kept in close proximity to $v_i$.

Given $m$ and $n$, three parameters per polytope listed below govern the final configurations of $P_m$ and $P_n$.

1. the exterior-dihedral angle $\alpha$ at the edge $\overline{v_{j_0} v_{j_3}}$,
2. the angle $\beta = \angle v'_{j_4} o v'_{j_5}$, and
3. the angle $\gamma = \angle v_{j_0} o v_{j_1 - 1}$.

The settings of these angles must satisfy certain conditions, which in turn enable all the necessary intersections of edges in the Gaussian map of the Minkowski sum. We denote the face $\overline{v_{j_5+1} v_{j_5} v_{j_1} v_{j_1-1}}$ adjacent to $f^u$ by $f^x$. The vertex $x = G(f^x)$ is the nearest vertex to $u$. The $y$-coordinate of the vertex $w_n$ must be greater than the $y$-coordinate of the edge $\overline{xv}_m$ at $z = 0$ in $P_m$'s coordinate system. Similarly, the $y$-coordinate of the vertex $w_m$ must be greater than the $y$-coordinate of the edge $\overline{xv}_n$ at $z = 0$ in $P_n$'s coordinate system.[3] This is best seen in Figure 4.5(c). The values of the $y$-coordinates of $w_n$ and $w_m$ are simply $\sin(\alpha_n)$ and $\sin(\alpha_m)$, respectively. The value of the $y$-coordinate of the edge $\overline{xv}_m$ at $z = 0$ however depends on all the three parameters $\alpha_m$, $\beta_m$, and $\gamma_m$. Similarly, the $y$-coordinate of the edge $\overline{xv}_n$ at $z = 0$ in the respective coordinate system depends on $\alpha_n$, $\beta_n$, and $\gamma_n$. Instead of deriving an expression that directly evaluates these $y$-coordinates, we suggest an iterative procedure that decreases the angles at every iteration until the conditions above are met, and argue that this procedure eventually terminates, because at the limit, we are back at the case where $m = n = 5$, for which valid settings exist.

[3]The rotation of, say $P_n$, is performed about the $Y$ axis. Thus, it has no bearing on $y$-coordinates.

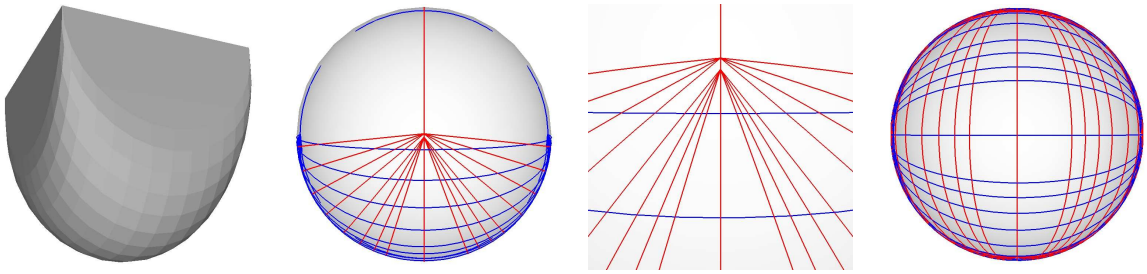

(a) (b) (c) (d)

Figure 4.5: (a) The Minkowski sum $M_{11,11} = P_{11} \oplus P'_{11}$, where $P'_{11}$ is $P_{11}$ rotated 90° about the $Y$ axis. (b) The Gaussian map of $M_{11,11}$ looked at from $z = \infty$. (c) A scaled up view of the Gaussian map of $M_{11,11}$ looked at from $z = \infty$. (d) The Gaussian map of $M_{11,11}$ looked at from $y = -\infty$.

### 4.2.3 Constructing $P_4$

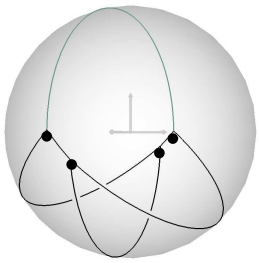

Recall that $P_4$ has 4 facets, 6 edges, and 4 vertices. Therefore, it cannot be constructed according to the prescription provided in the previous section. Applying the same principles though, we place two vertices of $G_4$ near the pole $(0, 0, -1)$, and two vertices near the opposite pole $(0, 0, 1)$. One edge, which connects a vertex near one pole to a vertex near the other, lightly shaded in the figure on the left, is entirely contained in $H^+$. The other three edges that connect vertices near opposite poles mostly lie in $H^-$. They form a set of $2i - 5 = 3$ edges, denoted as $E'_4$. The length of every edge in $E'_4$ is almost $\pi$. In contrast to the case $i \geq 5$, two out of the three edges in $E'_4$ cross the plane $y = 0$. Namely, small sections of them lie in $H^+$. As in the case $i > 4$, one edge, the lightly shaded one, is entirely contained in $H^+$.

We construct $P_4$, such that the two facets $f^1 = \overline{v_0v_1v_2}$ and $f^2 = \overline{v_0v_2v_3}$ are visible when looked at from $z = \infty$, and when looked at from $z = -\infty$, the remaining two facets $f^3 = \overline{v_3v_1v_0}$ and $f^4 = \overline{v_3v_2v_1}$ are visible. As depicted on the right, the projection of all four vertices onto the plane $z = 0$ lie on the unit circle. The vertices $v_0$ and $v_2$ lie on the plane $z = 0$, and the vertices $v_1$ and $v_3$ lie in a parallel plane. The distance between the planes is small to form small exterior-dihedral angles at the edges $\overline{v_0v_2}$ and $\overline{v_1v_3}$.

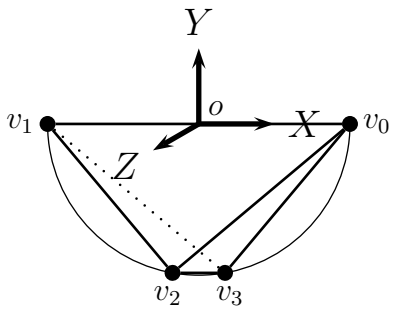


As in the general case, two parameters govern the exact placement of $v_1$, $v_2$, and $v_3$. One is the size of the exterior-dihedral angle at the edge $\overline{v_0v_2}$. The other parameter is the size of the angle $\angle v_2ov'_3$, where $v'_3$ is the projection of $v_3$ onto the plane $z = 0$. The sizes of these angles are determined by the same rationale as in the general case.

This concludes the proof of the lower bound of Theorem 4.1 for the special case $k = 2$.

## 4.3 Maximum Complexity of Minkowski Sums of Many Polytopes

Let $P_1, P_2, \ldots, P_k$ be a set of $k$ polytopes in $\mathbb{R}^3$, such that the number of facets of $P_i$ is $m_i$ for $i = 1, 2, \ldots, k$. In this section we present a tight bound on the number of facets of the Minkowski sum $M = P_1 \oplus P_2 \oplus \ldots \oplus P_k$ generalizing the arguments presented above for $k = 2$.

### 4.3.1 The Lower Bound

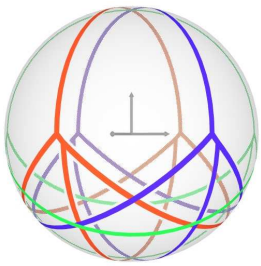

Figure 4.6: The overlay of the Gaussian maps of three tetrahedra rotated about the $Y$ axis $0°$, $60°$, and $120°$, respectively.

Given $k$ positive integers $m_1, m_2, \ldots, m_k$, such that $m_i \geq 4$, we describe how to construct $k$ polytopes in $\mathbb{R}^3$ with corresponding number of facets, such that the number of facets of their Minkowski sum is exactly $\sum_{1 \leq i < j \leq k}(2m_i - 5)(2m_j - 5) + \binom{k}{2} + \sum_{i=1}^{k} m_i$. More precisely, given $i$, we describe how to construct a skeleton of a polytope $P_i$ with $i$ facets, $3i - 6$ edges, and $2i - 4$ vertices, and prove that the number of facets of the Minkowski sum $M = P_1 \oplus P_2 \oplus \ldots \oplus P_k$ of the $k$ polytopes properly adjusted and oriented is exactly the expression above. We use the same construction described in Section 4.2.

The number of facets in the Minkowski sum of $P_i, i = 1, 2, \ldots, k$ is maximal, when the number of vertices in the overlay of $G_i, i = 1, 2, \ldots, k$ is maximal. This occurs, for example, when $G_i$ is rotated $180°(i-1)/k$ about the $Y$ axis for $i = 1, 2, \ldots, k$, as depicted on the left for the case of $m_1 = m_2 = m_3 = 4$. (Recall, that $E_i'$ refers to the set of edges that span the lowest hemispheres, and its cardinality is smaller than cardinality of $E$ by one.) In this configuration, all the $2m_i - 5$ edges in $E_i'$ intersect all the $2m_j - 5$ edges in $E_j'$, for $1 \leq i < j \leq k$. All intersections occur in $H^-$. In addition, the edge $\overline{uv}_{m_i}$ intersects the edge $\overline{uv}_{m_j}$ for $1 \leq i < j \leq k$. These intersection points lie in $H^+$ near the pole $(0, 1, 0)$. Counting all these intersections results with $\sum_{1 \leq i < j \leq k}(2m_i - 5)(2m_j - 5) + \binom{k}{2}$. Adding the original vertices of $G(P_i), i = 1, 2, \ldots, k$, yields the bound asserted in Theorem 4.1.

### 4.3.2 The Upper Bound

We can apply the special case $k = 2$ of Theorem 4.1 to obtain

$$\begin{aligned} f(m_1, m_2, \ldots, m_k) &\leq f(m_1, f(m_2, m_3, \ldots, m_k)) \\ &\leq 4m_1 f(m_2, m_3, \ldots, m_k) - 9m_1 - 9f(m_2, m_3, \ldots, m_k) + 26 \\ &\leq 4^k \prod_{i=1}^{k} m_i + \ldots \end{aligned}$$

However, we can apply a technique similar to the one used in Section 4.1 and improve this upper bound, but first we must extend Lemma 4.3.

**Lemma 4.5.** *Let $G_1, G_2, \ldots, G_k$ be a set of $k$ Gaussian maps of convex polytopes, and let $G$ be their overlay. Let $f_i$ denote the number of faces of $G_i$, and let $f$ denote the number of faces of $G$. Then, $f \leq \sum_{1\leq i<j\leq k} f_i f_j - (k-2)\sum_{1\leq i\leq k} f_i + (k-1)(k-2)$.*

*Proof.* Let us choose two antipodal points on the sphere $\mathbb{S}^2$, such that no arc of the overlay is aligned with them. In particular, the points are in the interior of two distinct faces. We consider these two points to be the north pole and south pole of the sphere, and define the direction *west* to be the clockwise direction when looking from the north pole toward the south pole. We define a *western-most corner* to be a pair of a face and one of its vertices, which is to the west of all of its other vertices. Apart from the two faces, which contain the poles, any face has a unique western-most corner, since no edge is aligned with the poles, and all faces of any Gaussian map are spherically convex. So for any overlay with $f$ faces, there are $f-2$ such western-most corners.

The maximal number of faces is attained when the overlay $G$ is non-degenerate. Thus, a vertex of $G$ is either the intersection of two edges of some distinct $G_i$ and $G_j$, or a vertex of some $G_i$. Therefore, a western-most corner for a face of $G$ is either a western-most corner for the overlay of some $G_i$ and $G_j$, or a western-most corner for some $G_i$, in which case it also is a western-most corner for any overlay involving $G_i$. The number of western-most corners in the Gaussian map $G_i$ is $f_i - 2$, and the maximal number of western-most corners in the overlay of some $G_i$ and $G_j$ is $f_i f_j - 2$.

We can therefore write:

$$f \leq \sum_{1\leq i<j\leq k} (f_i f_j - 2) - (k-2)\sum_{i=1}^{k}(f_i - 2) + 2.$$

This corresponds to summing the western-most corners appearing in the overlay of all pairs of Gaussian maps, and subtracting $(k-2)$ times the western-most corners appearing in all original Gaussian maps, since each of them appeared $(k-1)$ times in the first sum. Finally, we have:

$$\sum_{1\leq i<j\leq k} (f_i f_j - 2) - (k-2)\sum_{i=1}^{k}(f_i - 2) + 2 = \sum_{1\leq i<j\leq k} f_i f_j - (k-2)\sum_{i=1}^{k} f_i + (k-1)(k-2)\ .$$

□

Let $P_1, P_2, \ldots, P_k$ be $k$ polytopes in $\mathbb{R}^3$ with $m_1, m_2, \ldots, m_k$ facets, respectively. Let $G(P_i)$ denote the Gaussian map of $P_i$, and let $v_i$, $e_i$, and $f_i$ denote the number of vertices, edges, and faces of $G(P_i)$, respectively. Let $v_x$ denote the number of intersections of edges of $G(P_i)$ and edges of $G(P_j)$, $i \neq j$ in $G(M)$. Applying the same technique as in Section 4.1, that is, counting the total degrees of vertices in $G(M)$ implies that $\sum_{i=1}^{k} e_i + 2v_x = e$. Using Euler's formula, we get $\sum_{i=1}^{k} e_i + 2v_x = f + v - 2$. Applying Lemma 4.5 and respecting $v = \sum_{1\leq i\leq k} v_i + v_x$, we can bound $v_x$ from above:

$$v_x \leq \sum_{1\leq i<j\leq k} f_i f_j - (k-2)\sum_{i=1}^{k} f_i + (k-1)(k-2) + \sum_{i=1}^{k}(v_i - e_i) - 2\ . \tag{4.2}$$

According to Corollary 4.4 the maximum number of facets of the Minkowski sum of two polytopes is attained when the number of edges of each summand is maximal. We need to establish a similar property for the general case. Generalizing the derivation procedure in Section 4.1, we introduce $k$ non-negative integers $\ell_i, i = 1, 2, \ldots, k$, such that $e_i = 3v_i - 6 - \ell_i$ and $f_i = 2v_i - 4 - \ell_i$. Substituting $e_i$ in (4.2) we get:

$$\begin{aligned} v_x &\leq \sum_{1\leq i<j\leq k} f_i f_j - (k-2)\sum_{i=1}^{k} f_i + (k-1)(k-2) + \sum_{i=1}^{k}(v_i - 3v_i + 6 + \ell_i) - 2 \\ &\leq \sum_{1\leq i<j\leq k} f_i f_j - (k-2)\sum_{i=1}^{k} f_i - \sum_{i=1}^{k}(2v_i - 5) + \sum_{i=1}^{k}\ell_i + k^2 - 2k \ . \end{aligned} \tag{4.3}$$

Substituting $f_i$ in (4.3) we get:

$$\begin{aligned} v_x &\leq \sum_{1\leq i<j\leq k} (2v_i - 4 - \ell_i)(2v_j - 4 - \ell_j) - (k-2)\sum_{i=1}^{k}(2v_i - 4 - \ell_i) - \sum_{i=1}^{k}(2v_i - 5 - \ell_i) + k^2 - 2k \\ &= \sum_{1\leq i<j\leq k} (2v_i - 5)(2v_j - 5) + \binom{k}{2} + h(\ell_1, \ell_2, \ldots, \ell_k) \ , \end{aligned}$$

where

$$\begin{aligned} h(\ell_1, \ell_2, \ldots, \ell_k) &= \sum_{1\leq i<j\leq k} (\ell_i\ell_j - \ell_j(2v_i - 5) - \ell_i(2v_j - 5)) \\ &= \sum_{i=1}^{k} \ell_i(\sum_{j\neq i}(\ell_j/2 - (2v_j - 5))) \ . \end{aligned}$$

Connectivity of $G(P_i)$ implies that $\ell_i \leq 2v_i - 5$, which in turn implies that $h(\ell_1, \ell_2, \ldots, \ell_k) \leq 0$. Thus, we have:

$$v_x \leq \sum_{1\leq i<j\leq k} (2v_i - 5)(2v_j - 5) + \binom{k}{2} \ . \tag{4.4}$$

We conclude that the exact maximum number of facets of the Minkowski sum of $k$ polytopes cannot exceed $\sum_{1\leq i<j\leq k}(2m_i - 5)(2m_j - 5) + \sum_{1\leq i\leq k} m_i + \binom{k}{2}$, which completes the proof of Theorem 4.1. For example, the exact maximum number of facets of the Minkowski sum of $k$ tetrahedra is $5k^2 - k$. For $k = 2$ the expression evaluates to 18.

*Divide each difficulty into as many parts as is feasible and necessary to resolve it.*

Rene Descartes

# 5 Assembly Planning

Assembly partitioning with an infinite translation is the application of an infinite translation to partition an assembled product into two complementing subsets of parts, referred to as subassemblies, each treated as a rigid body. We present an exact implementation of an efficient algorithm based on the general framework described in [HLW00, WL94] to obtain such a motion and subassemblies given an assembly of polyhedra in $\mathbb{R}^3$. As usual, we do not assume general position. Namely, we handle degenerate input, and produce exact results. As often occurs, motions that partition a given assembly or subassembly might be isolated in the infinite space of motions. Any perturbation of the input or of intermediate results, caused by, for example, imprecision, might result with dismissal of valid partitioning-motions. In the extreme case, there is only a finite number of valid partitioning motions, as occurs in the assembly shown in Figure 5.1, no motion may be found, even though such exists. Proper handling requires significant enhancements applied to the original algorithmic framework. The implementation is based on software components introduced in Chapters 2 and 3. They

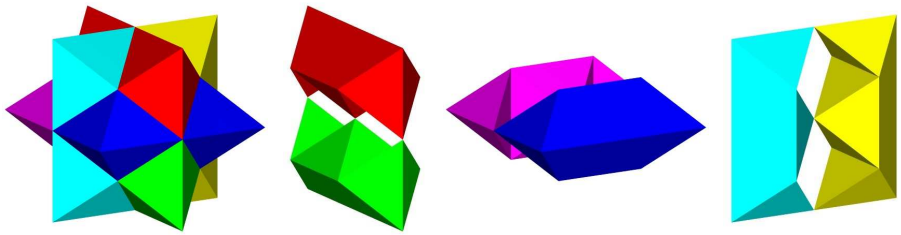

(a) (b) (c) (d)

Figure 5.1: (a) The Split Star assembly, and (b),(c), and (d) the Split Star six parts divided into three pairs of symmetric parts. The six parts are named according to their color $R$(ed), $G$(reen), $B$(lue), $P$(urple), $Y$(ellow), and $T$(urquoise).

paved the way to a complete, efficient, and concise implementation.

## 5.1 Introduction

Assembly planning is the problem of finding a sequence of motions that transform the initially separated parts of an assembly to form the assembled product. The reverse order of sequenced motions separates an assembled product to its parts. Thus, for rigid parts, assembly planning and disassembly planning refer to the same problem, and used interchangeably. In this chapter we concentrate on the case where the assembly consists of polyhedra in $\mathbb{R}^3$ and the motions are infinite translations.

The motion space is the space of possible motions that assembly parts may undergo. For each motion in a motion space, a subset of parts of a given assembly may collide with a different subassembly, when transformed as a rigid body according to the motion. Pairs of subassemblies that collide constitute constraints. The motion space approach dictates the precomputation of a decomposition of a motion space into regions, such that the constraints among the parts in the assembly are the same for all the motions in the same region. All constraints over a region are represented by a graph, called the *directional blocking graph* (DBG) [WL94]. The collection of all regions in a motion space together with their associated DBGs, collectively referred to as the *nondirectional blocking graph* (NDBG), can be used to obtain assembly (or disassembly) sequences.

The general framework and some of the techniques presented here have already been described in a series of papers and reports published in the past mainly during the late 90's. Halperin, Latombe, and Wilson made the connection between previously presented techniques that had used the motion space approach, and introduced a unified general framework [HLW00] at the end of the previous millennium. Only few publications related to this topic appeared ever since, to the best of our knowledge, which creates a long gap in the time line of the respective research. We certainly hope that the tools exposed in this chapter will help revive the research on algorithmic assembly planing, a research subject of considerable importance. Moreover, we believe that the machinery presented here, together with other recent advances in the practice of computational-geometry algorithms, can more generally support the development of new and improved techniques in *algorithmic automation* [2].

Solution to the assembly planning problem enables better feedback to designers. It provides a design team with additional tools to asses a design, prior to the construction of physical mock-ups, and helps creating products that are more cost-effective to manufacture and maintain. This is emphasized in light of the strategy to "plan anywhere, build anywhere" many Computer Aided Design (CAD) and Computer Aided Manufacturing (CAM) companies are trying to adopt. Assembly sequences are also useful for selecting assembly tools and equipment, and for laying out manufacturing facilities.

We restrict ourselves to two-handed partitioning steps, meaning that we partition the given assembly into two complementing subsets each treated as a rigid body. Even for two-handed partitioning, if we allow arbitrary translational motions (and not restrict ourselves to infinite translations) the problem is NP-hard [KK95]. The more general problem of assembly sequencing, namely planning a total ordering of assembly operations that merge

the individual parts into the assembled product, is PSPACE-hard, even when each part is a polygon with a constant number of vertices [Nat88].

Notice that the problem that we address in this chapter, namely partitioning with *infinite translations*, is technically considerably more complex than partitioning with *infinitesimal motions*. Although the latter may sound more general, as it handles infinitesimal translations and *rotations*, it is far simpler to implement, since it deals only with constraints that can be described linearly. Thus, the problem can be reduced to solving linear programs. Indeed, there are several implementations for partitioning with infinitesimal motions (see, e.g., [GHH+98, SS94]), but none that we are aware of dealing robustly with infinite translations. The shortcoming of using infinitesimal motions only is that suggested disassembly moves may not be extendible to practical finite-length separation motions.

Infinite-translation partitioning was not fully robustly implemented until recently, in spite of being more useful than infinitesimal partitioning, most probably due to the hardship of accurately constructing the underlying geometric primitives. What enables the solution that we present here, is the significant headway in the development of computational-geometry software over the past decade, the availability of stable code in the form of the Computational Geometry Algorithms Library (CGAL) in general and code for Minkowski sums and arrangements in particular [WFZH07b].

The implementation presented in this chapter is based on the `Arrangement_on_surface_2` package of CGAL; see Chapter 2 for more details. The implementation uses in particular arrangements of geodesic arcs embedded on the sphere; see Section 2.6. The ability to robustly construct such arrangements, and carry out exact operations on them using only (exact) rational arithmetic is a key property that enables an efficient implementation. The implementation exploits supported operations, and requires additional operations, e.g., central projection of polyhedra, which we implemented. We plan to make these new components available as part of a future public release of CGAL as well.

### 5.1.1 Split Star Puzzle

We use the assembly depicted in Figure 5.1 as a running example throughout the chapter. The name "Split Star" was given to this shape by Stewart Coffin in one of his Puzzle Craft booklet editions back in 1985. He uses the term *puzzle* to refer to any sort of geometric recreation having pieces that come apart and fit back together. We use it as an assembly. He describes how to produce the actual pieces out of wood [Cof06], and suggests that they are made very accurately. He observes that finding the solution requires dexterity and patience, when the pieces are accurately made with a tight fit. Even though the assembly seems relatively simple, this should come as little surprise, since the first partitioning motion is one out of only eight possible translations of four symmetric pairs of motions in opposite directions associated with two complementing subassemblies of three parts each. Evidently, any automatic process that introduces even the slightest error along the way, will most likely fail to compute the correct first motion in the sequence, and falsely claim that the assembly is interlocked.


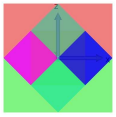


The Split Star assembly has the assembled shape of the first stellation of the rhombic dodecahedron [Luk57], illustrated atop the right pedestal in M. C. Escher's Waterfall woodcut [Boo82]. Its orthogonal projection along one of its fourfold axes of symmetry is a square, while the Star of David is obtained when it is projected along one of its threefold axes of symmetry, as seen on the left; for more details see [Cof06]. The assembly is a space-filling solid when assembled. It consists of six identical concave parts. Each part can be decomposed into eight identical tetrahedra yielding 48 tetrahedra in total. As manufacturing the pieces requires extreme precision, it is suggested to produce the 48 identical pieces and glue them as necessary. Each part can also be decomposed into three convex polytopes — two square pyramids and one octahedron, yielding 18 polytopes in total. The partitioning described in this chapter requires the decomposition of the parts into convex pieces. The choice of decomposition may have a drastic impact on the time consumption of the entire process, as observed in a different study in $\mathbb{R}^2$ [AFH02], and shown by experiments in Section 5.5.

### 5.1.2 Chapter Outline

The rest of this chapter is organized as follows. The partitioning algorithm is described in Section 5.2 along with the necessary terms and definitions. In Section 5.3 we provide implementation details. Section 5.4 presents optimizations that are not discussed in the preceding sections, some of which we have already implemented and proved to be useful. We report on experimental results in Section 5.5.

## 5.2 The Partitioning Algorithm

The main problem we address in this chapter, namely, *polyhedral assembly partitioning with infinite translations*, is formally defined as follows: Let $A = \{P_1, P_2, \ldots, P_n\}$ be a set of $n$ pairwise interior disjoint polyhedra in $\mathbb{R}^3$. $A$ denotes the assembly that we aim to partition. We look for a proper subset $S \subset A$ and a direction $\vec{d}$ in $\mathbb{R}^3$, such that $S$ can be moved as a rigid body to infinity along $\vec{d}$ without colliding with the rest of the parts of the assembly $A \setminus S$. (We allow sliding motion of one part over the other. We disallow the intersection of the interior of two polyhedra.)

We follow the NDBG approach [WL94], and describe it here using the general formulation and notation of [HLW00]. The *motion space* in our case, namely the space of all possible partitioning directions, is represented by the unit sphere $\mathbb{S}^2$. Every point $p$ on $\mathbb{S}^2$ defines the direction from the center of $\mathbb{S}^2$ towards $p$. Every direction $\vec{d}$ is associated with the directed graph $DBG(\vec{d}) = (V, E)$ that encodes the blocking relations between the parts in $A$ when moved along $\vec{d}$ as follows: The nodes in $V$ correspond to polyhedra in $A$; we denote a node corresponding to the polyhedron $P_i$ by $v(P_i) \in V$. There is an edge directed from $v(P_i)$ to $v(P_j)$, denoted $e(P_i, P_j) \in E$, if and only if the interior of the polyhedron $P_i$ intersects

the interior of the polyhedron $P_j$ when $P_i$ is moved to infinity along the direction $\vec{d}$, and $P_j$ remains stationary.

The key idea behind the NDBG approach is that in problems such as ours, where the number of parts is finite, and any allowable partitioning motion can be described by a small number of parameters, there is only a relatively small (polynomial) number of distinct DBGs that need to be constructed in order to detect a possible partitioning direction. Stated differently, the motion space can be represented by an arrangement comprising a finite number of cells each assigned with a fixed DBG. Once this arrangement is constructed, we construct the DBG over each cell of the arrangement, and check it for strong connectivity. A DBG that is not strongly connected is associated with a direction, or a set of directions in case the cell is not a singular point, that partition the given assembly. The desired movable subset $S \subset A$ is a byproduct of the algorithm that checks for strong connectivity. If all the DBGs over all the cells of the arrangement are strongly connected, we conclude that the assembly is *interlocked*, as a subset of the parts in $A$ that can be separated from the rest of the assembly by an infinite translation does not exist.

Next we show how to construct the motion-space arrangement and compute the DBG over each one of the arrangement cells. Each ordered pair of distinct polyhedra $< P_i, P_j >$ defines a region $Q_{ij}$ on $\mathbb{S}^2$, which is the union of all the directions $\vec{d}$, such that when $P_i$ is moved along $\vec{d}$ its interior will intersect the interior of $P_j$. How can we effectively compute this region? Let $M_{ij}$ denote the Minkowski sum $P_j \oplus (-P_i) = \{b - a \,|\, a \in P_i,\, b \in P_j\}$. We claim that the central projection of $M_{ij}$ onto $\mathbb{S}^2$ is exactly $Q_{ij}$.

**Lemma 5.1.** *A direction $\vec{d}$ is in the interior of the central projection of $M_{ij}$ onto $\mathbb{S}^2$ if and only if when $P_i$ is moved along $\vec{d}$ its interior will intersect the interior of $P_j$.*

*Proof.* Let $\vec{d}$ be some direction in the central projection of $M_{ij}$ onto $\mathbb{S}^2$. In other words, there exists a point $m \in M_{ij}$, such that $m = s \cdot \vec{d}$, for some positive scalar $s$. As $m$ is in $M_{ij}$, there exist two points $p_i \in P_i$ and $p_j \in P_j$, such that $m = p_j - p_i$. Thus, $p_j = p_i + s \cdot \vec{d}$, meaning that the point $p_i$ intersects $p_j$ when moved along $\vec{d}$. A similar argument can be used to show the converse. □

Next, we describe how, given two polyhedra $P_i$ and $P_j$, we compute the region $Q_{ij}$, using robust and efficient hierarchy of building blocks, which we have developed in recent years. The existing tools that we use are (i) computing the arrangement of spherical polygons [BFH$^+$07, FSH08b, FSH08a, WFZH07b], and (ii) construction of Minkowski sums of convex polytopes [BFH$^+$07, FH07, FSH08b, FSH08a]. We also need some extra machinery, as explained below.

Assume $P_i$ is given as the union of a collection of (not necessarily disjoint) convex polytopes $P_1^i, P_2^i, \ldots, P_{m_i}^i$, and similarly $P_j$ is given as the collection of convex polytopes $P_1^j, P_2^j, \ldots, P_{m_j}^j$. It is easily verified that $M_{ij} = \bigcup_{k=1,\ldots,m_i,\ell=1,\ldots,m_j} P_\ell^j \oplus (-P_k^i)$. So we compute the Minkowski sum of each pair $P_\ell^j \oplus (-P_k^i)$, and centrally project it onto $\mathbb{S}^2$. Finally, we take the union of all these projections to yield $Q_{ij}$.

There are several ways to effectively compute the central projection of a convex polyhedron $C$ (one of the polytopes $M_{k\ell}^{ij} = P_\ell^j \oplus (-P_k^i)$) from the origin onto $\mathbb{S}^2$. We opted for the

following. An edge $e$ of $C$ is called a *silhouette edge*, if the plane $\pi$ through the origin and $e$ is tangent to $C$ at $e$; namely, $\pi$ intersects $C$ in $e$ only. We assume for now that no tangent plane contains a facet of $C$; we relax this assumption in Section 5.3.5, where we provide a detailed description of the procedure. We traverse the edges of $C$ till we find a silhouette edge $e_1$. One can verify that the silhouette edges form a cycle on $C$. We start with $e_1$, and search for a silhouette edge adjacent to $e_1$. We proceed in the same manner, till we end up discovering $e_1$ again. Projecting this cycle of edges onto $\mathbb{S}^2$ is straightforward.

All the boundaries of the regions $Q_{ij}$ form an arrangement of geodesic arcs on the sphere. We traverse the motion-space arrangement in say a breadth-first fashion. For the first face we check which ones of the regions $Q_{ij}$ contain it. We construct the corresponding DBG and check it for strong connectivity. If it is not strongly connected, we stop and announce a solution as described above. Otherwise we move to an adjacent feature of the current face. During this move we may have stepped out from a set of regions $Q_{ij}$, and may have stepped into a new set of regions $Q_{ij}$. We update the current DBG according to the regions we left or entered, test the new DBG for strong connectivity, and so on till the traversal of all the arrangement cells is completed. Notice that it is important to visit also vertices and edges of the arrangement, since the solution may not lie in the interior of a face. Indeed, in our Split Star example, solutions are on vertices of the arrangement. Without careful exact constructions, such solutions could easily be missed.

## 5.3 Implementation Details

The implementation of the assembly-partitioning operation consists of eight phases listed below. They all exploit arrangements of geodesic arcs embedded on the sphere [BFH+07, FSH08a] in various ways. The `Arrangement_on_surface_2` package of CGAL already supports the construction and maintenance of such arrangements, the computation of union of faces of such arrangements, the construction of Gaussian maps of polyhedra represented by such arrangements, and the computation of their Minkowski sums. It provides the ground for efficient and generic implementation of the remaining required operations, such as central projection.

1. **Convex Decomposition**
2. **Sub-part Gaussian map construction**
3. **Sub-part Gaussian map reflection**
4. **Pairwise sub-part Minkowski sum construction**
5. **Pairwise sub-part Minkowski sum projection**
6. **Pairwise Minkowski sum projection**
7. **Motion-space construction**
8. **Motion-space processing**

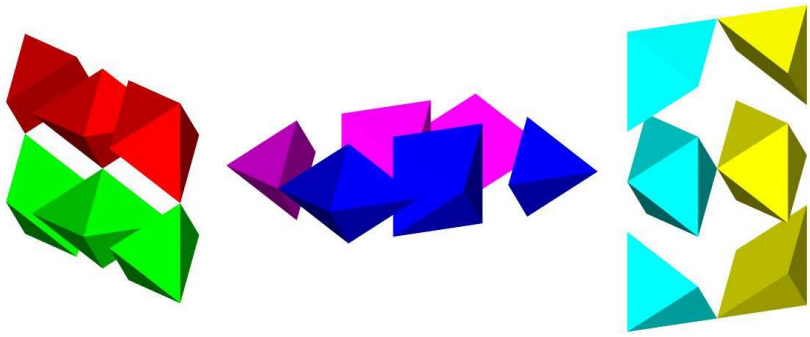

Figure 5.2: The Split Star six parts decomposed into three convex sub-parts each.

The partitioning process is implemented as a free function that accepts as input an ordered list of polyhedra in $\mathbb{R}^3$, which are the parts of the assembly. Each part is represented as a polyhedral mesh in $\mathbb{R}^3$; see Section 3.2.1 for a definition. We proceed with a detailed discussion of the implementation of each phase.

We deal below with various details that are typically ignored in reports on geometric algorithms (for example, under the general position assumption). However, in assembly planning, or more generally in movable-separability problems [Tou85] in tight scenarios, much of the difficulty shifts exactly to these technical details and in particular to handling degeneracies. This is especially emphasized in Phases 5 and 6 (Subsections 5.3.5 and 5.3.6 respectively), but prevails throughout the entire section.

### 5.3.1 Convex Decomposition

We decompose each concave part into convex polyhedra referred to as sub-parts. The output of this phase is an ordered list of parts, where each part is an ordered list of convex sub-parts represented as polyhedral surfaces. Each polyhedral surface is maintained as a CGAL `Polyhedron_3` [Ket07a] data structure, which consists of vertices, edges, and facets and incidence relations on them [Ket99]. A part that is convex to start with is simply converted into an object of type `Polyhedron_3`.

A new package of CGAL that supports convex decomposition of polyhedra has been recently introduced [Hac07], but has not become publicly available yet. As we aim for a fully automatic process, we intend to exploit such components, once they become available, and study their impact. For the time being we resorted to a manual procedure. A simple decomposition of the Split Star parts used in the running example is illustrated in Figure 5.2.

### 5.3.2 Sub-part Gaussian Map Construction

We convert each sub-part represented as a polyhedral surface into a Gaussian map represented as an arrangement of geodesic arcs embedded on the sphere, where each face $f$ of the arrangement is extended with the coordinates of its associated primal vertex $v = G^{-1}(f)$, resulting with a unique representation; see Section 3.1 for the exact definition of Gaussian

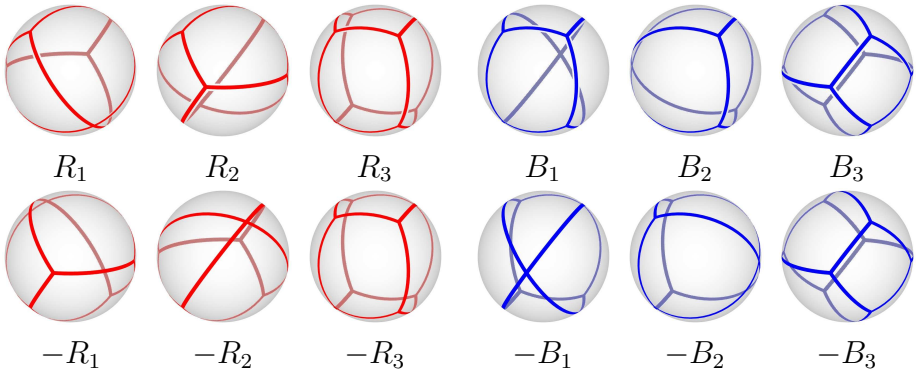


Figure 5.3: Samples of the Gaussian maps of sub-parts of the Split Star assembly. The bottom row contains the reflections of the Gaussian maps at the top row.

maps and see Section 3.2 the exact procedure to construct one from a polytope.

The output of this phase is an ordered list of parts, where each part is an ordered list of the Gaussian maps of the convex sub-parts. Figure 5.3 depicts the Gaussian maps of six of the 18 polytopes that comprise the set of sub-parts of our Split Star assembly.

### 5.3.3 Sub-part Gaussian Map Reflection

We reflect each sub-part $P_k^i$ through the origin to obtain $-P_k^i$. This operation can be performed directly on the output of the previous phase, reflecting the underlying arrangements of geodesic arcs embedded on the sphere, which represent the Gaussian maps, while handling the additional data attached to the arrangement faces. As a matter of fact, this phase can be reduced as part of an optimization discussed in Section 5.4.

The output of this phase is an ordered list of parts, where each part is an ordered list of Gaussian maps of the reflected convex sub-parts. Figure 5.3 depicts the Gaussian maps of six of the 18 polytopes that comprise the set of reflected sub-parts of the Split Star example.

### 5.3.4 Pairwise Sub-part Minkowski Sum Construction

| Construct Pairwise Sub-part Minkowski Sums |
|---|
| **for** $i$ **in** $\{1, 2, \ldots, n\}$ |
| **for** $j$ **in** $\{1, 2, \ldots, n\}$ |
| **if** $i == j$ **continue** |
| **for** $k$ **in** $\{1, 2, \ldots, m_i\}$ |
| **for** $\ell$ **in** $\{1, 2, \ldots, m_j\}$ |
| $M_{k\ell}^{ij} = P_\ell^j \oplus (-P_k^i)$ |

We compute the Minkowski sums of the pairwise sub-parts and reflected sub-parts. Aiming for an efficient output sensitive algorithm, the construction of an individual Minkowski sum from two Gaussian maps represented as two arrangements respectively is performed by overlaying the two arrangements. When the overlay operation progresses, new vertices, edges, and faces of the resulting arrangement are created based on features of the two operands. When a new feature is created its attributes are updated. There are ten cases that must be handled; see Sections 3.2.2 for details. The `Arrangement_on_surface_2` package conveniently supports the overlay operation allowing users to provide their own version of these ten operations. The overlay operation is exploited below in several different variants of arrangements of geodesic

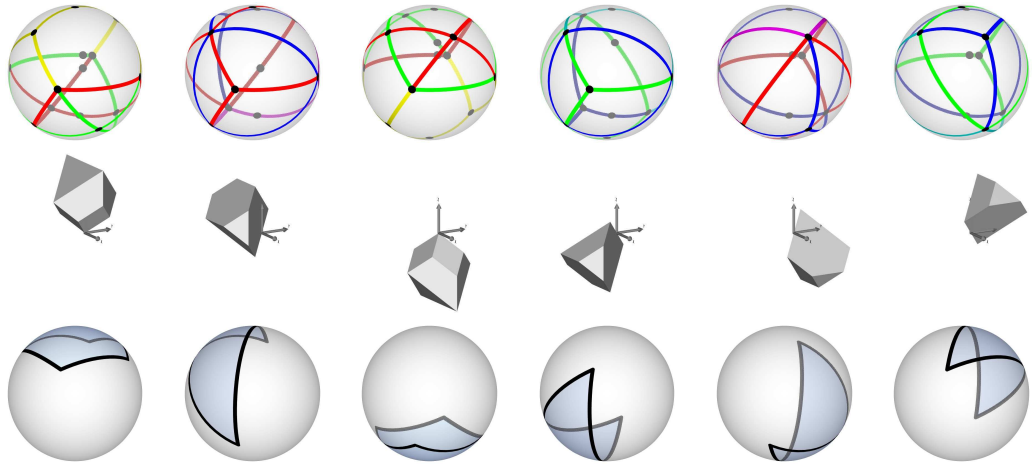


Figure 5.4: Samples of the pairwise Minkowski sums of sub-parts of the Split Star assembly. The middle row contains six Minkowski sums. The top row contains the corresponding Gaussian maps. The bottom row contains the corresponding central projection of the Minkowski sums on $\mathbb{S}^2$.

arcs embedded on the sphere. Each application requires the provision of a different set of those ten operations.

The output of this phase is a map from ordered pairs of distinct indices into lists of Minkowski sums represented as Gaussian maps. Each ordered pair $<i, j>, i \neq j$ is associated with the list of Minkowski sums $\{M_{k\ell}^{ij} \,|\, k = 1, 2, \ldots, m_i,\ \ell = 1, 2, \ldots, m_j\}$. In case of our Split Star the map consists of 30 entries that correspond to all configurations of ordered distinct pairs of parts. Each entry consists of a list of nine Minkowski sums, that is, 270 Minkowski sums in total.

### 5.3.5 Pairwise Sub-part Minkowski Sum Projection

Project Pairwise Sub-part Minkowski sums

**for** $i$ **in** $\{1, 2, \ldots, n\}$
  **for** $j$ **in** $\{1, 2, \ldots, n\}$
    **if** $i == j$ **continue**
    **for** $k$ **in** $\{1, 2, \ldots, m_i\}$
      **for** $\ell$ **in** $\{1, 2, \ldots, m_j\}$
        $Q_{k\ell}^{ij} = \text{project}(M_{k\ell}^{ij})$

We centrally project all pairwise sub-part Minkowski sums computed in the previous phase onto the sphere. Each projection is represented as an arrangement of geodesic arcs on the sphere, where each cell $c$ of the arrangement is extended with a Boolean flag that indicates whether all infinite rays emanating from the origin in all directions $\vec{d} \in c$ pierce the corresponding Minkowski sum. As the Minkowski sums are convex, their spherical projections are spherically convex.

Given a convex Minkowski sum $C$, we distinguish between four different cases as follows:

1. The origin is contained in the interior of a facet of $C$.
2. The origin lies in the interior of an edge of $C$.
3. The origin coincides with a vertex of $C$.

4. The origin is separated from $C$.

Computing the projection of a convex polytope $C$ can be done efficiently using dedicated procedures that handle the four cases, respectively. Recall that $C$ is represented as a Gaussian map, which is internally represented as an arrangement of geodesic arcs embedded on the sphere. We traverse the vertices of the arrangement. For each vertex $v$ we extract its associated primal facet $f = G^{-1}(v)$. We dispatch the appropriate computation based on the relative position of the origin with respect to the supporting plane to $f$, and the supporting plane to adjacent facets of $f$.

**If the origin is contained in the interior of a facet $f$ of $C$**, the projection of the silhouette of $C$ is a great (full) circle that divides the sphere into two hemispheres. The normal to the plane that contains the great circle is identical to the normal to the supporting plane to $f$, easily extracted from the arrangement representing the Gaussian map of $C$. The `Arrangement_on_surface_2` package conveniently supports the insertion of a great circle, provided by the normal to the plane that contains it, into an arrangement of geodesic arcs embedded on the sphere.

We omit the implementation details of the following two cases, and proceed to the general case. **If the origin is separated from $C$**, we traverse all edges of $C$ until we find a silhouette edge characterized as follows: Let $v_s$ and $v_t$ be the source and target vertices of some edge $e$ in the arrangement representing the Gaussian map of $C$, and let $f_s = G^{-1}(v_s)$ and $f_t = G^{-1}(v_t)$ be their associated primal facets, respectively. $e$ is a silhouette edge, if and only if, the origin is not in the negative side of the supporting plane to $f_s$ and not in the positive side of the supporting plane to $f_t$. We start with the first silhouette edge we find, and search for an adjacent silhouette edge in a loop, until we rediscover the first one. We project only the target vertices of significant silhouette edges, and connect consecutive projections using arcs of great circle. Let $e$ and $e'$ be adjacent silhouette edges. We skip $e$, if the projections of $e$ and $e'$ lie on the same great circle. For example, all but the last adjacent silhouette edges incident to a facet supported by a plane that contains the origin are redundant, as illustrated in the figure above. Here we skip $e_0$, $e_1$, and $e_2$, and project the target vertex of $e_3$.

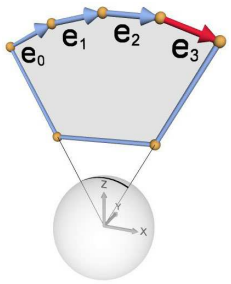


The output of this phase is a map from ordered pairs of distinct indices into lists of arrangements as described above. Each ordered pair $<i, j>, i \neq j$ is associated with the list of central projections of the pairwise Minkowski sums of $P_j$'s sub-parts and the reflection through the origin of $P_i$'s sub-parts.

### 5.3.6 Pairwise Minkowski Sum Projection

For each pair of distinct parts $P_i$ and $P_j$ we compute the union of projections of the pairwise Minkowski sums of all sub-parts of part $P_j$ and reflections of all sub-parts of part $P_i$.

The output of this phase is a map from ordered pairs of distinct indices into arrangements. Each ordered pair $<i, j>, i \neq j$ is associated with a single arrangement extended as described above, that represents the central projection $Q_{ij}$ of $M_{ij} = P_j \oplus (-P_i)$.

```
Unite Pairwise Sub-part
        Minkowski sums Projections
for i in {1, 2, ..., n}
    for j in {1, 2, ..., n}
        if i == j continue
        Q_ij = ∅
        for k in {1, 2, ..., m_i}
            for ℓ in {1, 2, ..., m_j}
                Q_ij = Q_ij ∪ Q^ij_kℓ
```

We exploit the overlay operation in this phase the second time throughout this process, this time in a loop. Given two distinct parts $P_i$ and $P_j$ we traverse all projections in the set $\{Q_{k\ell}^{ij} \,|\, k = 1, 2, \ldots, m_i, \ell = 1, 2, \ldots, m_j\}$, and accumulate the result in the arrangement $Q_{ij}$. As mentioned in Section 5.3.4, when the overlay operation progresses, new vertices, edges, and faces of the resulting arrangement are created. When a new face $f$ is created as a result of the overlay of a face $g$ in some projection $Q_{k\ell}^{ij}$, and a face in the accumulating arrangement, the Boolean flag associated with $f$, which indicates whether all directions $\vec{d} \in f$ pierce $M_{ij}$, is turned on, if $\vec{d}$ pierces $M_{k\ell}^{ij}$, that is, if the flag associated with the face of $g$ is on.

The intermediate result of this step are arrangements with potentially redundant edges and vertices. It is desired (but not necessary) to remove these cells, as it reduces the time consumption of the succeeding operations, which is directly related to the complexity of the arrangements. It has even a larger impact when the optimization described in Section 5.4 is applied, as the optimization decreases the number of preceding operation at the account of slightly increasing the number of succeeding operations. We remove all edges and vertices that are in the interior of the projection, that is all marked edges and vertices. We also remove spherically collinear vertices on the boundary of the projection, the degree of which decreased below three, as a result of the redundant-edge removal.

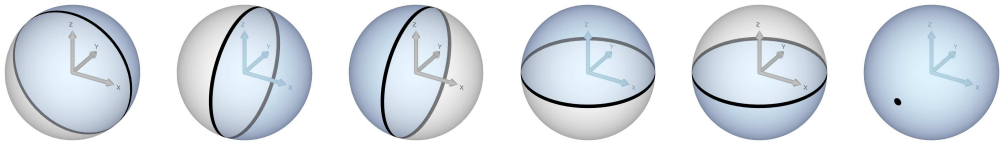

(a) (b) (c) (d) (e) (f)

Figure 5.5: Peg-in-the-hole Minkowski sum projections. (a), (b), (c), (d), and (e) are the sub-part projection. (f) is the union of the former.

CGAL also supports Boolean operations applied to general polygons[1] and in particular the union operation. However, it consumes and produces *regularized* general polygons; see Section 2.7.1. This regularization operation is harmful in the realm of assembly planning. Therefore, we work directly on the cells of the arrangements $Q_{ij}$. Quite often the projection contains isolated vertices and edges, as occurs in the example depicted on the right, referred to as "peg-in-the-hole". Here the assembled product is translucently viewed from two opposite directions. The blue part is stationary and is decomposed into five sub-parts. Figure 5.5 illustrates the corresponding five pairwise Minkowski sum projections, and their union. The complement of the union consists of a single isolated vertex.

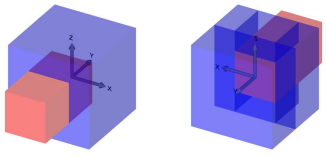

[1]The generic code supports point sets bounded by algebraic curves embedded on parametric surfaces referred to as general polygons.

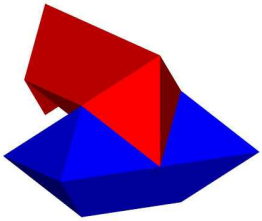

Recalling our Split Star assembly, the projection of the Minkowski sum of the red part and the reflection of the blue part, and its reflection, that is, the projection of the Minkowski sum of the blue part and the reflection of the red part are depicted on the left.

$B \oplus (-R)$

$R \oplus (-B)$

### 5.3.7 Motion-Space Construction

We compute a single arrangement that represents the motion space, where each cell $c$ of the arrangement is extended with a DBG. We use the adjacency-matrix storage format provided by BOOST [3] to represent each DBG. Recall that for a graph with $n$ vertices such as ours, an $n \times n$ matrix is used, where each element $a_{ij}^c$ of a DBG associated with cell $c$ is a Boolean flag that indicates whether part $P_i$ collides with part $P_j$ when moved along any direction $\vec{d} \in c$. In particular we use the `adjacency_matrix` class. It implements the Boost Graph Library (BGL) [SLL02] interface, which supports, among the other, easy insertions of new edges into existing graphs. Handling large assemblies with sparse blocking relations may require different representations of DBGs to reduce memory consumption.

We exploit the overlay operation in this phase the third time similar to its application in Section 5.3.6. We traverse all central projections in the set $\{Q_{ij} \,|\, 1 \leq i < j \leq n\}$, and accumulate the result in the final motion-space arrangement. As mentioned above in Section 5.3.4, when the overlay operation progresses, new vertices, edges, and faces of the resulting arrangement are created. When a new cell $c$ is created as a result of the overlay of a face $g$ in some projection $Q_{ij}$, and a cell in the accumulating arrangement, the DBG associated with $c$ is updated. That is, if the flag associated with $g$ is turned on, we insert an edge between vertex $i$ and vertex $j$ into the DBG associated with $c$.

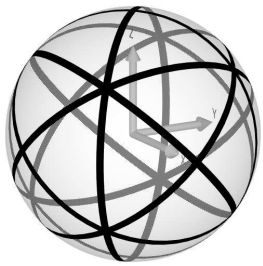

Depicted on the left is the motion-space arrangement computed by our program for the Split Star assembly.

### 5.3.8 Motion-Space Processing

Table 5.1: The Split Star valid partitioning directions and corresponding subassemblies.

| | Direction | Subset |
|---|---|---|
| 1. | −1,−1, −1 | *GBT* |
| 2. | −1,−1, 1 | *RBT* |
| 3. | −1, 1, −1 | *GPT* |
| 4. | −1, 1, 1 | *RPT* |
| 5. | 1,−1, −1 | *GBY* |
| 6. | 1,−1, 1 | *RBY* |
| 7. | 1, 1, −1 | *GPY* |
| 8. | 1, 1, 1 | *RPY* |

We traverse all vertices, edges, and faces of the motion-space arrangement in this order, and test the DBG associated with each cell for strong connectivity using the BOOST global function `strong_components()`. This function computes the strongly connected components of a directed graph using Tarjan's algorithm based on depth-first search (DFS) [Tar72]. The set of constraints associated with a vertex $v$ is a proper subset of the constraints associated with the edges incident to $v$. Similarly, the set of constraints associated with an edge $e$ is a proper subset of the constraints associated with the two faces incident to $e$. Therefore, if the DBGs of all vertices are strongly connected, we terminate with the conclusion that the

assembly is interlocked. Similarly, if we are interested in finding all solutions, and the DBGs of all edges are strongly connected, we terminate, as no further solutions on faces exist.

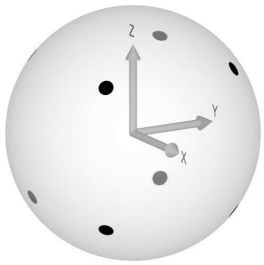


For the Split Star assembly, our program successfully identifies all the eight partitioning directions depicted on the right along with the corresponding subset of parts listed in Table 5.1.

## 5.4 Additional Optimization

The reflection of the sub-parts through the origin as described in Section 5.3.3 has been naively implemented. The computation is applied to the polyhedral-mesh representation of each sub-part. An immediate optimization calls for an application of the reflection operation directly on the arrangements that represent the Gaussian map. We are planning to introduce a generic implementation of the reflection operation that operates on any applicable arrangement. This operation alters the incidence relations between the arrangement features and their geometric embeddings. For each vertex, it negates its associated point, and inverts the order of the halfedges incident to it. For each edge, it negates the associated curve. For each face, it inverts the order of the halfedges along its outer boundary. Similar to the overlay operation (see Section 2.4.2), where the user can provide a set of ten functions, which are invoked when new vertices, edges, and faces of the resulting arrangement are created, while the overlay operation progresses, the user can provide a set of three functions that are invoked when a new vertex, halfedge, and face are created, while the reflection operation progresses. Extended data associated with these types, such as a primal vertex associated with an arrangement face as in the case of an arrangement representing a Gaussian map, can easily be updated with the provision of an appropriate function.

The trivial observation that $P \oplus (-Q) = -((-P) \oplus Q)$ leads to another optimization. Instead of reflecting all sub-parts in the set $\{P_k^i \,|\, i = 1, 2, \ldots, n, k = 1, 2, \ldots, m_i\}$, we reflect only the sub-parts in the set $\{P_k^i \,|\, i = 2, \ldots, n, k = 1, 2, \ldots, m_i\}$, and compute only the pairwise sub-parts Minkowski sums in the set $\{M_{k\ell}^{ij} \,|\, 1 \leq i < j \leq n, k = 1, 2, \ldots, m_j, \ell = 1, 2, \ldots, m_j\}$, their central projection, and the union of the appropriate projections to yield the set $\{Q_{ij} \,|\, 1 \leq i < j \leq n\}$. Then, we apply the reflection operation described above on each member of this set, and obtain the full set of projections $\{Q_{ij} \,|\, i = 1, 2, \ldots, n, j = 1, 2, \ldots, n\}$. The Boolean flag associated with a face of an arrangement that represents a central projection is equal to the flag associated with its reflection. In other words, a face of $Q_{ij}$ consists of directions that pierce $M_{ij}$, if and only if, its reflection in $Q_{ji}$ consists of directions that pierce $M_{ji}$.

Phase 8 is purely topological. Thus, we do not expect the time consumption of this phase to dominate the time consumption of the entire process for any input. Nevertheless, it might be possible to reduce its contribution to the total time consumption through efficient testing for strong connectivity applied to all the DBGs [KMW98], exploiting the similarity between DBGs associated with incident cells. Recall, that the set of arcs in a DBG associated with a vertex $v$ is a subset of the set of arcs associated with an edge incident to $v$. Similarly, the set of arcs in a DBG associated with an edge $e$ is a subset of the set of arcs associated with

Table 5.2: Time consumption (in seconds) of the execution of the eight phases applied to the Split Star assembly as input. Each one of the three rows refers to a different decomposition of the assembly. **A** — number of convex sub-parts per part. **B** — number of sub-part vertices per part. **C** — total number of convex sub-parts. **D** — total number of Minkowski sums. **E** — total number of arrangements of geodesic arcs embedded on the sphere constructed throughout the process.

| **A** | **B** | **C** | **D** | **E** | **1** | **2** | **3** | **4** | **5** | **6** | **7** | **8** |
|---|---|---|---|---|---|---|---|---|---|---|---|---|
| 3 | 16 | 18 | 270 | 607 | NA | 0.01 | 0.04 | 2.38 | 0.41 | 2.05 | | |
| 5 | 22 | 30 | 750 | 1591 | NA | 0.01 | 0.05 | 5.03 | 1.09 | 7.07 | 0.36 | 0.01 |
| 8 | 32 | 48 | 1920 | 3967 | NA | 0.01 | 0.06 | 11.12 | 2.41 | 27.99 | | |

a face incident to $e$. The proposed technique reduces the cost from $O(n^2)$ per DBG to an amortized cost of $O(n^{1.376})$, where $n$ is the maximum number of arcs in any blocking graph.

## 5.5 Experimental Results

Our program can handle all inputs. However, we limit ourselves to a representative set of test cases, where we compare the impact of different decompositions on the process time consumption. The results listed in Table 5.2 were produced by experiments conducted on a Pentium PC clocked at 1.7 GHz. In all three test cases we use the Split Star assembly as input. Naturally, in all three cases identical projections are obtained as the intermediate results of Phase 6, hence the identical time consumption of the succeeding last two phases. Evidently, it is desired to decompose each part into as few as possible sub-parts with as small as possible number of features. However, an automatic decomposition operation may require large amount of resources to arrive at optimal or near optimal decompositions. Notice that Phases 4 and 6 dominate the time complexity. This is due to the large number of geometric predicates that must be evaluated during the execution of the overlay operation.

*Seriousness is the only refuge of the shallow.*

Oscar Wilde

# 6 Conclusion and Future Work

In this thesis we show how a complete implementation of extendible arrangements with a rich set of operations enables a broad spectrum of robust applications that solve problems arising in domains such as motion planning, assembly planning, and solid modeling. For example, we describe how arrangements embedded on two-dimensional surfaces can be efficiently used to compute Minkowski sums of two polytopes in $\mathbb{R}^3$, which in turn, and in conjunction with several other operations based on such arrangements, can be used to partition an assembly with an infinite translation motion. The rest of this chapter is devoted to future prospects related to our research topics.

## 6.1 Arrangements on Two-Dimensional Surfaces

Constructing Minkowski Sums of polytopes in $\mathbb{R}^3$ has been successfully attempted in the past. We introduce a robust, yet efficient method. Table 3.5 shows that both our exact methods outperform the other exact methods. However, we believe that both of our methods, and in fact all CGAL based methods have great potential for further improvements through future optimizations applied to the infrastructure of CGAL, as CGAL is an evolving project. While the space consumption of the CGM method is greater than the space consumption of the spherical Gaussian-map method, the table also reveals that the CGM method is currently more efficient than its rival. We estimate that the gap will decrease, if not vanish, once all optimizations for the `Arrangement_on_surface_2` data-structure that are still pending are implemented and enabled.

We are constantly striving to improve the quality of our infrastructure, that is the `Arrangement_on_surface_2` package. We have already identified few weak spots. Eliminating them will increase the genericity, extendibility, efficiency, and functionality of the package. We provide one example in each category.

### 6.1.1 Generic Observers

There is a certain similarity between observers (see Section 2.4.4) and visitors (see Section 2.4.1), as typically each of their methods is triggered as a response to a certain event — a member of a pre-determined list of events. Technically, the main difference between them is that observers define a one-to-many mapping between objects, while visitors define a one-to-one mapping.[1] Recall, for example, that a single arrangement may register many observers, but it is only natural to relate a single visitor to a specific algorithmic framework in order to realize a certain concrete algorithm. Consequently, arrangement observers are derived from a common base class, and their methods must be virtual. This is how modules, which are closed for modification, are extended using object-oriented programming. However, composability of such modules is limited, since independently produced modules generally do not agree on common abstract interfaces from which supplied types must inherit. In addition, when techniques from the object-oriented programming and the generic programming paradigms are mixed, they often clash. There are known methods to replace lists of objects, derived from a common base class, and linked during run time, with a list of syntactically unrelated objects concatenated during compile time (coded using a generic programming technique) [Ale01, Chapter 3]. Nevertheless, we would like to simultaneously enjoy the benefits of both the object-oriented and the generic programming paradigms, that is, to enable the immediate production of composable modules that support dynamic polymorphism. A very important research direction in our context is to explore these possibilities, perhaps pushing the limits of the C++ programming language along the way.

### 6.1.2 Property Maps

In many cases we need to associate values (called "properties") with the vertices, the halfedges, and the faces of the arrangement. In addition, it is often necessary to associate multiple properties with each vertex, edge, or face; this is what Boost literature refers to as multi-parameterization. BGL [SLL02] graph classes have template parameters for vertex and edge "properties". A property specifies the parameterized type of the property and also assigns an identifying tag to the property.

There are various ways to associate properties with arrangement cells. One option is to extend the geometric types of the kernel, as the kernel is fully adaptable and extensible [HHK+07]. However, this indiscriminating extension may lead to an undue space-consumption, as every geometric object is extended, regardless of its use.[2] Another option, is to extend the vertex, halfedge, or face records of the Dcel; see Section 2.3.3. This may also lead to excessive space-consumption, for example, when the data associated with a halfedge is in fact tied to the embedded geometric curve. In this case the data, or at least a handle to the data, must be stored twice in both twin halfedges. A third option is to extend the curve (or point) types defined by the geometry-traits class; see Section 2.3.1. But even this option leads to unjustified space-consumption, when only a limited number of arrangement

[1] They also differ in essence. While an observer typically implements a notifier, a visitor is usually a coherent part of an algorithm based on a fundamental and flexible framework. [GHJV95]

[2] It also requires nontrivial knowledge about the kernel structure and the techniques to extend it.

features are associated with real data. In such cases it is advantageous to use external search structures that map individual arrangement features with their data.

Designing a useful and convenient interface, while taking all considerations above into account, is a research topic on its own, which may further push the limits of good usage of the C++ programming language.

### 6.1.3 Point Location for Surfaces

Point location is one of the most fundamental operations applied to arrangements; see Section 2.4.5. The contest between the different point-location strategies for arrangement embedded in the plane was settled in favor of the "landmark" variants for many types of arrangements [HH08]. Unfortunately, at this point, these strategies cannot be applied on arrangements embedded on surfaces other than the plane. This is due to limitations that arise from the specific implementations of geometry traits that support these types of embedded surfaces, e.g., the geometry traits that handles geodesic arcs embedded on the sphere; see Section 2.6. The problem should be attacked from both its ends. That is, we can try to enhance the geometry traits implementations, and add all ingredients required by the concept *ArrangementLandmarksTraits_2* as defined today, and at the same time, try to come up with alternative, perhaps similar, strategies that induce different requirements that are easier to satisfy by the geometry-traits classes.

### 6.1.4 Geometry-Traits Models

Continuous and steady effort is made to further extend the arsenal of geometry-traits models, or simply to improve the existing ones; see Section 2.5.2. Supporting arrangements induced by rich families of curves opens the door for numerous applications.

The dominant bottleneck of all applications mentioned in this thesis is the application of the geometry operations implemented in the geometry-traits classes. Expediting their performance, while containing the growth of their memory footprint is always desired. For example, the arrangement package provides two traits classes that handle line segments. Both are parameterized by a geometric kernel; see Section 1.3.3. Segments defined by most CGAL kernels are represented only by their two endpoints. When a segment is split several times, the bit-length needed to represent the coordinates of its endpoints may grow exponentially (see [FWH04] for a discussion), which may significantly slow down the computation. Therefore, one of the two traits classes represents a segment by its supporting line in addition to its two endpoints. When the traits class computes an intersection point of two line segments, it uses the coefficients of their supporting lines. When a segment is split at an intersection point, the underlying line of the two resulting sub-segments remains the same, and only its endpoints are updated. This traits class thus overcomes the undesired effect of cascading intersection-point representation, as described above, at the account of a larger memory footprint. A similar idea can be applied to the traits class that handles geodesic arcs embedded on the sphere. An implementation of a geometry-traits that handles such arcs that stores the projections of all the arrangement geometric features once calculated, and

retrieves them when subsequently needed, has great potential to reduce time consumption at the price of growth in space consumption.

Another direction is to expand existing implementations to meet the requirements of the various concepts in the hierarchy described in Chapter 2. Consider, for example, the geometry traits class that handles geodesic arcs embedded on the sphere. Currently, it supports the basic operations required to construct and maintain arrangements induced by such arcs. As mentioned in the previous section, it might be possible to enhance it to enable the use of one or more of the variants of the "landmark" point-location strategies. Similarly, enabling Boolean set operations of spherical patches bounded by geodesic arcs embedded on the sphere requires the provision of few additional operations by the traits class.

## 6.2 Three-Dimensional Arrangements

Consider the following task: Given a set $\mathcal{S} = \{S_1, S_2, \ldots, S_n\}$ of two-dimensional surfaces in $\mathbb{R}^3$, construct the three-dimensional arrangement $\mathcal{A}(\mathcal{S})$ induced by $\mathcal{S}$. Fulfilling this task in an efficient, complete, and robust manner has not been attempted yet, and is considered challenging. Implementing various strategies of point-location that operate on arrangements in $\mathbb{R}^3$ and a plane-sweep and zone-construction frameworks for such a data structure is greatly desired, but extremely ambitious. In analogy to two-dimensional arrangements, a generic implementation of a plane-sweep framework can enable various operations, such as the overlay of spatial subdivisions and ordinary and regularized Boolean set operations of point sets bounded by general algebraic surfaces. These operations, in turn, can enable the implementation of a multitude of applications.

Arrangements embedded on two-dimensional surfaces can be used as building blocks in the implementation of a data structure that represents a three-dimensional arrangement [Wei07]. We can consider each surface $S_k$ separately, and construct the arrangement $\mathcal{A}_k = \mathcal{A}_k(\mathcal{S})$ induced by intersection curves between $S_k$ and $\mathcal{S} \setminus S_k$ embedded on $\mathcal{S}$. The arrangements $\mathcal{A}_1$,$\mathcal{A}_2$,...,$\mathcal{A}_n$ can subsequently be connected together to properly represent the spatial subdivision $\mathcal{A}(\mathcal{S})$.

## 6.3 Boolean Set-Operations

In some sense and to some extent this thesis attempts to close gaps between theoretical results and practical needs. It is not accidental that great parts of the thesis are closely related to CGAL, as one of the goals of CGAL stated in the Introduction chapter of the thesis is to translate (theoretical) results into useful, reliable, and efficient programs for industrial and academic applications. Evidently, the Boolean set operations package of CGAL, which is based on the `Arrangement_on_surface_2` package (see Section 2.7.1) is one of the most popular packages among CGAL packages in the commercial market. Naturally, we would like to continue improving this package. The problems addressed in the next two subsections were raised during the $3^{rd}$ CGAL User Workshop [dW08] [1].

### 6.3.1 Fixing the Data

Input data of Boolean set operations, namely, a set of one or more polygons, used in real-world applications is occasionally corrupted, as it originates from measuring devices that are susceptive to noise and physical disturbances. In some other cases, it contains many degeneracies, which either disable computations based on fixed-precision arithmetic, or slow down further computation using exact geometric computation.

#### Invalid Data

A polygon $P$ is said to be *simple* (or Jordan), if the only points of the plane belonging to two edges of $P$ are vertices of consecutive edges $P$ [23]. Namely, no two edges intersect, except for every two consecutive edges, which share one endpoint. A simple polygon is topologically equivalent to a disk. A polygon $P$ is said to be *weakly simple*, if the chain of the edges of $P$ does not cross itself. A polygon $P$ is said to be *relatively simple*, if it is weakly simple and the edges of $P$ do not intersect in their relative interior. Observe, that a relatively simple polygon, the vertices of which appear only once in the boundary (the degree of each vertex is two), is simple.

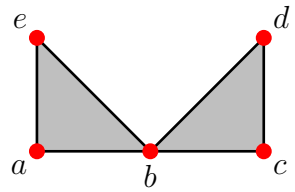

Figure 6.1: A *relatively simple* polygon that is not simple, given by its boundary $\{a, b, c, d, b, e\}$.

Input data for any Boolean set operation represents points set that may be bounded or unbounded, and may have holes. Items of such input take the form of general polygons or general polygons with holes with well-defined interiors and exteriors. A valid polygon must be weakly simple (but not necessarily simple) and its vertices must be ordered in counterclockwise direction around its interior. A valid polygon with holes that represents a bounded point set, has an outer boundary represented as a weakly simple (but not necessarily simple) polygon, the vertices of which are oriented in counterclockwise order around its interior. In addition, the set may contain holes, where each hole is represented as a simple polygon, the vertices of which are oriented in clockwise order around the interior of the hole. Note that an unbounded polygon without holes spans the entire plane. Vertices of holes may coincide with vertices of the boundary.

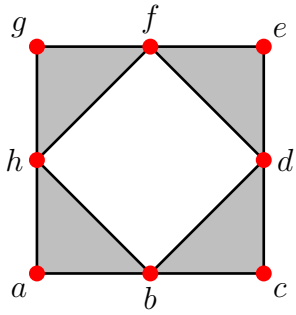

Figure 6.2: A polygon with a hole given by its outer boundary $\{a, b, c, d, e, f, g, h\}$ and its hole $\{h, f, d, b\}$.

As mentioned above, real-world data is often corrupted. Naturally, passing invalid polygons (polygons with holes, respectively) as input to a Boolean set operation must be avoided. Apparently, automatically "fixing" corrupted data, that is, converting invalid input polygons or polygons with holes to valid ones, is not a simple task. Consider, for example, the self intersecting star depicted in Figure 6.3(a). A point is considered inside the point set, if and only if the number of counterclockwise turns the oriented boundary makes around the point, also called the winding number, is greater than zero. It can be efficiently calculated using an `Arrangement_2` data structure as follows. We extend each halfedge $h$ with a Boolean flag that indicates whether the winding number increases or decreases when we cross $h$, that is,

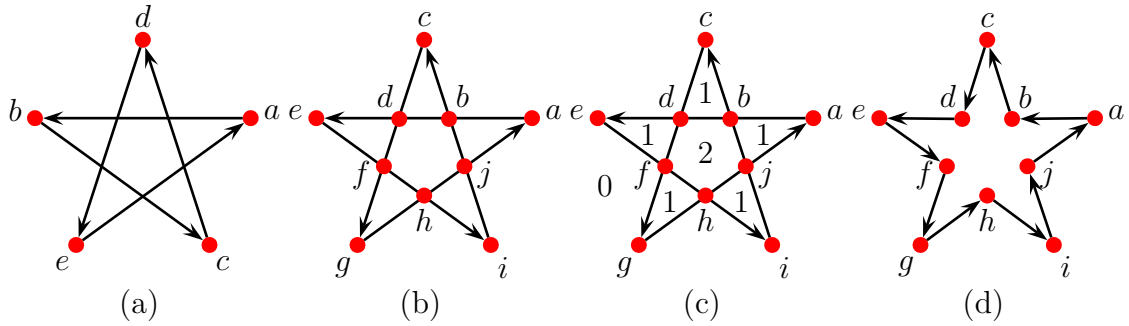


Figure 6.3: (a) A self crossing polygon given by $\{a, b, c, d, e\}$. (b) The `Arrangement_2` data structure constructed from the polygon edges. (c) The `Arrangement_2` data structure with updated face winding-numbers. (d) The `Arrangement_2` data structure with internal edges removed.

when we move from the face incident to $h$ to the face incident to the twin of $h$. Observe that twin halfedges always have opposite flag values. We extend each face with an integer that counts the winding number of every point in the face. Finally, we apply a Breath-First Search (BFS) on all the arrangement faces starting from the unbounded face and updating the face counters as we cross halfedges. The BGL, for example, can be employed for this task. Figure 6.3 illustrates the process. Once the winding number of every face is updated, we remove internal edges, as they are redundant, and convert the arrangement back into a valid polygon or polygon with holes.

The problem becomes more complicated when the input polygons or polygons with holes violate several validity properties at the same time. Naturally, converting corrupted data into valid data consumes time. The challenge is to perform this task flawlessly and efficiently, while presenting a convenient interface to the user.

### Degenerate Data

In computational geometry there are two main techniques to eliminate degeneracies and near-degeneracies. One is snap rounding [GM95, GGHT97, Hob99] and the other is controlled perturbation [HL04, MO06]. Both techniques aim at processing geometric data, e.g., curves of the boundaries of general polygons, to yield new data that can be further robustly and more efficiently processed, perhaps using only limited precision. Traditionally, snap rounding has been applied to linear objects embedded in the plane [HP01, HP02], where it replaces sets of linear segments with sets of polylines. It can be extended though to other types of curves in the plane, such as Bézier curves [EKW07], or even other curve types embedded on other surfaces that have a well defined grid (and perhaps other properties), such as geodesic arcs embedded on the sphere. Controlled perturbation has even a larger spectrum of applicable platforms. With respect to our polygons, applying any one of the two techniques above may result with (partially) overlapping curves, which belong to two different polygons, respectively. In this case, we need to merge the incremental winding contributions of the original curves mentioned above.

### 6.3.2 Improving the Efficiency

The `Boolean_set_operations_2` package provides efficient operations that compute the regularized union or the regularized intersection of a set of input polygons. There is no restriction on the polygons in the set; naturally, they may intersect each other. The package also provides an efficient predicate that determines whether all polygons in a given set intersect.

There are at least three different methods to compute the union of a set of polygons $P_1, \ldots P_m$. We can do it incrementally as follows. At each step we compute the union of $S_{k-1} = \bigcup_{i=1}^{k-1} P_i$ with $P_k$ and obtain $S_k$. A second option is to use a divide-and-conquer approach. First, we divide the set of polygons into two subsets. Then, we compute the union of each subset recursively, and obtain the partial results in $S_1$ and $S_2$, respectively. Finally, we compute the union $S_1 \cup S_2$. A third option aggregately computes the union of all polygons. We construct an arrangement inserting the polygon edges at once, utilizing the sweep-line framework, (see Section 2.4.1) and extract the result from the arrangement. Similarly, it is also possible to aggregately compute the intersection $\bigcap_{i=1}^{m} P_i$ of a set of input polygons.

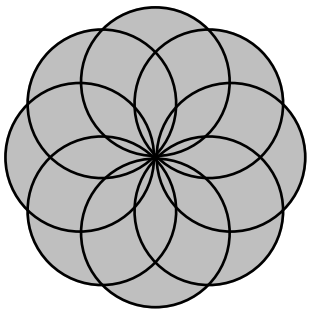

Figure 6.4: The union of eight discs.

The incremental method is more efficient for a small (constant) size of input polygons, and the aggregate method is more efficient for sparse polygons with a relatively small number of intersections. It is also possible to mix between the three methods, reaping the benefits of them all. We would like to figure out what are the exact conditions that should be used to determine when to use each method, or when to switch from one to another.

### 6.3.3 Non Regularized Operations

The CGAL package `Nef_2` supports ordinary set-operations on point sets in $\mathbb{R}^2$ [See07]. The point-set operands and results are rectilinear polygonal model. Such a point set can be defined by a finite set of open halfspaces, or obtained by set complement and set intersection operations. The package supports operations that consume and produce linear polygons defined by linear edges. The Boolean set operations package, on the other hand, supports only regularized set-operations, but the operations consume and produce general polygons. Recall, that a general polygon is a point set in $\mathbb{R}^2$ that has a topology of a polygon, but its boundary edges map to arcs of curves, which are not necessarily linear. Extending the package to support not only regularized operations, but also ordinary ones, will make it useful for more applications; see, for example, Section 5.3.6.

### 6.3.4 Operating in 3-Space

Boolean set operations are intuitive and therefore popular in many fields. For example, CSG is a representation model for solids based on Boolean set operations. Solids represented using CSG result from Boolean set operations applied to elementary solids called primitives, e.g., cubes, spheres, cones, and cylinders. A CSG solid is represented in a tree structure, where

the leaves represent primitives, and internal nodes represent Boolean operations.

The CGAL package `Nef_3` supports ordinary set-operations on point sets in $\mathbb{R}^3$ [HK07]. Similar to the planar case, the package supports operations that consume and produce (linear) polyhedra defined by (linear) halfspaces. Having the ability to construct and maintain arrangements in $\mathbb{R}^3$, will enable the development of a new package, that will support either regularized, or even non-regularized, robust Boolean set-operations that consume and produce general (curved) polyhedra in $\mathbb{R}^3$, the boundaries of which are general surfaces. Many fundamental problems in solid modeling, motion planning, and other domains, can benefit from such a package.

## 6.4 Collision Detection

One possible progression of the collision detection algorithm and its implementation described in Section 3.4 is a complete integrated framework that answers proximity queries about the relative placement of polytopes that undergo rigid motions including *rotation*. The framework may use either the spherical or the cubical Gaussian-map to represent polytopes. The interface of these two data structures should be consolidated to allow rapid interchanging.

Some of the methods we foresee compute only those portions of the Minkowski sum that are absolutely necessary, making our approach even more competitive. Briefly, instead of computing the Minkowski sum of $P$ and $-Q$, we walk simultaneously on the two respective CGM's, producing one feature of the Minkowski sum at each step of the walk. Such a strategy could be adapted to the case of rotation by rotating the trajectory of the walk, keeping the CGM of $-Q$ intact, instead of rotating the CGM itself.

## 6.5 Reflection Mapping and GIS

We have developed a new data structure that can be used to construct and maintain cubical Gaussian-maps and compute Minkowski sums of pairs of polytopes represented by the new data structure; see Chapter 3. The name of the data structure is `Cubical_gaussian_map_3`, and we are considering introducing a package by the same name to a prospective release of CGAL. The implementation is generic and can be used for other purposes, where six planar subdivisions embedded on a unit cube and stitched properly at the edges of the cube is useful, for example Cubical Environment Mapping; see, e.g., [FvDFH95, Section 16.6].

Figure 6.5: Environment of the St. Peters Cathedral mapped on a teapot with a silver material applied. Taken in RTHDRIBLE [22].

In computer graphics, *reflection mapping* is an efficient method of simulating a complex mirroring surface by means of a precomputed texture image. The texture is used to store the image of the environment surrounding the rendered ob-

ject. The surrounding environment can be represented, constructed, maintained, and stored in several ways; the most common ones are the Spherical Environment Mapping in which a single texture contains the image of the surrounding as reflected on a mirror ball, or the Cubical Environment Mapping in which the environment is unfolded onto the six faces of a cube and stored therefore as six square textures.

Reflection Mapping can be categorized as some sort of a geographic information system (GIS). There are two broad methods used to store data in a GIS: Raster and Vector. In a GIS data is often related from different sources possibly of different storing types. Regardless of whether a single arrangement embedded on a sphere, or six arrangements embedded on the cube, are concerned, the connection to GIS is clear — both data-structures can accommodate geographic vector data in a natural way.

## 6.6 Exact Complexity of Minkowski Sums

| **Dimension** | **Exact Maximum Complexity** |
|---|---|
| $d = 2$ | $m_1 + m_2 + \ldots + m_k$ |
| $d = 3$ | $\sum_{1 \le i < j \le k} (2m_i - 5)(2m_j - 5) + \sum_{1 \le i \le k} m_i + \binom{k}{2}$ |

The table to the right summarizes the known exact bounds on the maximum complexity of Minkowski sums of polytopes in terms of number of facets ($(d-1)$-faces) derived in Chapter 4. The exact bounds are unknown for higher Dimensions as far as we know.

It is known that the exact complexity (counting faces) of the Minkowski sum of two polytopes with $m$ and $n$ facets can be as low as $m$, when the two polytopes have the same number of facets $m$ and parallel features, but it is unknown what is the minimum exact complexity of Minkowski sums of polytopes that have only a limited number of parallel features, or none at all.

# A

# Software Components, Libraries, and Packages

## A.1 Visual Simulation

We have developed a toolkit, called SGAL (Scene Graph Algorithm Library),[1] that supports the construction and maintenance of directed acyclic graphs that represent scenes and models in $\mathbb{R}^3$. The toolkit includes, among the other, two interactive 3D applications. The first detects collisions and answers proximity queries for polytopes that undergo translation and rotation. The second enables users to visualize a scene in an interactive manner. It parses input files that describe the scene in a degenerate yet extended VRML format [27]. The format is degenerate, as not all VRML features are supported (yet). However, it has been significantly extended as described below.

Both applications are linked with (i) CGAL, (ii) a library that provides the exact rational number-type, (iii) several BOOST libraries, (iv) imagemagick [15] — a library that creates, edits, and composes bitmap images, and (v) internal libraries that construct and maintain 3D scene-graphs, written in C++, and built on top of `OpenGL`. The internal code is divided into two libraries; `SGAL` — The main 3D scene-graph library and `SCGAL` — Extensions that depend on CGAL.

We added several geometry nodes that represent polytopes using various sub-representations, such as Gaussian maps, a few other related nodes that handle coordinates, and many other miscellaneous nodes that provide services, such as antialiasing and snapshoting. The descriptions of some of the geometry nodes follows.

`ArrangementOnSphere` This node represents models as arrangements of geodesic arcs embedded on the sphere.

`ExactPolyhedron` This node represents polyhedra as meshes using the CGAL `Polyhedron_3`

[1] We plan to offer SGAL with an open-source license in the future, making it available to the public.

data structure.

`SphericalGaussianMap` This node represents polytopes as spherical Gaussian maps using the `Arrangement_on_surface_2` data structure instantiated as an arrangement embedded on the sphere.

`CubicalGaussianMap` This node represents polytopes as cubical Gaussian maps using the `Cubical_gaussian_map_3` data structure.

The implementation relies on inputing *exact* coordinates. To this end, the format was further extended with a node called `ExactCoordinate` that represents exact coordinates, and enables the provision of exact rational coordinates as input.

The entire partitioning process described in Chapter 5 is realized within Sgal. The library contains all the necessary ingredients required to represent and visualize the input and the output, and to simulate the process. In particular, it has been extended with two geometry node types: the `Assembly` node type represents assemblies or subassemblies, and the `AssemblyPart` node type represents parts of assemblies. Notice, that each node object of the three types `AssemblyPart`, `SphericalGaussianMap`, and `ArrangementOnSphere` internally maintains the Cgal data structure that represents an arrangement of geodesic arcs embedded on the sphere [BFH+07], an instance of the `Arrangement_on_surface_2` class template.

## A.2 Software Availability

Compiling and executing the programs require the latest internal release of Cgal (post version 3.31) and the components listed above including an internal package of Cgal that supports the `Cubical_gaussian_map_3` data structure. The source code is available upon request.[2] Precompiled executables compiled either with `g++` 4.2.3 on Linux or with `VC 8` on Windows, data sets, and documentation can be downloaded from `http://www.cs.tau.ac.il/~efif/CD/3d`.

[2]Send email to `efifogel@gmail.com`.

# Bibliography


[AFH02] Pankaj Kumar Agarwal, Eyal Flato, and Dan Halperin. Polygon decomposition for efficient construction of Minkowski sums. *Computational Geometry: Theory and Applications*, 21:39–61, 2002.

[AK00] Franz Aurenhammer and Rolf Klein. Voronoi diagrams. In Jörg-Rüdiger Sack and Jorge Urrutia, editors, *Handbook of Computational Geometry*, chapter 5, pages 201–290. Elsevier Science Publishers, B.V. North-Holland, Amsterdam, North-Holland, 2000.

[Ale01] Andrei Alexandrescu. *Modern C++ Design*. Addison-Wesley, 2001.

[AS97] Boris Aronov and Micha Sharir. On translational motion planning of a convex polyhedron in 3-space. *SIAM Journal on Computing*, 26(6):1785–1803, 1997.

[AS00] Pankaj Kumar Agarwal and Micha Sharir. Arrangements and their applications. In Jörg-Rüdiger Sack and Jorge Urrutia, editors, *Handbook of Computational Geometry*, chapter 2, pages 49–119. Elsevier Science Publishers, B.V. North-Holland, Amsterdam, North-Holland, 2000.

[AS01] Marcus Vinícius Alvim Andrade and Jorge Stolfi. Exact algorithms for circles on the sphere. *International Journal of Computational Geometry and Applications*, 11(3):267–290, jun 2001.

[Aus99] Matthew H. Austern. *Generic Programming and the STL*. Addison-Wesley, 1999.

[BdLT97] Jean-Daniel Boissonnat, Eduard E. de Lange, and Monique Teillaud. Minkowski operations for satellite antenna layout. In *Proceedings of 13th Annual ACM Symposium on Computational Geometry (SoCG)*, pages 67–76. Association for Computing Machinery (ACM) Press, 1997.

[BDTY00] Jean-Daniel Boissonnat, Olivier Devillers, Monique Teillaud, and Mariette Yvinec. Triangulations in CGAL. In *Proceedings of 16th Annual ACM Symposium on Computational Geometry (SoCG)*, pages 11–18. Association for Computing Machinery (ACM) Press, 2000.

[BEH+02] Eric Berberich, Arno Eigenwillig, Michael Hemmer, Susan Hert, Kurt Mehlhorn, and Elmar Schömer. A computational basis for conic arcs and

Boolean operations on conic polygons. In *Proceedings of 10th Annual European Symposium on Algorithms (ESA)*, volume 2461 of *LNCS*, pages 174–186. Springer-Verlag, 2002.

[BEH+05] Eric Berberich, Arno Eigenwillig, Michael Hemmer, Susan Hert, Lutz Kettner, Kurt Mehlhorn, Joachim Reichel, Susanne Schmitt, Elmar Schömer, and Nicola Wolpert. EXACUS: Efficient and exact algorithms for curves and surfaces. In *Proceedings of 13th Annual European Symposium on Algorithms (ESA)*, volume 3669 of *LNCS*, pages 155–166. Springer-Verlag, 2005.

[BFH+07] Eric Berberich, Efi Fogel, Dan Halperin, Kurt Melhorn, and Ron Wein. Sweeping and maintaining two-dimensional arrangements on surfaces: A first step. In *Proceedings of 15th Annual European Symposium on Algorithms (ESA)*, volume 4698 of *LNCS*, pages 645–656. Springer-Verlag, 2007.

[BFH+09a] Eric Berberich, Efi Fogel, Dan Halperin, Michael Kerber, and Ophir Setter. Arrangements on parametric surfaces ii: Concretizations and applications, 2009. Manuscript.

[BFH+09b] Eric Berberich, Efi Fogel, Dan Halperin, Kurt Melhorn, and Ron Wein. Arrangements on parametric surfaces i: General framework and infrastructure, 2009. Manuscript.

[BFHW07] Eric Berberich, Efi Fogel, Dan Halperin, and Ron Wein. Sweeping over curves and maintaining two-dimensional arrangements on surfaces. In *Abstracts of 23rd European Workshop on Computational Geometry*, pages 223–226, 2007.

[BGRR96] Julien Basch, Leonidas J. Guibas, G. D. Ramkumar, and L. Ramshaw. Polyhedral tracings and their convolution. In *Proceedings of 2nd Workshop on Algorithmic Foundations of Robotics*, 1996.

[BHK+05] Eric Berberich, Michael Hemmer, Lutz Kettner, Elmar Schömer, and Nicola Wolpert. An exact, complete and efficient implementation for computing planar maps of quadric intersection curves. In *Proceedings of 21st Annual ACM Symposium on Computational Geometry (SoCG)*, pages 99–106. Association for Computing Machinery (ACM) Press, 2005.

[BK08] Eric Berberich and Michael Kerber. Exact arrangements on tori and Dupin cyclides. In *Proceedings of ACM Symposium on Solid and Physical Modeling (SPM)*, pages 59–66. Association for Computing Machinery (ACM) Press, 2008.

[BM07] Eric Berberich and Michal Meyerovitch. Computing envelopes of quadrics. In *Abstracts of 23rd European Workshop on Computational Geometry*, pages 235–238, 2007.

[BO79] Jon Louis Bentley and Thomas Ottmann. Algorithms for reporting and counting geometric intersections. *IEEE Transactions on Computers*, 28(9):643–647, 1979.

[Boo82] F. H. Bool et al. *M. C. Escher: His Life and Complete Graphic Work*. Harry N. Abrams, Inc., 1982.

[BR01] Henk Bekker and Jos B. T. M. Roerdink. An efficient algorithm to calculate the Minkowski sum of convex 3D polyhedra. In *Proceedings of International Conference on Computational Science Part I*, volume 2073 of *LNCS*, pages 619–628. Springer-Verlag, 2001.

[Cam97] Stephen A. Cameron. Enhancing GJK: Computing minimum and penetration distances between convex polyhedra. In *Proceedings of IEEE International Conference on Robotics and Automation*, pages 3112–3117, 1997.

[CC86] Stephen A. Cameron and R. K. Culley. Determining the minimum translational distance between two convex polyhedra. In *Proceedings of IEEE International Conference on Robotics and Automation*, pages 591–596, 1986.

[CDR92] John Canny, Bruce Donald, and Eugene K. Ressler. A rational rotation method for robust geometric algorithms. In *Proceedings of 8th Annual ACM Symposium on Computational Geometry (SoCG)*, pages 251–260. Association for Computing Machinery (ACM) Press, 1992.

[cga07] CGAL *User and Reference Manual*, 3.3 edition, 2007. `http://www.cgal.org/Manual/3.3/doc_html/cgal_manual/index.html`.

[CKF+04] Tim Culver, John Keyser, Mark Foskey, Shankar Krishnan, and Dinesh Manocha. ESOLID — a system for exact boundary evaluation. *Computer-Aided Design*, 36(2):175–193, 2004.

[CL06] Frederic Cazals and Sebastien Loriot. Computing the exact arrangement of circles on a sphere, with applications in structural biology. Technical Report 6049, INRIA Sophia-Antipolis, 2006.

[Cof06] Stewart T. Coffin. *Geometric Puzzle Design*. A.K. Peters, Ltd., 2nd edition, 2006.

[COLYKT03] Daniel Cohen-Or, Shuly Lev-Yehudi, Adi Karol, and Ayellet Tal. Inner-cover of non-convex shapes. *International Journal on Shape Modeling*, 9(2):223–238, Dec 2003.

[dBvKOS00] Mark de Berg, Mark van Kreveld, Mark Overmars, and Otfried Schwarzkopf. *Computational Geometry: Algorithms and Applications*. Springer-Verlag, Berlin, Germany, 2nd edition, 2000.

[dCPT07] Pedro M. M. de Castro, Sylvain Pion, and Monique Teillaud. Exact and efficient computations on circles in CGAL. In *Abstracts of 23rd European Workshop on Computational Geometry*, pages 219–222, 2007.

[DHH01] Duong Anh Duc, Nguyen Dong Ha, and Lethi Thuy Hang. Proposing a model to store and a method to edit spatial data in topological maps. Technical report, Ho Chi Minh University of Natural Sciences, Ho Chi Minh City, Vietnam, 2001.

[DK90] David P. Dobkin and David G. Kirkpatrick. Determining the separation of preprocessed polyhedra — a unified approach. In *Proceedings of 17th International Colloquium on Automata, Languages and Programming*, volume 443 of *LNCS*, pages 400–413. Springer-Verlag, 1990.

[dW08] Michiel de Wilde. Using CGAL for robust planar geometry processing in agilent ADS. 3rd CGAL User Workshop, 2008. `http://www.cgal.org/UserWorkshop/index.html`.

[EK08] Arno Eigenwillig and Michael Kerber. Exact and efficient 2D-arrangements of arbitrary algebraic curves. In *Proceedings of 19th Annual ACM-SIAM Symposium on Discrete Algorithms (SODA)*, pages 122–131, Philadelphia, PA, USA, 2008. Society for Industrial and Applied Mathematics (SIAM).

[EKP+04] Ioannis Z. Emiris, Athanasios Kakargias, Sylvain Pion, Monique Teillaud, and Elias P. Tsigaridas. Towards and open curved kernel. In *Proceedings of 20th Annual ACM Symposium on Computational Geometry (SoCG)*, pages 438–446. Association for Computing Machinery (ACM) Press, 2004.

[EKSW04] Arno Eigenwillig, Lutz Kettner, Elmar Schömer, and Nicola Wolpert. Complete, exact and efficient computations with cubic curves. In *Proceedings of 20th Annual ACM Symposium on Computational Geometry (SoCG)*, pages 409–418. Association for Computing Machinery (ACM) Press, 2004.

[EKW07] Arno Eigenwillig, Lutz Kettner, and Nicola Wolpert. Snap rounding of Bézier curves. In *Proceedings of 23rd Annual ACM Symposium on Computational Geometry (SoCG)*, pages 158–167. Association for Computing Machinery (ACM) Press, 2007.

[EL00] Stephen A. Ehmann and Ming C. Lin. Accelerated proximity queries between convex polyhedra by multi-level Voronoi marching. In *Proceedings of IEEE Conference on Intelligent Robots and Systems*, pages 2101–2106, 2000.

[EOR92] Roger C. Evans, Michael A. O'Connor, and Jarek R. Rossignac. Construction of Minkowski sums and derivatives morphological combinations of arbitrary polyhedra in CAD/CAM systems, 1992. US Patent 5159512.

[ES86] Herbert Edelsbrunner and Raimund Seidel. Voronoi diagrams and arrangements. *Discrete & Computational Geometry*, 1:25–44, 1986.

[FFHL02] Eyal Flato, Efi Fogel, Dan Halperin, and Eyal Leiserowitz. Movie: Exact Minkowski sums and applications. In *Proceedings of 18th Annual ACM Symposium on Computational Geometry (SoCG)*, pages 273–274. Association for Computing Machinery (ACM) Press, 2002.

[FGK+00] Andreas Fabri, Geert-Jan Giezeman, Lutz Kettner, Stefan Schirra, and Sven Schönherr. On the design of CGAL a computational geometry algorithms library. *Software — Practice and Experience*, 30(11):1167–1202, 2000.

[FH95] Ulrich Finke and Klaus H. Hinrichs. Overlaying simply connected planar subdivisions in linear time. In *Proceedings of 11th Annual ACM Symposium on Computational Geometry (SoCG)*, pages 119–126. Association for Computing Machinery (ACM) Press, 1995.

[FH05] Efi Fogel and Dan Halperin. Movie: Exact Minkowski sums of convex polyhedra. In *Proceedings of 21st Annual ACM Symposium on Computational Geometry (SoCG)*, pages 382–383. Association for Computing Machinery (ACM) Press, 2005.

[FH06] Efi Fogel and Dan Halperin. Exact and efficient construction of Minkowski sums of convex polyhedra with applications. In *Proceedings of 8th Workshop on Algorithm Engineering and Experiments*, 2006.

[FH07] Efi Fogel and Dan Halperin. Exact and efficient construction of Minkowski sums of convex polyhedra with applications. *Computer-Aided Design*, 39(11):929–940, 2007.

[FH08] Efi Fogel and Dan Halperin. Polyhedral assembly partitioning with infinite translations or the importance of being exact. 2008. Proceedings of 8th Workshop on Algorithmic Foundations of Robotics.

[FHH+00] Eyal Flato, Dan Halperin, Iddo Hanniel, Oren Nechushtan, and Ester Ezra. The design and implementation of planar maps in CGAL. *The ACM Journal of Experimental Algorithmics*, 5:1–23, 2000.

[FHK+07] Efi Fogel, Dan Halperin, Lutz Kettner, Monique Teillaud, Ron Wein, and Nicola Wolpert. Arrangements. In J.-D. Boissonnat and M. Teillaud, editors, *Effective Computational Geometry for Curves and Surfaces*, chapter 1, pages 1–66. Springer-Verlag, 2007.

[FHW] Efi Fogel, Dan Halperin, and Christophe Weibel. On the exact maximum complexity of Minkowski sums of convex polyhedra. *Discrete & Computational Geometry*. Accepted for publication.

[FHW+04] Efi Fogel, Dan Halperin, Ron Wein, Sylvain Pion, Monique Teillaud, Ioannis Emiris, Athanasios Kakargias, Elias Tsigaridas, Eric Berberich, Arno Eigenwillig, Michael Hemmer, Lutz Kettner, Kurt Mehlhorn, Elmar Schomer, and Nicola Wolpert. An empirical comparison of software for constructing arrangements of curved arcs (preliminary version). Technical Report ECG-TR-361200-01, Tel-Aviv University, INRIA Sophia-Antipolis, MPI Saarbrücken, 2004.

[FHW07] Efi Fogel, Dan Halperin, and Christophe Weibel. On the exact maximum complexity of Minkowski sums of convex polyhedra. In *Proceedings of 23rd Annual ACM Symposium on Computational Geometry (SoCG)*, pages 319–326. Association for Computing Machinery (ACM) Press, 2007.

[FSH08a] Efi Fogel, Ophir Setter, and Dan Halperin. Exact implementation of arrangements of geodesic arcs on the sphere with applications. In *Abstracts of 24th European Workshop on Computational Geometry*, pages 83–86, 2008.

[FSH08b] Efi Fogel, Ophir Setter, and Dan Halperin. Movie: Arrangements of geodesic arcs on the sphere. In *Proceedings of 24th Annual ACM Symposium on Computational Geometry (SoCG)*, pages 218–219. Association for Computing Machinery (ACM) Press, 2008.

[FT07] Efi Fogel and Monique Teillaud. Generic programming and the CGAL library. In J.-D. Boissonnat and M. Teillaud, editors, *Effective Computational Geometry for Curves and Surfaces*, chapter 8, pages 313–320. Springer-Verlag, 2007.

[Fuk04] Komei Fukuda. From the zonotope construction to the Minkowski addition of convex polytopes. *Journal of Symbolic Computation*, 38(4):1261–1272, 2004.

[FvDFH95] James D. Foley, Andries van Dam, Steven K. Feiner, and John F. Hughes. *Computer Graphics: Principles and Practice in C*. Addison-Wesley, 2nd edition, 1995.

[FW07] Komei Fukuda and Christophe Weibel. f-vectors of Minkowski additions of convex polytopes. *Discrete & Computational Geometry*, 37:503–516, 2007.

[FWH04] Efi Fogel, Ron Wein, and Dan Halperin. Code flexibility and program efficiency by genericity: Improving CGAL's arrangements. In *Proceedings of 12th Annual European Symposium on Algorithms (ESA)*, volume 3221 of *LNCS*, pages 664–676. Springer-Verlag, 2004.

[FWZH07] Efi Fogel, Ron Wein, Baruch Zukerman, and Dan Halperin. 2d regularized boolean set-operations. In CGAL Editorial Board, editor, CGAL *User and Reference Manual*. 3.3 edition, 2007.

[GGHT97] Michael T. Goodrich, Leonidas J. Guibas, John Hershberger, and Paul J. Tanenbaum. Snap rounding line segments efficiently in two and three dimensions. In *Proceedings of 13th Annual ACM Symposium on Computational Geometry (SoCG)*, pages 284–293. Association for Computing Machinery (ACM) Press, 1997.

[GHH+98] Leonidas J. Guibas, Dan Halperin, Hirohisa Hirukawa, Jean-Claude Latombe, and Randall H. Wilson. Polyhedral assembly partitioning using maximally covered cells in arrangements of convex polytopes. *International Journal of Computational Geometry and Applications*, 8(2):179–200, 1998.

[GHJV95] Erich Gamma, Richard Helm, Ralph Johnson, and John M. Vlissides. *Design Patterns — Elements of Reusable Object-Oriented Software*. Addison-Wesley, 1995.

[Gho93] Pijush K. Ghosh. A unified computational framework for Minkowski operations. *Computers & Graphics*, 17(4):357–378, 1993.

[GHZ99] Leonidas J. Guibas, David Hsu, and Li Zhang. H-walk: Hierarchical distance computation for moving convex bodies. In *Proceedings of 15th Annual ACM Symposium on Computational Geometry (SoCG)*, pages 265–273. Association for Computing Machinery (ACM) Press, 1999.

[GJK88] Elmer G. Gilbert, Daniel W. Johnson, and Sathiya S. Keerthi. A fast procedure for computing the distance between complex objects. 4(2):193–203, 1988.

[GM95] Leonidas J. Guibas and David H. Marimont. Rounding arrangements dynamically. In *Proceedings of 11th Annual ACM Symposium on Computational Geometry (SoCG)*, pages 190–199. Association for Computing Machinery (ACM) Press, 1995.

[GRS83] Leonidas J. Guibas, Leo Ramshaw, and Jorge Stolfi. A kinetic framework for computational geometry. In *Proceedings of 24th Annual IEEE Symposium on the Foundations of Computer Science*, pages 100–111, 1983.

[GS87] Leonidas J. Guibas and Raimund Seidel. Computing convolutions by reciprocal search. *Discrete & Computational Geometry*, 2:175–193, 1987.

[GS93] Peter Gritzmann and Bernd Sturmfels. Minkowski addition of polytopes: Computational complexity and applications to Gröbner bases. *SIAM Journal on Discrete Math*, 6(2):246–269, 1993.

[Hac07] Peter Hachenberger. Exact Minkowski sums of polyhedra and exact and efficient decomposition of polyhedra into convex pieces. In *Proceedings of 15th Annual European Symposium on Algorithms (ESA)*, volume 4698 of *LNCS*, pages 669–680. Springer-Verlag, 2007.

[Hal04] Dan Halperin. Arrangements. In Jacob E. Goodman and Joseph O'Rourke, editors, *Handbook of Discrete and Computational Geometry*, chapter 24, pages 529–562. Chapman & Hall/CRC, 2nd edition, 2004.

[Han00] Iddo Hanniel. The design and implementation of planar arrangements of curves in CGAL. M.Sc. thesis, School of Computer Science, Tel Aviv University, 2000.

[HH00] Iddo Hanniel and Dan Halperin. Two-dimensional arrangements in CGAL and adaptive point location for parametric curves. In *Proceedings of International Workshop on Algorithm Engineering (WAE)*, volume 1982 of *LNCS*, pages 171–182. Springer-Verlag, 2000.

[HH03] Shai Hirsch and Dan Halperin. Hybrid motion planning: Coordinating two discs moving among polygonal obstacles in the plane. In Jean-Daniel Boissonnat, Joel Burdick, Ken Goldberg, and Seth Hutchinson, editors, *Algorithmic Foundations of Robotics V*, pages 239–255. Springer-Verlag, 2003.

[HH08] Idit Haran and Dan Halperin. An experimental study of point location in planar arrangements in CGAL. *The ACM Journal of Experimental Algorithmics*, 13, 2008.

[HHK+07] Susan Hert, Michael Hoffmann, Lutz Kettner, Sylvain Pion, and Michael Seel. An adaptable and extensible geometry kernel. *Computational Geometry: Theory and Applications*, 38(1-2):16–36, 2007.

[HK07] Peter Hachenberger and Lutz Kettner. 3D Boolean operations on nef polyhedra. In CGAL Editorial Board, editor, CGAL *User and Reference Manual*. 3.3 edition, 2007.

[HKL+99] Kenneth E. Hoff III, John Keyser, Ming Lin, Dinesh Manocha, and Tim Culver. Fast computation of generalized voronoi diagrams using graphics hardware. In *Proceedings of 26th Annual International Conference on Computer Graphics and Interactive Techniques*, pages 277–286. Association for Computing Machinery (ACM) Press, 1999.

[HKL04] Dan Halperin, Lydia E. Kavraki, and Jean-Claude Latombe. Robotics. In Jacob E. Goodman and Joseph O'Rourke, editors, *Handbook of Discrete and Computational Geometry*, chapter 48, pages 1065–1093. Chapman & Hall/CRC, 2nd edition, 2004.

[HKM07] Peter Hachenberger, Lutz Kettner, and Kurt Mehlhorn. Boolean operations on 3D selective Nef complexes: Data structure, algorithms, optimized implementation and experiments. *Computational Geometry: Theory and Applications*, 38(1-2):64–99, 2007. Special issue on CGAL.

[HL04] Dan Halperin and Eran Leiserowitz. Controlled perturbation for arrangements of circles. volume 14, pages 277–310, 2004.

[HLW00] Dan Halperin, Jean-Claude Latombe, and Randall H. Wilson. A general framework for assembly planning: The motion space approach. *Algorithmica*, 26:577–601, 2000.

[Hob99] John D. Hobby. Practical segment intersection with finite precision output. *Computational Geometry: Theory and Applications*, 13(4):199–214, 1999.

[Hof04] Christoph M. Hoffmann. Solid modeling. In Jacob E. Goodman and Joseph O'Rourke, editors, *Handbook of Discrete and Computational Geometry*, chapter 56, pages 1257–1278. Chapman & Hall/CRC, 2nd edition, 2004.

[HP01] Dan Halperin and Eli Packer. Snap rounding revisited. In *Abstracts of 17th European Workshop on Computational Geometry*, pages 82–85. Freie Universität Berlin, 2001.

[HP02] Dan Halperin and Eli Packer. Iterated snap rounding. *Computational Geometry: Theory and Applications*, 23:209–225, 2002.

[HRS92] Craig D. Hodgson, Igor Rivin, and Warren D. Smith. A characterization of convex hyperbolic polyhedra and of convex polyhedra inscribed in the sphere. *Bull. (New Series) of the AMS*, 27:246–251, 1992.

[HS98] Dan Halperin and Christian R. Shelton. A perturbation scheme for spherical arrangements with application to molecular modeling. *Computational Geometry: Theory and Applications*, 10:273–287, 1998.

[HW07] Iddo Hanniel and Ron Wein. An exact, complete and efficient computation of arrangements of Bézier curves. In *Proceedings of ACM Symposium on Solid and Physical Modeling (SPM)*, pages 253–263. Association for Computing Machinery (ACM) Press, 2007.

[IIM85] Hiroshi Imai, Masao Iri, and Kazuo Murota. Voronoi diagram in the Laguerre geometry and its applications. *SIAM Journal on Computing*, 14(1):93–105, 1985.

[KCMK00] John Keyser, Tim Culver, Dinesh Manocha, and Shankar Krishnan. Efficient and exact manipulation of algebraic points and curves. *Computer-Aided Design*, 32(11):649–662, 2000.

[Ket99] Lutz Kettner. Using generic programming for designing a data structure for polyhedral surfaces. *Computational Geometry: Theory and Applications*, 13(1):65–90, 1999.

[Ket07a] Lutz Kettner. 3D polyhedral surfaces. In CGAL Editorial Board, editor, CGAL *User and Reference Manual*. 3.3 edition, 2007.

[Ket07b] Lutz Kettner. Halfedge data structures. In CGAL Editorial Board, editor, CGAL *User and Reference Manual*. 3.3 edition, 2007.

[KK95] Lydia E. Kavraki and Mihail N. Kolountzakis. Partitioning a planar assembly into two connected parts is NP-complete. *Information Processing Letters*, 55:159–165, 1995.

[KLPY99] Vijay Karamcheti, Chen Li, Igor Pechtchanski, and Chee K. Yap. A core library for robust numeric and geometric computation. In *Proceedings of 15th Annual ACM Symposium on Computational Geometry (SoCG)*, pages 351–359. Association for Computing Machinery (ACM) Press, 1999.

[kLsKE98] In kwon Lee, Myung soo Kim, and Gershon Elber. Polynomial/rational approximation of Minkowski sum boundary curves. *Graphical Models and Image Processing*, 60(2):136–165, 1998.

[KMP+08] Lutz Kettner, Kurt Mehlhorn, Sylvain Pion, Stefan Schirra, and Chee Yap. Classroom examples of robustness problems in geometric computations. *Computational Geometry: Theory and Applications*, 40(1):61–78, 2008.

[KMW98] Sanjeev Khanna, Rajeev Motwani, and Randall H. Wilson. On certificates and lookahead in dynamic graph problems. *Algorithmica*, 21(4):377–394, 1998.

[KN04] Lutz Kettner and Stefan Näher. Two computational geometry libraries: LEDA and CGAL. In Jacob E. Goodman and Joseph O'Rourke, editors, *Handbook of Discrete and Computational Geometry*, chapter 65, pages 1435–1463. Chapman & Hall/CRC, Boca Raton, FL, 2nd edition, 2004.

[KR91] Anil Kaul and Jarek R. Rossignac. Solid-interpolating deformations: Construction and animation of PIPs. In *Proceedings of European Computer Graphics Conference (Eurographics)*, pages 493–505, 1991.

[Lat91] Jean-Claude Latombe. *Robot Motion Planning*. Kluwer Academic Publishers, Boston, 1991.

[LC91] Ming C. Lin and John F. Canny. A fast algorithm for incremental distance calculation. In *Proceedings of IEEE International Conference on Robotics and Automation*, pages 1008–1014, 1991.

[LM04] Ming C. Lin and Dinesh Manocha. Collision and proximity queries. In Jacob E. Goodman and Joseph O'Rourke, editors, *Handbook of Discrete and Computational Geometry*, chapter 35, pages 787–807. Chapman & Hall/CRC, 2nd edition, 2004.

[LPT08] Sylvain Lazard, Luis Peñaranda, and Elias Tsigaridas. A CGAL based algebraic kernel based on RS and application to arrangements. In *Abstracts of 24th European Workshop on Computational Geometry*, pages 91–94, 2008.

[Luk57] Dorman Luke. Stellations of the rhombic dodecahedron. *The Mathematical Gazette*, 41(337):189–194, 1957.

[Mey06] Michal Meyerovitch. Robust, generic and efficient construction of envelopes of surfaces in three-dimensional space. In *Proceedings of 14th Annual European Symposium on Algorithms (ESA)*, volume 4168 of *LNCS*, pages 792–803. Springer-Verlag, 2006.

[Mir98] Brian Mirtich. V-clip: Fast and robust polyhedral collision detection. *ACM Transactions on Graphics*, 17(3):177–208, 1998.

[MN00] Kurt Mehlhorn and Stefan Näher. LEDA*: A Platform for Combinatorial and Geometric Computing*. Cambridge University Press, Cambridge, UK, 2000.

[MO06] Kurt Mehlhorn and Ralf Osbild. Reliable and efficient computational geometry via controlled perturbation. In *Automata, Languages and Programming*, volume 4051 of *LNCS*, pages 299–310. Springer-Verlag, 2006.

[MS88] David A. Musser and Alexander A. Stepanov. Generic programming. In *Proceedings of International Conference on Symbolic and Algebraic Computation*, volume 358 of *LNCS*, pages 13–25. Springer-Verlag, 1988.

[MS03] Kurt Mehlhorn and Michael Seel. Infimaximal frames: A technique for making lines look like segments. *International Journal of Computational Geometry and Applications*, 13(3):241–255, 2003.

[Mul90] Ketan Mulmuley. A fast planar partition algorithm, I. *Journal of Symbolic Computation*, 10(3-4):253–280, 1990.

[MWZ07] Michal Meyerovitch, Ron Wein, and Baruch Zukerman. 3D envelopes. In CGAL Editorial Board, editor, CGAL *User and Reference Manual*. 3.3 edition, 2007.

[Mye98] Nathan Myers. A new and useful template technique: "Traits". In Stanly B. Lippman, editor, *C++ Gems*, volume 5 of *SIGS Reference Library*, pages 451–458. Cambridge University Press, Cambridge, UK, 1998.

[Nat88] B. K. Natarajan. On planning assemblies. In *Proceedings of 4th Annual ACM Symposium on Computational Geometry (SoCG)*, pages 299–308. Association for Computing Machinery (ACM) Press, 1988.

[NLC02] Hyeon-Suk Na, Chung-Nim Lee, and Otfried Cheong. Voronoi diagrams on the sphere. *Computational Geometry: Theory and Applications*, 23(2):183–194, 2002.

[OBSC00] Atsuyuki Okabe, Barry Boots, Kokichi Sugihara, and Sung Nok Chiu. *Spatial Tessellations: Concepts and Applications of Voronoi Diagrams*. John Wiley & Sons, NYC, 2nd edition, 2000.

[Ove96] Mark H. Overmars. Designing the computational geometry algorithms library CGAL. In *Proceedings of ACM Workshop on Applied Computational Geometry, Towards Geometric Engineering*, volume 1148, pages 53–58, London, UK, 1996. Springer-Verlag.

[PF06] Sylvain Pion and Andreas Fabri. A generic lazy evaluation scheme for exact geometric computations. In *2nd Library-Centric Software Design Workshop*, 2006.

[PS85] Franco P. Preparata and Michael Ian Shamos. *Computational Geometry: An Introduction*. Springer-Verlag, New York, NY, 1985.

[PY07] Sylvain Pion and Mariette Yvinec. 2D triangulation data structure. In CGAL Editorial Board, editor, CGAL *User and Reference Manual*. 3.3 edition, 2007.

[Rog03] Vadim Rogol. Maximizing the area of an axially-symmetric polygon inscribed by a simple polygon. Master's thesis, Technion, Haifa, Israel, 2003.

[Sch00] Stefan Schirra. Robustness and precision issues in geometric computation. In Jörg-Rüdiger Sack and Jorge Urrutia, editors, *Handbook of Computational Geometry*, chapter 14, pages 597–632. Elsevier Science Publishers, B.V. North-Holland, Amsterdam, North-Holland, 2000.

[See07] Michael Seel. 2D Boolean operations on nef polygons. In CGAL Editorial Board, editor, CGAL *User and Reference Manual*. 2007.

[SH75] Michael Ian Shamos and Dan Hoey. Closest-point problems. In *Proceedings of 16th IEEE Symposium on the Foundations of Computer Science*, pages 151–162, 1975.

[SH89] Jack Snoeyink and John Hershberger. Sweeping arrangements of curves. In *Proceedings of 5th Annual ACM Symposium on Computational Geometry (SoCG)*, pages 354–363. Association for Computing Machinery (ACM) Press, 1989.

[Sha04] Micha Sharir. Algorithmic motion planning. In Jacob E. Goodman and Joseph O'Rourke, editors, *Handbook of Discrete and Computational Geometry*, chapter 47, pages 1037–1064. Chapman & Hall/CRC, 2nd edition, 2004.

[SKS02] Joon-Kyung Seong, Myung-Soo Kim, and Kokichi Sugihara. The Minkowski sum of two simple surfaces generated by slope-monotone closed curves. In *Geometric Modeling and Processing — Theory and Applications*, pages 33–42, 2002.

[SLL02] Jeremy G. Siek, Lie-Quan Lee, and Andrew Lumsdaine. *The B*OOST *Graph Library*. Addison-Wesley, 2002.

[SS94] Jack Snoeyink and Jorge Stolfi. Objects that cannot be taken apart with two hands. *Discrete & Computational Geometry*, 12:367–384, 1994.

[SSH08] Ophir Setter, Micha Sharir, and Dan Halperin. Construction two-dimensional Voronoi diagrams via divide and conquer of envelopes in space, 2008. Manuscript.

[Sug02] Kokichi Sugihara. Laguerre Voronoi diagram on the sphere. *Journal for Geometry and Graphics*, 6(1):69–81, 2002.

[SWK03] Kevin Sahr, Denis White, and A. Jon Kimerling. Geodesic discrete global grid systems. *Cartography and Geographic Information Science*, 30(2):121–134, 2003.

[Tar72] Robert E. Tarjan. Depth first search and linear graph algorithms. *SIAM Journal on Computing*, 1(2):146–160, 1972.

[Tou85] Godfried Toussaint. *Movable separability of sets*. North-Holland, 1985.

[VKSM05] Gokul Varadhan, Shankar Krishnan, T. V. N. Sriram, and Dinesh Manocha. A simple algorithm for complete motion planning of translating polyhedral robots. *International Journal of Robotics Research*, 24(11):983–995, 2005.

[VM06] Gokul Varadhan and Dinesh Manocha. Accurate Minkowski sum approximation of polyhedral models. *Graphical Models and Image Processing*, 68(4):343–355, 2006.

[Wei02] Ron Wein. High-level filtering for arrangements of conic arcs. In *Proceedings of 10th Annual European Symposium on Algorithms (ESA)*, volume 2461 of *LNCS*, pages 884–895. Springer-Verlag, 2002.

[Wei05] Ron Wein. Efficient implementation of red-black trees with split and catenate operations. Technical report, Tel-Aviv University, 2005. `http://www.cs.tau.ac.il/~wein/publications/pdfs/rb_tree.pdf`.

[Wei07] Ron Wein. *The Integration of Exact Arrangements with Effective Motion Planning*. Ph.D. thesis, The Blavatnik School of Computer Science, Tel Aviv University, 2007.

[WF05] Ron Wein and Efi Fogel. The new design of CGAL's arrangement package. Technical report, Tel-Aviv University, 2005. `http://www.cs.tau.ac.il/~wein/publications/pdfs/Arr_new_design.pdf`.

[WFZH05] Ron Wein, Efi Fogel, Baruch Zukerman, and Dan Halperin. Advanced programming techniques applied to CGAL's arrangement package. In *1st Library-Centric Software Design Workshop*, 2005.

[WFZH07a] Ron Wein, Efi Fogel, Baruch Zukerman, and Dan Halperin. 2D arrangements. In CGAL Editorial Board, editor, CGAL *User and Reference Manual*. 3.3 edition, 2007.

[WFZH07b] Ron Wein, Efi Fogel, Baruch Zukerman, and Dan Halperin. Advanced programming techniques applied to CGAL's arrangement package. *Computational Geometry: Theory and Applications*, 38(1–2):37–63, 2007. Special issue on CGAL.

[WL94] Randall H. Wilson and Jean-Claude Latombe. Geometric reasoning about mechanical assembly. *Artificial Intelligence*, 71(2):371–396, 1994.

[WSD03] Yanyan Wu, Jami J. Shah, and Joseph K. Davidson. Improvements to algorithms for computing the Minkowski sum of 3-polytopes. *Computer-Aided Design*, 35(13):1181–1192, 2003.

[WvH07] Ron Wein, Jur P. van den Berg, and Dan Halperin. The visibility-Voronoi complex and its applications. *Computational Geometry: Theory and Applications*, 36(1):66–87, 2007.

[Yap04] Chee K. Yap. Robust geomtric computation. In Jacob E. Goodman and Joseph O'Rourke, editors, *Handbook of Discrete and Computational Geometry*, chapter 41, pages 927–952. Chapman & Hall/CRC, 2nd edition, 2004.

# Links


[1] Using CGAL for robust planar geometry processing in Agilent ADS.
http://acg.cs.tau.ac.il/projects/external-projects/agilent-ads/project-page.

[2] Algorithmic automation.
http://goldberg.berkeley.edu/algorithmic-automation.

[3] BOOST — portable C++ libraries.
http://www.boost.org.

[4] BOOST, Generic Programming Techniques.
http://www.boost.org/community/generic_programming.html.

[5] CGAL — computational geometry algorithms library.
http://www.cgal.org.

[6] The CORE number library homepage.
http://cs.nyu.edu/exact/core_pages.

[7] ECG — effective computational geometry for curves and surfaces.
http://www-sop.inria.fr/prisma/ECG.

[8] ESOLID — exact boundary evaluation of low-degree curved solids.
http://www.cs.unc.edu/~geom/ESOLID.

[9] EXACUS — efficient and exact algorithms for curves and surfaces.
http://www.mpi-inf.mpg.de/projects/EXACUS.

[10] Function object.
http://en.wikipedia.org/wiki/Function_object.

[11] GEOMETRYFACTORY.
http://www.geometryfactory.com.

[12] GMP — GNU multiple precision arithmetic library.
http://gmplib.org.

[13] Gnuplot homepage.
http://www.gnuplot.info.

[14] Google maps.
http://maps.google.com.

[15] Imagemagick homepage.
http://www.imagemagick.org/script/index.php.

[16] CGAL arrangement of IRIT free-form curves.
http://www.cs.technion.ac.il/~cs234326/projects/IRIT_CGAL/index.htm.

[17] LEDA — library for efficient data types and algorithms.
http://www.algorithmic-solutions.com/enleda.htm.

[18] LEDA external package: Sphere geometry.
http://www.mpi-inf.mpg.de/LEDA/friends/SphereGeometry.html.

[19] MAPC — efficient and exact manipulation of algebraic points and curves.
http://www.cs.unc.edu/~geom/MAPC.

[20] Minkowski sum related movies.
http://acg.cs.tau.ac.il/movies.

[21] The QUICKCD library homepage.
http://www.ams.sunysb.edu/~jklosow/quickcd/QuickCD.html.

[22] Real-time high dynamic range image-based lighting.
http://www.daionet.gr.jp/~masa/rthdribl.

[23] Wolfram Mathworld simple polygon. Simple polygon.
http://mathworld.wolfram.com/SimplePolygon.html.

[24] The SOLID library homepage.
http://www.win.tue.nl/cs/tt/gino/solid/.

[25] STL — C++ standard template library.
http://www.sgi.com/tech/stl.

[26] SWIFT++ library homepage.
http://gamma.cs.unc.edu/SWIFT++/.

[27] The web3D homepage.
http://www.web3d.org.

[28] Christophe Weibel. Minkowski sums.
http://roso.epfl.ch/cw/poly/public.php.

# Index